



## 저작자표시-변경금지 2.0 대한민국

이용자는 아래의 조건을 따르는 경우에 한하여 자유롭게

- 이 저작물을 복제, 배포, 전송, 전시, 공연 및 방송할 수 있습니다.
- 이 저작물을 영리 목적으로 이용할 수 있습니다.

다음과 같은 조건을 따라야 합니다:



저작자표시. 귀하는 원저작자를 표시하여야 합니다.



변경금지. 귀하는 이 저작물을 개작, 변형 또는 가공할 수 없습니다.

- 귀하는, 이 저작물의 재이용이나 배포의 경우, 이 저작물에 적용된 이용허락조건을 명확하게 나타내어야 합니다.
- 저작권자로부터 별도의 허가를 받으면 이러한 조건들은 적용되지 않습니다.

저작권법에 따른 이용자의 권리는 위의 내용에 의하여 영향을 받지 않습니다.

이것은 [이용허락규약\(Legal Code\)](#)을 이해하기 쉽게 요약한 것입니다.

[Disclaimer](#) 

이학박사학위논문

**Morphological diversity of  
self-assembled block copolymers  
containing high-density functional  
groups and their applications**

고밀도 작용기를 포함하는 블록공중합체의 수용액  
상의 자기조립체의 구조적 다양성 탐구와 응용

2023 년 2 월

서울대학교 대학원  
화학부 고분자화학전공  
이 수 정

Ph. D. Dissertation

**Morphological diversity of  
self-assembled block copolymers  
containing high-density functional  
groups and their applications**

Soo Jeong Lee

Research Advisor: Prof. Kyoung Taek Kim

**Department of Chemistry  
Seoul National University**

# Morphological diversity of self-assembled block copolymers containing high-density functional groups and their applications

고밀도 작용기를 포함하는 블록공중합체의 수용액  
상의 자기조립체의 구조적 다양성 탐구와 응용

지도교수 김 경 택

이 논문을 이학박사 학위논문으로 제출함.

2023년 2월

서울대학교 대학원  
화학부 고분자화학 전공  
이 수 정

이 수 정의 이학박사 학위논문을 인준함

2023년 2월

위 원 장 이 연 (인)

부 위 원 장 김 경 택 (인)

위 원 손 병 혁 (인)

위 원 송 윤 주 (인)

위 원 이 인 환 (인)

## Abstract

# **Morphological diversity of self-assembled block copolymers containing high-density functional groups and their applications**

Soo Jeong Lee

Major in polymer chemistry

Department of Chemistry

Seoul National University

Solution self-assembly of block copolymers is a facile way to synthesize nanostructures. For this, it is essential to synthesize well-defined block copolymers. The synthesized block copolymer contains hydrophobic block and hydrophilic block in one molecule, so it is similar to surfactant. Through the interaction between each block and the solvent, it has the advantage of being able to generate various microstructures compared to bulk assembly. There are many factors in the assembly structure of these amphiphilic molecules, however they can be defined based on the most influential block ratio and critical packing parameters. Previous studies have revealed that these factors are closely related to chemical structures, this dissertation also tried to reveal and apply various structures based on further results.

We reported a self-assembled structure that has never been reported in previous

studies through a binary blend of block copolymers with the same chemical structure and extreme molecular weight differences of the hydrophobic block. In addition, through labeling experiments using functionalized block copolymers and gold nanoparticles, the assumption that low molecular weight polymers are concentrated in areas with high surface energy to stabilize the structure was experimentally proven.

In addition, we endowed high-density functional groups to the surface of the polymer cubosome with well-defined two independent channels among known self-assembly structures and a large surface area due to the mesoporous structure. Alkyne groups were introduced to the surface of polymer cubosome, and the activity of the functional groups was confirmed using Copper catalysed alkyne azide cycloaddition (CuAAC). It was expected that cubosome with high density alkyne groups could be used as a nanoreactor for aldol reaction through the introduction of L-proline.

Futhermore, the morphological transition of the solution-self-assembly structures were observed by modifying the hydrophilic block ends of block copolymers with Benzyl, hydroxy, t-Boc-glycine, and amine. In conclusion, polymer cubosomes containing high-density amine groups on the surface, which had not been found in previous studies, was implemented and a Ni-NTA complex was introduced to function as a stationary phase for immobilized metal affinity chromatography to selectively purify histidine-tagged proteins.

In addition, following the genealogy of functionalized polymer synthesis research, 4-pentenoic acid was modified to synthesize sequence defined discrete polymers through Passerini 3-component reaction. This method is expected to be a new means to control the properties of polymer by combining the previously reported iterative exponential growth with multicomponent reaction for more efficient synthesis and

imparting functional groups to specific position on the backbone of the sequence-defined polymers.

**Keywords: Block copolymer, solution self-assembly, Polymer cubosomes, Discrete polymer, Functionalized polymer, Polymer nanostructures**

**Student Number: 2016-20357**

# Contents

<i>Abstract</i> .....	i
<i>Contents</i> .....	iv
<i>List of Schemes</i> .....	vii
<i>List of Tables</i> .....	ix
<i>List of Figures</i> .....	x
<i>Abbreviation</i> .....	xx

## **Chapter 1. Introduction**

1.1 Overview .....	1
1.2 Nonergodic behavior in self-assembly of polymers .....	2
1.3 Polymer cubosomes and applications .....	6
1.4 Synthesis of discrete polymer using multi component reaction .....	11
1.5 Summary .....	15
1.6 References .....	15

## **Chapter 2. Morphological Diversity from the Solution Self-Assembly of Block Copolymer Blends Containing High Molecular-Weight Hydrophobic Blocks**

2.1 Abstract .....	19
2.2 Introduction .....	19



<b>2.3 Results and discussion</b> .....	<b>23</b>
<b>2.4 Conclusion</b> .....	<b>33</b>
<b>2.5 Experimental</b> .....	<b>34</b>
<b>2.6 References</b> .....	<b>53</b>

### **Chapter 3. Polymer cubosomes with high-density surface functional groups**

<b>3.1 Abstract</b> .....	<b>58</b>
<b>3.2 Introduction</b> .....	<b>59</b>
<b>3.3 Results and discussion</b> .....	<b>60</b>
<b>3.4 Conclusion</b> .....	<b>66</b>
<b>3.5 Experimental</b> .....	<b>66</b>
<b>3.6 References</b> .....	<b>81</b>

### **Chapter 4. Polymer cubosomes as a stationary phase for affinity chromatography of proteins**

<b>4.1 Abstract</b> .....	<b>85</b>
<b>4.2 Introduction</b> .....	<b>85</b>
<b>4.3 Results and discussion</b> .....	<b>87</b>
<b>4.4 Conclusion</b> .....	<b>96</b>
<b>4.5 Experimental</b> .....	<b>97</b>
<b>4.6 References</b> .....	<b>107</b>

## **Chapter 5. Synthesis of Sequence defined polymer using Passerini 3-component reaction**

<b>5.1 Abstract .....</b>	<b>111</b>
<b>5.2 Introduction .....</b>	<b>111</b>
<b>5.3 Results and discussion .....</b>	<b>114</b>
<b>5.4 Conclusion .....</b>	<b>121</b>
<b>5.5 Experimental .....</b>	<b>121</b>
<b>5.6 Reference .....</b>	<b>127</b>
<b>Abstract (in Korean) .....</b>	<b>129</b>

## List of Schemes

**Scheme 2.1** Preparation of hydrophilic block (1). Dendritic hydrophilic block used in this study was synthesized as previously reported.

**Scheme 2.2** Preparation of amphiphilic block copolymers (3)-(6).

**Scheme 2.3** Preparation of hydrophilic block.

**Scheme 2.4** Preparation of hydrophobic block.

**Scheme 2.5** Preparation of amphiphilic block copolymers.

**Scheme 2.6** Preparation of azide functionalized Bunte Salt.

**Scheme 2.7** Preparation of Bunte Salt.

**Scheme 2.8** Preparation of azide-functionalized AuNPs.

**Scheme 3.1** Chemical structure of branched-linear block copolymer containing functional groups: a) one acetylene group; b) three acetylene groups.

**Scheme 3.2** Scheme for Copper (I)-catalyzed azide-alkyne cycloadditions (CuAAC) of polymers with alkyne groups and azido coumarin in water condition.

**Scheme 3.3** Reaction conditions for each step: (i)  $\text{CH}_3(\text{OCH}_2\text{CH}_2)_{11}\text{OTs}$ ,  $\text{K}_2\text{CO}$ , KI, Acetone, 80 °C; (ii) Pd/C (5%), Dry MeOH, 55 °C, reflux; (iii)  $\text{HCCCH}_2(\text{OCH}_2\text{CH}_2)_{12}\text{OTs}$ ,  $\text{K}_2\text{CO}_3$ , KI, Acetone, 80 °C; (iv) KOH, EtOH, reflux.

**Scheme 3.4** Reaction conditions for each step: (i)  $\text{HCCCH}_2(\text{OCH}_2\text{CH}_2)_{12}\text{OTs}$ ,  $\text{K}_2\text{CO}_3$ , KI, Acetone, 80 °C; (ii) KOH, EtOH, reflux.

**Scheme 3.5** Reaction conditions for each step: (i) DMF,  $\text{NaN}_3$ , R.T, 12h; (ii) Dry THF,  $\text{LiAlH}_4$ , 70°C, 3h.

**Scheme 3.6** Reaction conditions: (i) Dry MC, DCC, DMAP, 0 °C.

**Scheme 3.7** Synthetic procedure for 3-Azidocoumarin.

**Scheme 4.1** a) Synthesis of BCPs via ATRP. b) Post-modification process of BCPs.

**Scheme 4.2** Synthesis of dendritic hydrophilic block.

**Scheme 4.3** Synthesis of 2-hydroxyethyl 2-bromoisobutyrate.

**Scheme 4.4** Synthesis of ATRP macroinitiator.

**Scheme 4.5** Reaction conditions for each step: (i) Pd/C (10%), Acetone, H<sub>2</sub>; (ii) t-Boc-glycine, dryMC, EDC, DPTS, 0 °C; (iii) TFA, Dry MC, R.T, 1h.

**Scheme 5.1** a) Passerini 3-component reaction. b) Concerted mechanism of Passerini 3-component reaction.

**Scheme 5.2** The monomer modification processes: a) Steglich-type esterification of 4-pentenoic acid and benzyl alcohol. b) Lemieux–Johnson oxidation of benzyl 4-pentenoate. c) Protection of aldehyde groups with neopentyl glycols using Dean-Stark method to prepare the AB type monomer.

**Scheme 5.3** a) Passerini 3-component reaction using AB type monomers. b) Cross-convergent synthesis of sequence-defined polymers via Passerini 3-component reaction.

**Scheme 5.4** Preparation of benzyl 4-pentenoate.

**Scheme 5.5** Preparation of benzyl 4-oxobutanoate.

**Scheme 5.6** Preparation of AB type monomer.

**Scheme 5.7** Preparation of 3-(5,5-dimethyl-1,3-dioxan-2-yl)propanoic acid.

**Scheme 5.8** Preparation of dimer.

**Scheme 5.9** Hydrogenation of dimer.

**Scheme 5.10** Deacetalization of dimer.

**Scheme 5.11** Preparation of trimer.

## **List of Table**

**Table 2.1** Characterization of BCPs.

**Table 2.2** Characterization of BCPs.

**Table 2.3** Characterization of BCPs.

**Table 3.1** Characterization of polymers.

**Table 4.1** Characterization of BCPs.

## List of Figures

**Figure 1.1** Energy diagram of kinetic traps vs thermodynamic equilibrium states.

Transition between the kinetic traps and the thermodynamic equilibrium state is possible under external stimuli.

**Figure 1.2** End-caps and Y-junction points which is the defects of cylindrical micelles system.

**Figure 1.3** a) End cap and associated undulations in a cylindrical micelles. b) Y-junction that connects cylindrical micelles. c) A transition from a bilayer to a cylinder which is the structural element of the octopus morphology.

**Figure 1.4** a) Cryo-TEM image of polymer blended micelles. b) Transport of diblock copolymer molecules along the cylindrical portions would permit evolution of a connected bilayer sheet.

**Figure 1.5** Critical packing parameter (Shape factor).  $v$ : Volume of hydrophobic block.  $l_c$ : Effective maximum chain extension.  $a_0$ : Optimum head group area.

**Figure 1.6** Self-assembly of PEG<sub>3</sub>-PS block copolymer into polymer cubosomes.

**Figure 1.7** Polymer cubosome with lattice structure of the primitive cubic phase ( $Im\bar{3}m$ ): a) SEM image of the polymer cubosome. b) TEM image showing the internal structure of the polymer cubosome. c) High resolution SEM image of the internal structure of the polymer cubosome. d) The SAXS result of the polymer cubosome (lattice parameter,  $a = 93.4$  nm).

**Figure 1.8** Schematic illustration of SDEMS process and the film consisting of the IBC structures.

**Figure 1.9** a) SEM images of the top layer of the film having evenly distributed

nanopores (~10 nm). The inset shows a picture of the polymer film. b) SEM images of the cross-section of the film.

**Figure 1.10** a) SAXS results of the Polymer cubosomes (black,  $Pn\bar{3}m$ , lattice parameter,  $a = 213$  nm), single networks of silica (red,  $Fd\bar{3}m$ ,  $a = 361$  nm) and titania (blue,  $Fd\bar{3}m$ ,  $a = 247$  nm). b), c) SEM and TEM images for single networks of silica. d) UV–vis reflectance spectrometry of the Polymer cubosomes (black), silica networks (red) and titania networks (blue). e) SEM image of fractured titania single cubic network. i) Optical microscope images of silica (top) and titania (bottom) networks.

**Figure 1.11** a), b) SEM images of Ni networks ( $Fd\bar{3}m$ ). c) SEM image of carbonaceous network. d) High resolution SEM images showing the internal single diamond ( $Fd\bar{3}m$ ) lattice of carbonaceous network.

**Figure 1.12** a) Scheme of polymers synthesized from an Ugi 4-CR Product. b) Synthetic scheme for polymers using ROMP.

**Figure 1.13** a) Chemical structure of stearic acid (monomer with carboxylic acid). b) Synthetic process for a sequence-defined tetramer (starting from 1a) or a sequence-defined block copolymer (starting from 1b). c) Chemical structure of the tetramer with different side chains. d) GPC traces after Passerini 3-CR and thiol–ene reactions in the synthesis of tetramer. e) Chemical structure of the sequence-defined block-copolymer. f) GPC traces of the PEG copolymer after each Passerini 3-CR.

**Figure 1.14** a) Synthetic scheme for sequence-defined polymers. b) Chemical structure of the decamer having different side chains. c) GPC traces of the products after each Passerini 3-CR.

**Figure 1.15** a) Synthetic scheme for the self-metathesis reaction. b) GPC traces of the products, indicating the clear shift of the 20-mer compared to the decamer.

**Figure 2.1** Schematic illustrating of the self-assembly of the blend of H-BCP and L-BCP. The average structural parameters, such as packing parameters and block ratio, would be decided by the composition of two BCPs in the blend, which dictates the morphology of the self-assembled structures.

**Figure 2.2** Representative EM images of the self-assembled structures of BCP: a) SEM and e) TEM images of polymersomes of 3 self-assembled by cosolvent method. b) SEM and f) TEM images of polymer hexosomes of 5 self-assembled by solvent diffusion-evaporation self-assembly method. c,d) SEM and g,h) TEM images of polymer cubosomes of 4 self-assembled by solvent diffusion-evaporation self-assembly method.

**Figure 2.3** a–d) Representative SEM and e–h) TEM images of the self-assembled structures of BCP 3/6 blends: a,e) Polymersomes and sponge-phase particles (95:5 w/w). b,f) Polymersomes (85:15 w/w). c,g) Cylindrical micelles tethered to flat lamellae (80:20 w/w). d,h) Spherical micelles (70:30 w/w).

**Figure 2.4** a–d) Representative SEM and e–h) TEM images of the self-assembled structures of BCP 4/6 blends: a,e) Smaller cubosomes (95:5 w/w). b,f) Spherically entangled worm-like micelles (90:10 w/w). c,g) Worm-like micelles (75:25 w/w). d,h) Small vesicular structures (50:50 w/w).

**Figure 2.5** Representative SEM and TEM images of the self-assembled structures of BCP 5/6 blends: a,f) Polymer cubosomes (95:5 w/w). b,g) Ill-defined



cubosomes-like particles (90:10 w/w). c,h) Spherically entangled worm-like micelles (85:15 w/w). d,i) Unwinding of the entanglement of worm-like micelles (80:20 w/w). e,j) Short worm-like micelles (70:30 w/w).

**Figure 2.6** SIM image of the BCP 5/6 blends: Nile red-labeled Spherically entangled worm-like micelles (80:20 w/w). a–d) Cross-sectional CLSM images of Nile red-labeled spherically entangled worm-like micelles at different focal planes along the  $z$ -axis.

**Figure 2.7.** Representative SEM and TEM images of the self-assembled structures of BCP 5/6 blends: a,f) The composition of 6 is 22% (78:22 w/w). b,g) 25% (75:25 w/w). c,h) 28% (72:28 w/w). d,i) 30% (70:30 w/w). e,j) 50% (50:50 w/w).

**Figure 2.8.** TEM images of structures of BCP 4/7 blends (75:25 w/w): a) purified Y-junctioned micelles after the mixing with AuNPs (25nm) without click reaction. b,c) Purified the micelles after click reaction with AuNPs (5, 25 nm), respectively.

**Figure 2.9** a)  $^1\text{H}$  NMR spectrum of the macroinitiator PEG2000<sub>3</sub>-Br, 1. b) MALDI-TOF MS spectrum of the precursor of the macroinitiator, PEG2000<sub>3</sub>-OH.

**Figure 2.10** a) GPC elugrams (DMF as an eluent) and b)  $^1\text{H}$  NMR in  $\text{CD}_2\text{Cl}_2$  spectra of BCPs.

**Figure 2.11** Plot of column volume vs intensity of the entire absorbance of gradient column chromatography by Isolera™ Spektra system showing a successful separation of homo-PS The yield of block copolymers was ~17%.

**Figure 2.12** a ) Plot of polymerization time vs the number average of molecular

weight ( $M_n$ ) and molecular dispersity ( $D$ ) for 3. ( $M_n = 81,700 \text{ g mol}^{-1}$ ,  $D = 1.65$ ) b) GPC (THF as an eluent) results showing the progress during the polymerization time for 3. c) GPC (DMF as an eluent) and d)  $^1\text{H}$  NMR spectra showing the reaction mixture before purification process (black), the homo-PS separated as a first fraction of the gradient chromatography (red), and 3 separated as the second fraction (blue).

**Figure 2.13**  $^1\text{H}$  NMR in  $\text{CD}_2\text{Cl}_2$  spectrum of the macroinitiator  $\text{PEG1000}_3\text{-Br}$ , 2.

**Figure 2.14** a) GPC elugram (THF as an eluent) and b)  $^1\text{H}$  NMR in  $\text{CD}_2\text{Cl}_2$  spectrum of LBCP 6.

**Figure 2.15** DLS plots of polymersomes of 3 self-assembled by co-solvent method.

**Figure 2.16** a) SEM and b) TEM images of self-assembled structures of 4 by the co-solvent method. c) SEM and d) TEM images of self-assembled structures of 5 by the co-solvent method.

**Figure 2.17** Small-angle x-ray scattering result obtained from the dried polymer cubosomes of 4 ( $Im\bar{3}m$  symmetry,  $a = 190 \text{ nm}$ ).

**Figure 2.18** TEM images of the polymersomes of a)  $\text{PEG2000-PS}_{228}$  and b)  $\text{PEG2000}_3\text{-PS}_{1683}$  3 showing the thickness of the bilayer membrane.

**Figure 2.19** TEM image of the polymer cubosome of 4 by SDEMS method and the representative lattice of Schwarz P surface of BCP bilayers. The computer-generated (100) plane of Schwarz P surface was superimposed on TEM image to indicate the lattice parameter.

**Figure 2.20** TEM image of the self-assembled spherical micelle structure of the L-BCP6.

**Figure 2.21** a)  $^1\text{H}$  NMR in  $\text{CDCl}_3$  and b) MALDI spectrum of alkyne functionalized

hydrophilic block 7b.

**Figure 2.22** a)  $^1\text{H}$  NMR in  $\text{CDCl}_3$  and b) MALDI spectrum of alkyne functionalized hydrophilic block 7a.

**Figure 2.23** GPC (THF as an eluent) elugrams of hydrophobic block before 7c (black) and after 7d (red) click reaction.

**Figure 2.24** a)  $^1\text{H}$  NMR spectrum and b) GPC elugram of the L-BCP7.

**Figure 2.25** TEM image of the self-assembled spherical micelle structure of the L-BCP7.

**Figure 2.26**  $^1\text{H}$  NMR in  $\text{CDCl}_3$  spectrum of (a) 8b and (b) 8c.

**Figure 2.27**  $^1\text{H}$  NMR in  $\text{D}_2\text{O}$  spectrum of (a) 8d and (b) 8e.

**Figure 2.28** a) UV-vis spectra of azide-functionalized AuNPs 5nm ( $\lambda_{\text{max}} = 520\text{nm}$ , blue) and 25nm ( $\lambda_{\text{max}} = 525\text{nm}$ , red), respectively. b),c) TEM images of azide-functionalized AuNPs 5nm and 25nm.

**Figure 3.1** Characterization of polymer cubosomes containing one acetylene group (14a): a),b) SEM images of surface mesopores and c),d) TEM images of internal structures. e) The peaks of polymer cubosomes corresponding to  $Pn\bar{3}m$  symmetry analyzed by SAXS (lattice constant  $a = 50.3\text{ nm}$ ).

**Figure 3.2** Characterization of polymer cubosomes containing three acetylene groups (14b): a),b) SEM images of surface mesopores and c),d) TEM images of internal structures. e) The peaks of polymer cubosomes corresponding to  $Pn\bar{3}m$  symmetry analyzed by SAXS (lattice constant  $a = 37.2\text{ nm}$ ).

**Figure 3.3** Characterization of polymer cubosomes after CuAAC (15a and 15b): SEM image of a) 15a and b) 15b. TEM image of c) 15a and d) 15b. Blue luminescence of e) 15a and f) 15b analysed by CLSM images ( $\lambda_{\text{Ex}} = 404$

nm,  $\lambda_{Em} = 477$  nm). The SAXS spectra for g) 15a ( $a = 53.1$  nm) and h) 15b ( $a = 52.8$  nm).

**Figure 3.4** MALDI-TOF mass spectrum of compound 5 (MW= 1,489.75 g mol<sup>-1</sup>).

**Figure 3.5** MALDI-TOF mass spectrum of compound 7 (MW= 2,011.76 g mol<sup>-1</sup>).

**Figure 3.6** MALDI-TOF mass spectrum of compound 9 (MW= 2,186.16 g mol<sup>-1</sup>).

**Figure 3.7** <sup>1</sup>H NMR spectrum of compound 4.

**Figure 3.8** <sup>1</sup>H NMR spectrum of compound 5.

**Figure 3.9** <sup>1</sup>H NMR spectrum of compound 6.

**Figure 3.10** <sup>1</sup>H NMR spectrum of compound 7.

**Figure 3.11** <sup>1</sup>H NMR spectrum of compound 8.

**Figure 3.12** <sup>1</sup>H NMR spectrum of compound 9.

**Figure 3.13** <sup>1</sup>H NMR spectrum of compound 10.

**Figure 3.14** Characterization of amine terminated polystyrene (NH<sub>2</sub>-PS):<sup>1</sup>H NMR spectrum of a) 13a (Mn= 19,439 g mol<sup>-1</sup>,  $D=1.0759$ ) and b) 13b (Mn= 23,785 g mol<sup>-1</sup>,  $D=1.0548$ ). MALDI-TOF mass spectrum of c) 13a (MW= 21,235.53 g mol<sup>-1</sup>) and d) 13b (MW= 25,406.96 g mol<sup>-1</sup>).

**Figure 3.15** Characterization of block copolymers: <sup>1</sup>H NMR spectrum of a) 14a and b) 14b. THF GPC spectrum of c) 14a (Mn= 22,511 g mol<sup>-1</sup>,  $D=1.0739$ ) and d) 14b (Mn= 28,164 g mol<sup>-1</sup>,  $D=1.0301$ ).

**Figure 3.16** <sup>1</sup>H NMR spectrum of 3-azidocoumarin.

**Figure 4.1** SEM images of self-assembly structures in acetone: a) polymer cubosomes of 4a, b) hexosome of 5a, c) flat tubes were tethered to particles with micropores in the core of 6a, d) spherical micelles of 7a; In 1,4-dioxane e) filled-polymer cubosomes of 4a, f), g) hexosome of 5a and 6a,

h) vesicles of 7a.

**Figure 4.2** SEM images of self-assembly structures in acetone: a) polymer cubosomes of 4b, b) sponge structure of 5b, c), d) vesicles of 6b and 7b; In 1,4-dioxane e) filled-polymer cubosomes of 4b, f), g) hexosome of 5b and 6b, h) vesicles of 7b.

**Figure 4.3** SEM images of self-assembly structures of 7a: the case of 7a precipitated in mixed solution of MeOH and 10 mM HCl a), b) in acetone, the particles covered with a smooth surface without pores on one side and tethered with very small vesicular petals on the other side and c), d) in 1,4-dioxane, small vesicles and polymer cubosomes.; the case of self-assembly with 10mM HCl e), f) in acetone, particles in which fine vesicular petals were tethered and g), h) in 1,4-dioxane, well-defined polymer cubosomes.

**Figure 4.4** SEM images of self-assembly structures of 7b: the case of 7b precipitated in mixed solution of MeOH and 10 mM HCl a), b) in acetone, fine vesicles and some particles with a broken surface structure and c), d) in 1,4-dioxane, cylindrical micelles and particles having multiple layers.; the case of self-assembly with 10mM HCl e), f) in acetone, particles in which fine vesicular petals were tethered and g), h) in 1,4-dioxane, well-defined polymer cubosomes.

**Figure 4.5** TEM image of the structures self-assembled with 10mM HCl: a), b) polymer cubosome internal channels of 7a and c), d) polymer cubosome internal channels of 7b.

**Figure 4.6** Schematic illustration of introducing the Ni-NTA complex to polymer cubosome surface with high density amine groups. Reaction conditions for

each step: (i) p-Phenylene diisothiocyanate, MeOH, 40°C; (ii) NTA, water, NiSO<sub>4</sub>.

**Figure 4.7** a), b) <sup>1</sup>H NMR spectra of PEGs.

**Figure 4.8** a) <sup>1</sup>H and b) <sup>13</sup>C NMR spectra of compound 1.

**Figure 4.9** MALDI-TOF mass spectrum of compound 1 (MW= 2,257.79 g mol<sup>-1</sup>).

**Figure 4.10** a) <sup>1</sup>H and b) <sup>13</sup>C NMR spectrum of 2-hydroxyethyl 2-bromoisobutyrate.

**Figure 4.11** <sup>1</sup>H NMR spectrum of compound 2.

**Figure 4.12** a) <sup>1</sup>H and b) <sup>13</sup>C NMR spectra of compound 3.

**Figure 4.13** <sup>1</sup>H NMR spectra of compound a) 4a, b) 5a, c) 6a, d) 7a.

**Figure 4.14** THF GPC spectra of a) 4a (M<sub>n</sub>= 22,274 g mol<sup>-1</sup>, *D* =1.0832), b) 4b (M<sub>n</sub>= 23,408 g mol<sup>-1</sup>, *D* =1.1022) and DMF GPC spectra of c) 5a (M<sub>n</sub>= 17,055 g mol<sup>-1</sup>, *D* =1.1812), d) 5b (M<sub>n</sub>= 18,118 g mol<sup>-1</sup>, *D* =1.1620) and e) 7a (M<sub>n</sub>= 18,044 g mol<sup>-1</sup>, *D* =1.062), f) 7b (M<sub>n</sub>= 18,776 g mol<sup>-1</sup>, *D* =1.0931).

**Figure 5.1** <sup>1</sup>H NMR spectrum of benzyl 4-pentenoate.

**Figure 5.2** <sup>1</sup>H NMR spectrum of benzyl 4-oxobutanoate.

**Figure 5.3** <sup>1</sup>H NMR spectrum of AB type monomer containing both aldehyde and carboxylic acid groups protected with each of orthogonal protection groups, respectively.

**Figure 5.4** <sup>1</sup>H NMR spectrum of AB type monomer.

**Figure 5.5** <sup>1</sup>H NMR spectrum of benzyl deprotected dimer.

**Figure 5.6** <sup>1</sup>H NMR spectrum of deacetalized dimer.

**Figure 5.7** <sup>1</sup>H NMR spectrum of trimer synthesized through Passerini 3-component reaction.

**Figure 5.8** <sup>1</sup>H NMR spectrum of 3-(5,5-dimethyl-1,3-dioxan-2-yl)propanoic acid.

**Figure 5.9**  $^1\text{H}$  NMR spectrum of deactalized trimer.

## List of Abbreviations

- D**: Polydispersity
- 3D**: Three-dimensional
- ATRP**: Atom transfer radical polymerization
- BCP**: Block copolymer
- CLSM**: Confocal laser scanning microscopy
- CR**: Component reaction
- CuAAC**: Copper(I)-catalyzed azide-alkyne cycloaddition
- DCC**: Dicyclohexyl carbodiimide
- D.I water**: Deionized water
- DLS**: Dynamic light scattering
- DMAP**: 4-Dimethylaminopyridine
- DMF**: Dimethylformamide
- DNA**: Deoxyribo nucleic acid
- DP<sub>n</sub>**: Degree of polymerization
- DPTS**: 1,4-Dimethylpyridinium p-toluenesulfonate
- EA**: Ethyl acetate
- EDC**: 1-Ethyl-3-(3-dimethylaminopropyl)carbodiimide
- EM**: Electron microscopy
- EtOH**: Ethyl alcohol
- FE-SEM**: Field emission-scanning electron microscopy
- GPC**: Gel permeation chromatography
- His**: Histidine
- IBC**: Inverse bicontinuous cubic
- IDA**: Iminodiacetic acid
- MALDI-TOF**: Matrix-assisted laser desorption ionization time-of-flight
- MC**: Methylene chloride
- MCR**: Multicomponent reaction
- MeOH**: Methyl alcohol
- M<sub>n</sub>**: Number-average molecular weight



**NMR:** Nuclear magnetic resonance  
**NP:** Nanoparticle  
**NTA:** Nitrilotriacetic acid  
**PC:** Polymer cubosome  
**PEG:** Poly(ethylene glycol)  
**PLGA:** Polylactide-co-glycolide  
**PMDETA:** Pentamethyldiethyltriamine  
**PS:** Polystyrene  
**ROMP:** Ring opening metathesis polymerization  
**SAXS:** Small-angle x-ray scattering  
**SDEMS:** Solvent diffusion evaporation self-assembly  
**SEM:** Scanning electron microscopy  
**SIM:** Structured illumination microscopy  
**TBDMS:** tert-Butyldimethylsilyl  
**TEM:** Transmission electron microscopy  
**THF:** Tetrahydrofuran  
**TPMS:** Triply periodic minimal surfaces

# Chapter 1. Introduction

## 1.1 Overview

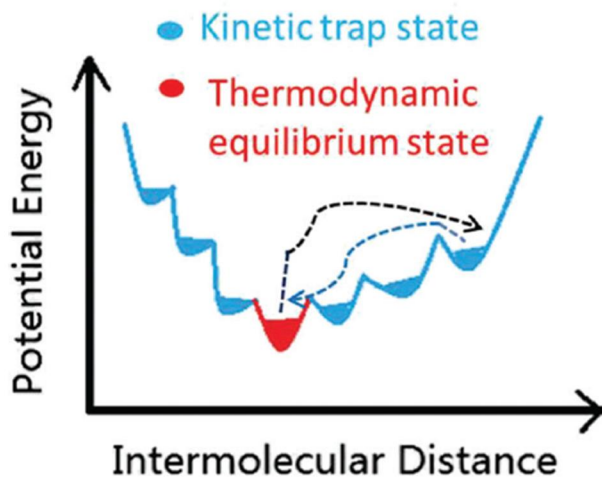
Polymers with various properties are abundant in nature.<sup>[1]</sup> Depending on their characteristics, they have played a useful role in many fields. Since the advent of synthetic polymers, tailored polymers with desired physiochemical properties were synthesized by modeling the natural polymers. Among these attempts, imparting functional groups to polymers has attracted much attention as one of the methods for controlling specific chemical or optical properties. This is because factors such as steric, polarity, and reactivity are affected by the chemical structure of the backbone or the functional groups included.<sup>[2]</sup> Also, unlike small molecules containing functional groups, polymers containing functional groups have various potentials.<sup>[3]</sup> These are required as an excellent material that corresponds well to fields such as polymeric pharmaceuticals, polymeric drugs, electronics, separation, energy harvesting and storage.<sup>[3,4]</sup> For this reason, direct anionic polymerization, cationic polymerization, free radical polymerization and coordination polymerization, as well as the bulk and surface modification of preformed polymer backbones have been steadily reported as studies on how to synthesize polymers containing functional groups.<sup>[2]</sup>

Recently, interest in a method for synthesizing a sequence-defined polymer to more precisely control physical properties by introducing a desired functional group at a desired position as well as simply introducing a functional group has increased. DNA is a representative naturally occurring sequence-defined polymer.<sup>[5]</sup> Just as specific

genetic information can be transmitted without any error through the sequence combination of four monomers, expectations have grown that polymers suitable for the desired purpose can be obtained through the introduction of sequences and functional groups through synthetic polymers.<sup>[6]</sup> In this process, researches on the synthesis of discrete polymers were also developed to maximize the role of functional groups by reducing the effect of molecular weight distribution. Merrifield solid-phase synthesis and iterative exponential growth are representative methods.<sup>[6-8]</sup>

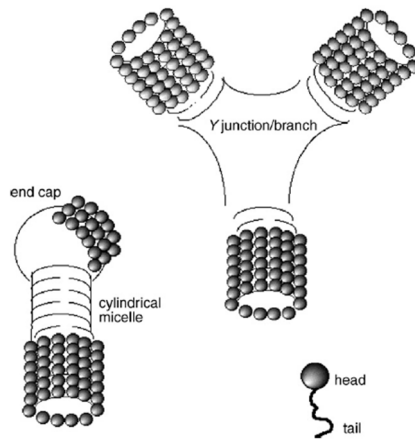
## 1.2 Nonergodic behavior in self-assembly of polymers

Molecular self-assembly is an association of molecules based on noncovalent interactions to form microstructures.<sup>[9]</sup> The first molecular structures were colloidal clusters made from surfactant solutions, later called 'micelles' by Hartley in 1936.<sup>[10,11]</sup> The Noncovalent interactions, which are the source of this molecular self-assembly, are generally weaker than covalent ones, such as hydrogen bonding, hydrophobic interaction, and van der Waals force, *etc.*<sup>[12]</sup> Therefore, the self-assembly structure is inevitably affected by external stimuli.<sup>[13]</sup> Recently, it has been shown that kinetic factors play an important role in determining the self-assembled structure. There are several cases, but in general, slow assembly processes reach thermal equilibrium, whereas fast assembly processes result in kinetically trap. It is said that the higher the temperature, the lower the concentration, and the longer-time course, the more the thermodynamic state is preferred. Also, since the energy barrier between the kinetic trap and the thermal equilibrium state is not that high, switching between these states is possible (Figure 1.1). Due to this phenomenon, various self-assembly strategies using kinetic issues have been proposed.<sup>[12-14]</sup>

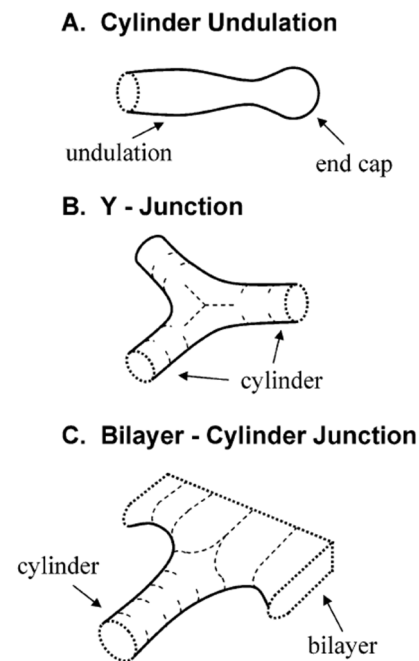


**Figure 1.1** Energy diagram of kinetic traps vs thermodynamic equilibrium states. Transition between the kinetic traps and the thermodynamic equilibrium state is possible under external stimuli.<sup>[12]</sup>

The preferred geometry of self-assembled structures is fixed by the spontaneous curvature of amphiphilic molecules. Spontaneous curvature is the difference between the effective packing areas of two different molecular units that describes properties such as MW, chain rigidity or the presence of large side groups. Relatively symmetric molecules show low spontaneous curvature and locally flat interfaces. In the cylindrical micelles system, a lot of end-caps are created in case of high spontaneous curvature, and as a result, the length of linear micelles is shortened.<sup>[15]</sup> On the other hand, when the spontaneous curvature is low, the tendency to expand branch points or micellar networks is preferred. These are two types of defects resulting from the generation of differences in energetic penalty and the formation of regions with differences in local curvature, but defects caused by amphiphile spontaneous curvature (Figure 1.2).<sup>[16,17]</sup>



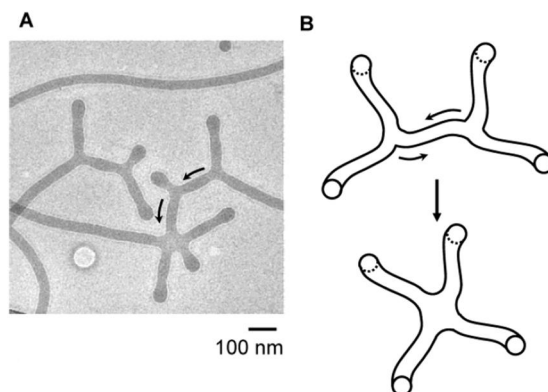
**Figure 1.2** End-caps and Y-junction points which is the defects of cylindrical micelles system.<sup>[15]</sup>



**Figure 1.3** a) End cap and associated undulations in a cylindrical micelles. b) Y-junction that connects cylindrical micelles. c) A transition from a bilayer to a cylinder which is the structural element of the octopus morphology.<sup>[18]</sup>

Furthermore, in the field of polymer self-assembly, morphological transitions by

non-energetic behavior of polymers have been reported.<sup>[19,20]</sup> Bates et al.<sup>[20]</sup> deal with the formation of micelles in aqueous dispersions of nonionic block copolymer amphiphiles: nonergodicity and morphology of binary mixtures. In this study, changes in the number of end caps in structures assembled from blends of poly-(ethylene oxide)-poly(butadiene) with different molecular weights were observed and interpreted. They reported that as the proportion of high molecular weight polymers increased, spherical micelles or cylindrical micelles changed to bilayer structures (Figure 1.3a-c).<sup>[19,21]</sup> Then, they inferred that the different interfacial curvatures are caused by intramolecular segregation resulting from the bimodal distribution of PEO blocks of different molecular weights.<sup>[20,22]</sup> In addition, internally segregated micelles resist fracturing into separate unique structures. As a result, the nonergodicity of the self-assembled polymer structure is an overall non-equilibrium with significant consequences on the distribution of morphologies found in PEO-PB-based dispersions (Figure 1.4).<sup>[20]</sup>

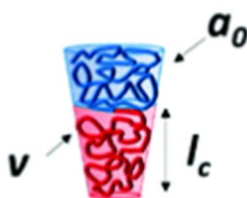


**Figure 1.4** a) Cryo-TEM image of polymer blended micelles. b) Transport of diblock copolymer molecules along the cylindrical portions would permit evolution of a connected bilayer sheet.<sup>[20]</sup>

### 1.3 Polymer cubosomes and applications

### 1.3.1 Polymer cubosomes

Molecular self-assembly is a fairly common phenomenon in nature. Cell membranes of living things are the result of self-assembly of phospholipids, and soap bubbles are also generated by self-assembly of surfactants.<sup>[23]</sup> In this way, depending on the type of building block, various self-assembled structures were observed and among these structures, especially polymer self-assembled structures are in the spotlight due to their higher stability and durability induced from unique mechanical and physical properties of polymers. For this reason, numerous studies are being conducted to apply these structures to various fields.<sup>[24]</sup>

$$p = \frac{v}{a_0 l_c}$$
A diagram of a polymer micelle, which is a spherical aggregate of polymer chains. The micelle is divided into two regions: a blue upper region representing the hydrophilic head groups and a red lower region representing the hydrophobic tails. The volume of the hydrophobic core is labeled as  $v$ . The effective maximum chain extension is labeled as  $l_c$ . The optimum head group area is labeled as  $a_0$ .

**Figure 1.5** Critical packing parameter (Shape factor).  $v$ : Volume of hydrophobic block.  $l_c$ : Effective maximum chain extension.  $a_0$ : Optimum head group area.<sup>[26]</sup>

There is a parameter defining the self-assembled structure of amphiphilic block copolymer, and a representative one is the packing parameter (Figure 1.5).<sup>[25]</sup> There are three elements that make up the packing parameter.  $a_0$  is the optimal head group area of the hydrophilic moiety, and  $v$  and  $l_c$  are the volume and length of the hydrophobic moiety, respectively. This  $p$  value is closely related to the structure of the polymer.<sup>[26]</sup>

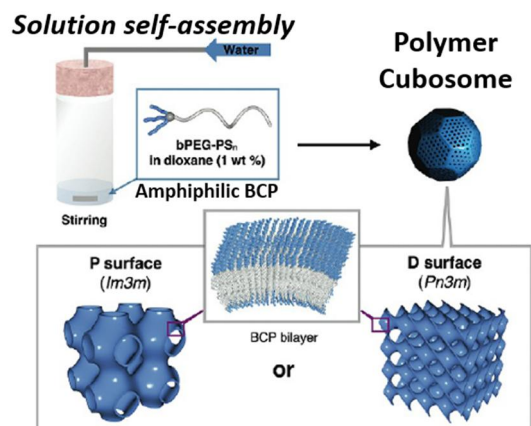


**Figure 1.6** Self-assembly of PEG<sub>3</sub>-PS block copolymer into polymer cubosomes.<sup>[28]</sup>

Kim et al,<sup>[27,28]</sup> they tried to change the  $p$  value and control the self-assembled structure by changing the chemical architecture of the polymer in addition to the block ratio. Amphiphilic block copolymers with polystyrene hydrophobic block were easily synthesized using branched PEG hydrophobic block as a macro initiator by atom transfer radical polymerization (ATRP). In conclusion, they reported for the first time a structure called a polymer cubosome through the aforementioned method. Polymer cubosome is inverse bicontinuous cubic (IBC) mesophases in solution which indicates three dimensionally periodic porous nanostructures composed of the minimal surfaces of self-assembled bilayers of BCPs (Figure 1.6). This structure also has highly defined two independent water channel networks inside. The lattice structures of  $Im\bar{3}m$  (Figure 1.7a-d),  $Pn\bar{3}m$  and  $Ia\bar{3}d$  were reported by SEM, TEM and small angle x-ray scattering (SAXS) analysis. Then, this structure has an average diameter of about 2-10  $\mu\text{m}$  and has mesopores of up to 50 nm on the surface, so the large surface area is about 1370 to 1530  $\text{\AA}^2$ .<sup>[29]</sup>



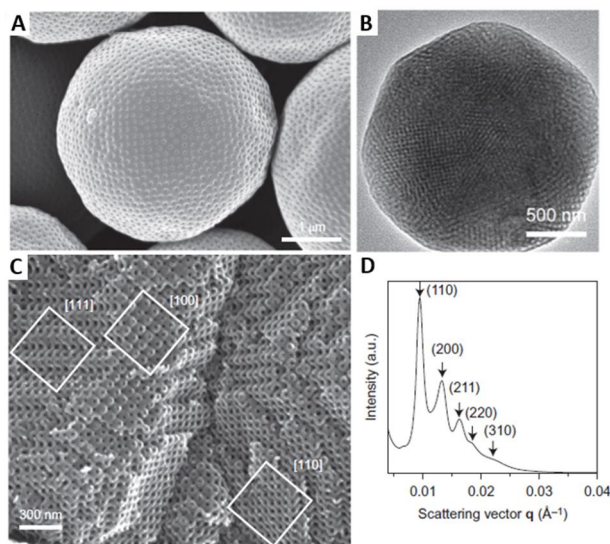


**Figure 1.7** Polymer cubosome with lattice structure of the primitive cubic phase ( $Im\bar{3}m$ ): a) SEM image of the polymer cubosome. b) TEM image showing the internal structure of the polymer cubosome. c) High resolution SEM image of the internal structure of the polymer cubosome. d) The SAXS result of the polymer cubosome (lattice parameter,  $a = 93.4 \text{ nm}$ ).<sup>[27]</sup>

### 1.3.2 Applications

Polymer cubosome has a mesoporous structure and is attracting attention as a useful material that can be applied to various fields such as drug delivery, nanotemplates, nanoreactor, lithography, separation, etc.<sup>[30]</sup>

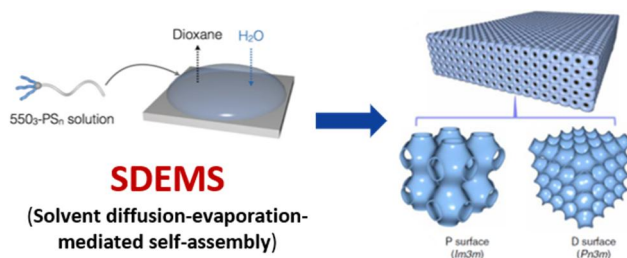


**Figure 1.8** Schematic illustration of SDEMS process and the film consisting of the IBC structures.<sup>[30]</sup>

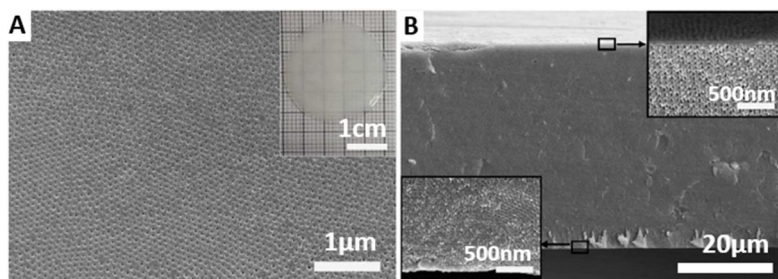


**Figure 1.9** a) SEM images of the top layer of the film having evenly distributed nanopores ( $\sim 10$  nm). The inset shows a picture of the polymer film. b) SEM images of the cross-section of the film.<sup>[30]</sup>

In 2015, Kim's group succeeded in making a polymer cubosome film using Solvent diffusion-evaporation-mediated self-assembly (SDEMS) method (Figure 1.8 and Figure 1.9a,b).<sup>[30]</sup> And the film was replicated with inorganic materials such as Ti and Si. In 2018, Subsequent studies also succeeded in replicating polymer cubosome particles into a single network structures using Ti and Si(Figure 1.10b,c and e).<sup>[31]</sup> As a result, both Ti and Si particles replicated the internal structure of the cubosome, and the products with the lattice structure of  $Fd\bar{3}m$  were analyzed by SAXS (Figure 1.10a). And in the case of replicating particles other than film, optical properties were also shown (Figure 1.10d, f and g).

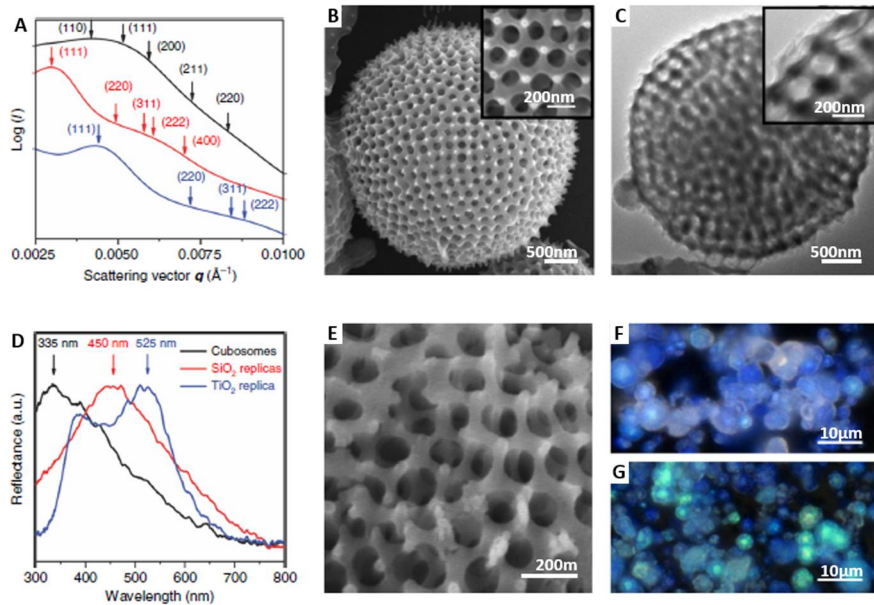


**Figure 1.10** a) SAXS results of the Polymer cubosomes (black,  $Pn\bar{3}m$ , lattice parameter,  $a = 213$  nm), single networks of silica (red,  $Fd\bar{3}m$ ,  $a = 361$  nm) and titania (blue,  $Fd\bar{3}m$ ,  $a = 247$  nm). b), c) SEM and TEM images for single networks of silica. d) UV-vis reflectance spectrometry of the Polymer cubosomes (black), silica networks (red) and titania networks (blue). e) SEM image of fractured titania single cubic network. i) Optical microscope images of silica (top) and titania (bottom) networks.<sup>[31]</sup>

Subsequently, in 2020 and 2022, the same group reported application studies that replicated polymer cubosome particles as Ni and carbon sources and utilize them as conductive materials (Figure 1.11a-d).<sup>[32,33]</sup> These conductive particles also had an  $Fd\bar{3}m$  lattice structure and were predicted to be well used as electrode materials in the future through the expression of electrical properties. Even now, researches to utilize the advantages of these polymer cubosomes are steadily progressing.

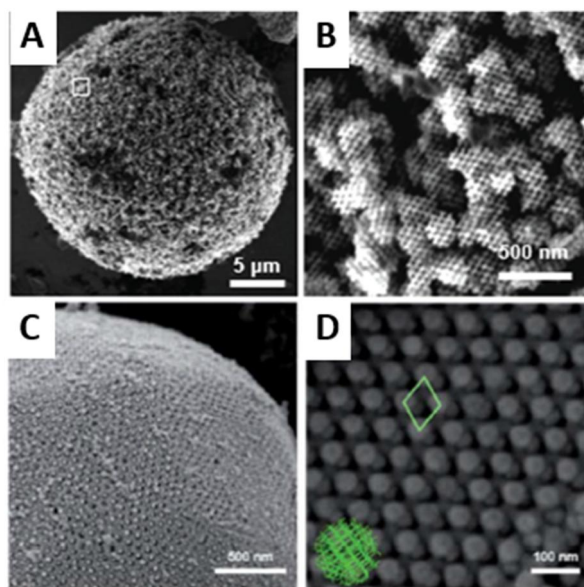


**Figure 1.11** a), b) SEM images of Ni networks ( $Fd\bar{3}m$ ). c) SEM image of carbonaceous network. d) High resolution SEM images showing the internal single diamond ( $Fd\bar{3}m$ ) lattice of carbonaceous network.<sup>[32,33]</sup>

## 1.4 Synthesis of polymers using multicomponent reaction

The first multicomponent reaction used to synthesize polymers was the Ugi 4-component reaction (CR). In 2003, Wright's group synthesized 4 types of norbornene monomers using Ugi 4-CR (Figure 1.12a).<sup>[34]</sup> The synthesized monomer was polymerized via Ring opening metathesis polymerization (ROMP) (Figure 1.12b). However, when the 1<sup>st</sup> grubbs catalyst was used, the reaction was slowed down due to the interaction of the catalyst with the functional group of the monomer, so polymer synthesis was not successful.

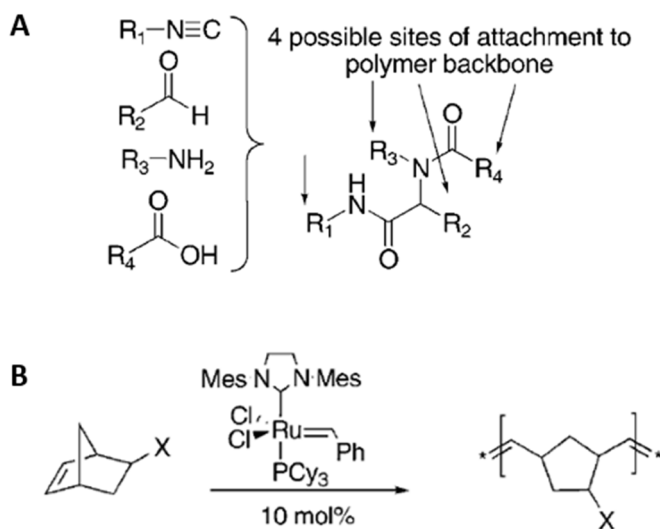


**Figure 1.12** a) Scheme of polymers synthesized from an Ugi 4-CR Product. b) Synthetic scheme for polymers using ROMP.<sup>[34]</sup>

In 2014, Meier's group synthesized a polymer with a defined sequence beyond simple synthesis using MCRs (Figure 1.13a,b).<sup>[35]</sup> Here, a sequence was given to the polymer through the merging of MCRs and thiol-ene reaction. Although it was not high molecular weight, it was confirmed that even tetramers were well formed. Then, by introducing PEG2000, a sequence-defined block copolymer was synthesized (Figure 1.13c-f).

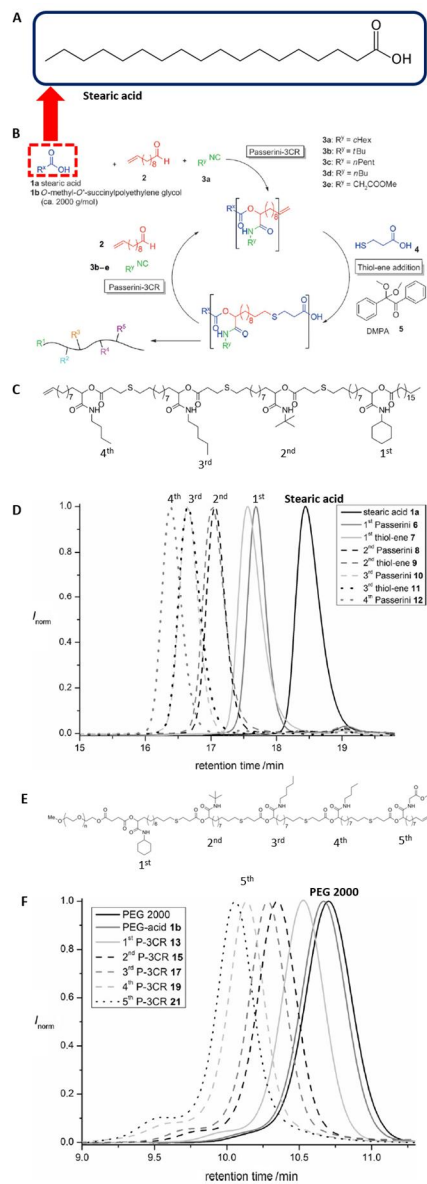


**Figure 1.13** a) Chemical structure of stearic acid (monomer with carboxylic acid). b) Synthetic process for a sequence-defined tetramer (starting from 1a) or a sequence-defined block copolymer (starting from 1b). c) Chemical structure of the tetramer with different side chains. d) GPC traces after Passerini 3-CR and thiol-ene reactions in the synthesis of tetramer. e) Chemical structure of the sequence-defined block-copolymer. f) GPC traces of the PEG copolymer after each Passerini 3-CR. [35]

And in 2016, there is research on the synthesis of polymers with more advanced types of sequences defined by the same group.<sup>[36]</sup> First, a monomer capable of having both functional groups was synthesized as an AB type monomer. Then, the polymer was synthesized by repeating deprotection and Passerini 3-CR process (Figure 1.14a). In this way, even the decamer was synthesized, significantly increased yield and synthesis efficiency were reported compared to previous studies (Figure 1.14b,c). And the decamer was made into a 20-mer through self-metathesis (Figure 1.15a,b). This research was the basis for synthesizing macromolecules with defined unique sequences.

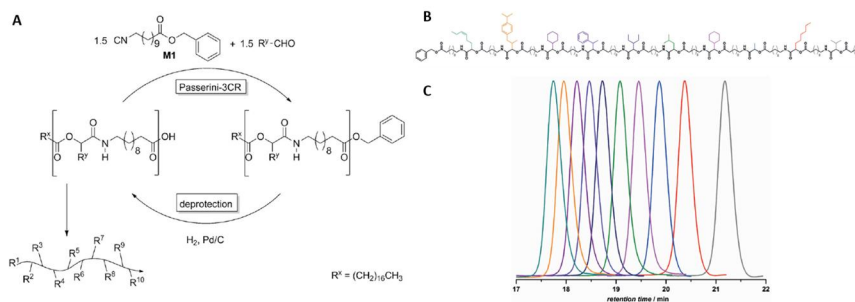


**Figure 1.14** a) Synthetic scheme for sequence-defined polymers. b) Chemical structure of the decamer having different side chains. c) GPC traces of the products after each Passerini 3-CR.<sup>[36]</sup>

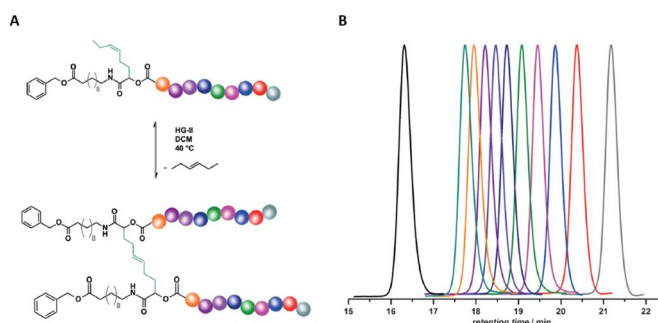


**Figure 1.15** a) Synthetic scheme for the self-metathesis reaction. b) GPC traces of the products, indicating the clear shift of the 20-mer compared to the decamer.<sup>[36]</sup>

## 1.5 Summary

In the following chapters, the details of the researches that are closely related to the contents introduced in Chapter 1 and overview so far are elucidated. In Chapter 2, we report the various morphological diversity in binary blend of the block copolymers with extremely different molecular weight of hydrophobic blocks. Then in Chapter 3 and 4, we suggest the polymer cubosomes with high density surface functional groups. One has alkyne groups (chapter3), and the other has amine groups (chapter4). All of these polymer structures were utilized as a nanoreactor and stationary phase of selective Histidine tagged protein purification resins, respectively. Finally, in Chapter 5, we discussed a new method for the synthesis of sequence-defined discrete polymers that combines Iterative exponential growth with multi-component reactions. This would be an efficient and facile way to create polymers with desired properties.

Portions of this thesis have been published.

Chapter 2: Lee, S. J.; Cho, A.; Kim, K. T., “Morphological Diversity from the Solution Self-Assembly of Block Copolymer Blends Containing High Molecular-Weight Hydrophobic Blocks” *Macromol. Rapid Commun.* **2022**, *43*, 2100893.

## 1.6 Reference

- [1] Fréchet, J. M. J. *Science*. **1994**, *263*, 1710–1715.
- [2] Schulz, D. N.; Patil, A. O. *Functional Polymers ACS Symposium Series*, American Chemical Society, Washington DC **1998**.
- [3] Vogl, O. *Pure Appl. Chem.* **1979**, *51*, 2409–2419.
- [4] Tang et al. *Mater. Chem. Front.* **2020**, *4*, 1803. [5] Lutz, J. F. *Polym. Chem.* **2010**, *1*, 55–62.
- [6] Badi, M.; Lutz, J. F. *Chem. Soc. Rev.* **2009**, *38*, 3383–3390.

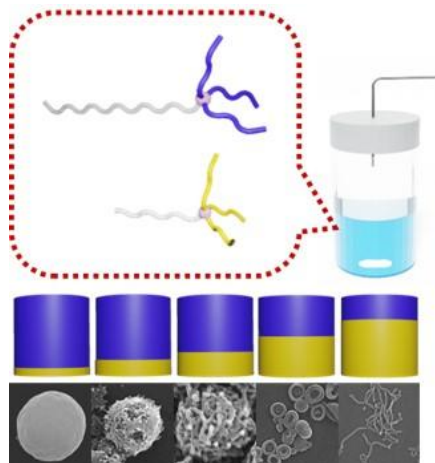


- [7] Meier, M. A. R.; Kowollik, C. B. *Adv. Mater.* **2019**, *31*, 1806027.
- [8] Lutz, J. F.; Ouchi, M.; Liu, D. R.; Sawamoto, M. *Science* **2013**, *341*, 1238149.
- [9] Whitesides, G. M.; Mathias, J. P.; Seto, C. T. *Science* **1991**, *254*, 1312–1319.
- [10] McBain, J. W. *Trans. Faraday Soc.* **1913**, *9*, 99–101.
- [11] Hartley, G. S. *Aqueous Solutions of Paraffin Chain Salts, A Study in Micelle Formation*, Paris **1936**.
- [12] Yan, Y.; Huang, J.; Tang, B. Z. *Chem. Commun.* **2016**, *52*, 11870.
- [13] Wang, A. D.; Shi, W. Y.; Huang, J. B.; Yan, Y. *Soft Matter* **2016**, *12*, 337–357.
- [14] Tidhar, Y.; Weissman, H.; Wolf, S. G.; Gulino, A.; Rybtchinski, B. *Chem. J. Eur.* **2011**, *17*, 6068–6075.
- [15] Dan, N. Safran, S. A. *Adv. Colloid Interface Sci.* **2006**, *123–126*, 323–331.
- [16] Tlusty, T.; Safran, S. A. *Science* **2000**, *290*, 1328–1331.
- [17] Tlusty, T.; Safran, S. A. *Philos. Trans. Royal Soc. A* **2001**, *359*, 879–881.
- [18] Tlusty, T.; Safran, S. A. *J. Phys. Condens. Matter* **2000**, *12*, A253–A262.
- [19] Jain, S.; Bates, F. S. *Science* **2003**, *300*, 460–464.
- [20] Jain, S.; Bates, F. S. *Macromolecules* **2004**, *37*, 1511–1523.
- [21] Israelachvili, J. *Intermolecular and Surface Forces, 2nd ed.*, Academic Press, San Diego **1992**.
- [22] Halperin, A. *J. Phys. (Paris)* **1988**, *49*, 131–137.
- [23] Galeotti, F.; Pisco, M.; Cusano, A. *Nanoscale*, **2018**, *10*, 22673–22700.
- [24] Mai, Y.; Eisenberg, A. *Chem. Soc. Rev.* **2012**, *41*, 5969–5985.
- [25] Doncom, K. E. B.; Blackman, L. D.; Wright, D. B.; Gibson, M. I.; O'Reilly, R. K. *Chem. Soc. Rev.* **2017**, *46*, 4119.
- [26] Karayianni, M.; Pispas, S. *J. Polym. Sci.* **2021**, *59*, 1874–1898.
- [27] La, Y.; Park, C.; Shin, T. J.; Joo, S. H.; Kang, S.; Kim, K. T. *Nat. Chem.* **2014**, *6*, 534–541.
- [28] An, T. H.; La, Y.; Cho, A.; Jeong, M. G.; Shin, T. J.; Park, C.; Kim, K. T. *ACS Nano*, **2015**, *9*, 3084–3096.
- [29] Ha, S.; La, Y.; Kim, K. T. *Acc. Chem. Res.* **2020**, *53*, 620–631.
- [30] Park, C.; La, Y.; An, T. H.; Jeong, H. Y.; Kang, S.; Joo, S. H.; Ahn, H.; Shin, T. J.; Kim, K. T. *Nat. Commun.* **2015**, *6*, 6392.

- [31] La, Y.; Song, J.; Jeong, M. G.; Cho, A.; Jin, S. M.; Lee, E.; Kim, K. T. *Nat. Commun.* **2018**, *9*, 5327.
- [32] Lee, H.; Kim, D.; Ma, H.; Kim, K. T. *Chem. Commun.* **2020**, *56*, 14059–14062.
- [33] Song, J.; Choi, S.; Lim, J.; Kim, K. T. *RSC Adv.* **2022**, *12*, 8429–8434.
- [34] Robotham, C. V.; Baker, C.; Cuevas, B.; Abboud, K.; Wright, D. L. *Molecular Diversity* **2003**, *6*, 237–244.
- [35] Solleder, S. C.; Meier, M. A. R. *Angew. Chem. Int. Ed.* **2014**, *53*, 711–714.
- [36] Solleder, S. C.; Zengel, D.; Wetzel, K. S.; Meier, M. A. R. *Angew. Chem. Int. Ed.* **2016**, *55*, 1204–1207.

# Chapter 2

## Morphological Diversity from the Solution Self-Assembly of Block Copolymer Blends Containing High Molecular-Weight Hydrophobic Blocks



### 2.1 Abstract

(This work was collaborated with Arah Cho and Prof. Kyoung Taek Kim, published in *Macromolecular rapid communications*, 2022)

Self-assembled structures of high molecular-weight block copolymers (BCPs) can prematurely settle to local energy minima without reaching a time-averaged equilibrium, resulting in the emergence of intriguing morphologies, such as 3D micellar networks. This nonergodic behavior is evident in binary blends of BCPs with different molecular weights. This study reports the solution self-assembly of the blends of two branched-linear BCPs with similar block chemistries but different molecular weights of the hydrophobic blocks. A progressive transition of morphologies from hexosomes and cubosomes to 3D micellar networks, short cylinders, and spherical micelles is demonstrated, which is driven by the increase in the composition of low-molecular-weight BCP in the blend. The labeling of the micellar networks using Au nanoparticles confirms that lower molecular-weight BCP concentrates at the surface of micellar networks.

## **2.2 Introduction**

The solution self-assembly of block copolymers (BCPs) creates polymer nanostructures with tailored morphology and surface chemistry to meet the requirements for applications, such as drug delivery, nanoreactors, and templates for constructing complex nanostructures.<sup>[1-5]</sup> The control of the self-assembled structures of BCPs, such as their shapes, sizes, and surface functions has been achieved by the rational design and precision-synthesis of polymer building blocks.<sup>[6-8]</sup> In particular, the molecular weights of the polymer blocks constituting a BCP exert a deciding effect on the self-assembly of macromolecular amphiphiles.<sup>[9]</sup> For instance, the relative ratio of the molecular weights of a solvophilic and

solvophobic block (block ratio) has served as the decisive parameter to predict and interpret the morphology of the self-assembly of a given BCP.<sup>[10,11]</sup> In addition, in a seminal report by Jain and Bates, the magnitude of the molecular weights of the polymer blocks has been shown to have a profound effect on the emergence of unusual morphologies.<sup>[12,13]</sup> This morphological complexity originates from the nonergodic behavior of high molecular-weight BCPs (H-BCPs) exhibiting extremely scarce molecular exchange between self-assembled structures.<sup>[14,15]</sup> These effects of BCP molecular weights on the self-assembly mandate the rigorous synthesis of polymer blocks to form a BCP via specific polymerization techniques, such as anionic polymerization and reversible deactivation radical polymerization.<sup>[16–18]</sup> Self-assembly of a BCP blend is a promising method to maneuver the morphology of BCP nanostructures without relying on a one-to-one correspondence between a rigorously synthesized BCP and the morphology of its self-assembled nanostructures.<sup>[19]</sup> The composition of two BCPs, each having a different block ratio, determines the effective block ratio of their blend for the coassembly, which provides a versatile means to achieve a new morphology without synthesizing a BCP having a block ratio corresponding to the targeted morphology.<sup>[20]</sup> Binary blends of BCPs sharing chemistries in both polymer blocks have been shown to form the nanostructures with a specific morphology guided by the effective block ratio of the binary blend determined by the composition of two BCPs.<sup>[21–23]</sup> This method also provides intriguing new morphologies of self-assembled structures that are difficult to obtain from the solution self-assembly of a single BCP.<sup>[13,24–26]</sup> Polymer cubosomes are bicontinuous cubic structures that are formed by the solution self-assembly of asymmetric BCPs having high molecular-weight solvophobic blocks

and low molecular-weight solvophilic blocks.<sup>[27]</sup> These structures have attracted considerable attention as promising candidates for applications, such as nanoreactors, separation materials, and nanotemplates.<sup>[28-30]</sup> Utilizing the proportionality of molecular weights of BCP building blocks to the size of their self-assembled structures, we have shown that H-BCP could self-assemble into cubosomes with large lattice parameters that are commensurate with optical wavelength.<sup>[31]</sup> These large lattice cubosomes could serve as templates for the synthesis of photonic crystals composed of a single-diamond cubic network. However, the predominant formation of ordered cubic mesoporous structures from the self-assembly of H-BCPs requires a narrow window of the block ratio and a sophisticated self-assembly strategy to overcome the trapping of BCP assemblies into premature structures. We imagined that the binary blends of BCPs sharing chemistries in both polymer blocks but greatly differing in the molecular weights of hydrophobic blocks could alleviate the difficulty of synthesizing H-BCPs that preferentially self-assemble into desired structures, such as cubosomes having large pore size and lattice parameter.<sup>[32]</sup> We envisaged that low molecular-weight BCP (L-BCP) in the blend could enhance the mobility of the H-BCP during self-assembly so that the self-assembly of the blend could reach thermodynamically stable structures (polymer cubosomes) without being trapped into premature structures.<sup>[33]</sup> In this study, we report the nonergodic behavior of the binary blends when self-assembled in solution. The blends were prepared from branched-linear BCPs, which were composed of a triarm poly(ethylene glycol) (PEG) and a linear polystyrene (PS) block in solution.<sup>[20]</sup> The blend was composed of two BCPs having similar molecular weights in the branched hydrophilic block but highly different molecular weights in the linear hydrophobic

blocks (Figure 2.1). We aimed to drive the self-assembly of binary blends towards the preferential formation of polymer cubosomes having large lattice parameters by adjusting the content of the L-BCP in the blend. It was found that giant hexosomes (colloidal particles having inverse hexagonal structures) of the H-BCP were gradually transformed into polymer cubosomes when the content of L-BCP in the blend was optimized. Surprisingly, however, a series of unusual morphologies including micellar networks and Y-junctioned micelles were found during the morphological transition from polymer hexosomes to cylindrical and spherical micelles, which arose from the nonergodic behavior of H-BCP during the self-assembly.<sup>[12,13]</sup>

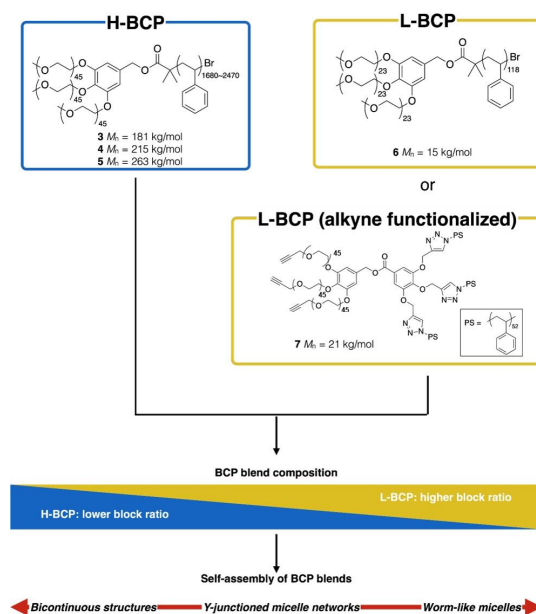


**Figure 2.1** Schematic illustrating of the self-assembly of the blend of H-BCP and L-BCP. The average structural parameters, such as packing parameters and block ratio, would be decided by the composition of two BCPs in the blend, which dictates the morphology of the self-assembled structures.

## 2.3 Results and discussion

### 2.3.1. Synthesis of High Molecular-Weight Branched-Linear BCPs

In this work, we aimed to investigate the solution self-assembly of binary blends composed of an H-BCP self-assembling into inverse mesophases and L-BCP forming spherical micelles. The details of synthesis and characterization are given in the Supporting Information. The H-BCPs were synthesized via atom transfer radical polymerization (ATRP) of styrene with a triarm PEG macroinitiator 1 (PEG2000<sub>3</sub>-Br, Figure 2.9).<sup>[34]</sup> Under the optimized ATRP conditions (20 equivalents of CuBr to 1), a series of H-BCPs with overall molecular weights in the range of 158–245 kg mol<sup>-1</sup> ( $D < 1.26$ ) (Table 2.1 and Figure 2.10) were synthesized, which were subsequently purified by performing the gradient chromatography on SiO<sub>2</sub> with a CH<sub>2</sub>Cl<sub>2</sub>/MeOH mixture (100:0 to 96:4 v/v) as an eluent utilizing the marked difference of the affinity of PEG and PS blocks toward silica (Figures 2.11 and 2.12). The number average molecular weight (Mn) was adjusted by controlling the duration of the polymerization. The BCP with the highest molecular weight, PEG2000<sub>3</sub>-PS<sub>2476</sub> (5) was obtained by quenching the ATRP at 12 h. The block ratios ( $f_{\text{PEG}}$ ) of the resulting BCPs (3–5), determined via <sup>1</sup>H NMR integration, were in the range of 2.4–3.5%. The L-BCP (6) was synthesized via the ATRP of styrene using a macroinitiator 2 (PEG1000<sub>3</sub>-Br) using CuBr (1.3 eq. to 2) (Table 2.2 and Figure 2.14).

### 2.3.2. Self-Assembly of High Molecular-Weight Branched-Linear BCPs

The high asymmetric block ratio ( $f_{\text{PEG}} < 3.5\%$ ) of H-BCPs suggested that these BCPs could self-assemble into inverse bicontinuous structures in solution.<sup>[29]</sup> Under



the standard conditions of the self-assembly via the cosolvent method (see experimental for details), H-BCP 3 self-assembled into polymer vesicles having an average diameter of 557 nm as determined using dynamic light scattering (DLS) (Figure 2.15). Scanning electron microscopy (SEM) and transmission electron microscopy (TEM) images showed polymersomes composed of thick bilayer membranes formed by the high molecular weight PS blocks (Figure 2.2a,e; Figure 2.18). By contrast, the self-assembly of H-BCPs 4 and 5 only produced colloidal nanoparticles with ill-defined internal structures, even with a slower rate of water addition ( $0.2 \text{ mL h}^{-1}$ ) (Figure 2.16). The formation of ill-defined structures might be originated from the difficulty of BCPs with high-molecular-weight PS blocks (Degree of polymerization,  $DP_n > 2000$ ) to reach equilibrium during the self-assembly. Therefore, the solvent diffusion evaporation self-assembly (SDEMS) method was used to introduce a poor solvent (water) at a much-reduced rate into the dioxane solution of a BCP (see the experimental for details).<sup>[27]</sup> This allowed the H-BCPs, PEG2000<sub>3</sub>-PS<sub>2012</sub> (4) ( $f_{\text{PEG}} = 3.0\%$ ) and PEG2000<sub>3</sub>-PS<sub>2476</sub> (5) ( $f_{\text{PEG}} = 2.4\%$ ), to self-assemble into cubosomes and hexosomes, respectively. The SEM images of the cubosomes of 4 (Figure 2.2c,d) showed the presence of surface pores, indicating well-defined internal bicontinuous cubic mesophases. The distance between the surface pores was determined to be  $\approx 200 \text{ nm}$ . The TEM images (Figure 2.2g,h) suggested the presence of internal Schwarz P surface ( $Im\bar{3}m$  symmetry) by revealing the (100) projection of the lattices. From the TEM images, the lattice parameter of the internal P surface was estimated to be  $\approx 200 \text{ nm}$  (Figure 2.19). Small-angle X-ray scattering (SAXS) pattern featured only broad peaks due to lattice distortion and background scattering from the cubosomes of small diameters (Figure 2.17). From

the SAXS results, the lattice parameter of the internal P surface was estimated to be 190 nm, which is consistent with those estimated from SEM and TEM images. The SEM images of the hexosomes of **5** exhibited only spherical particles without any surface structure (Figure 2.2b). However, the TEM images clearly showed the presence of the internal mesophases composed of hexagonally arranged water channels (Figure 2.2f).

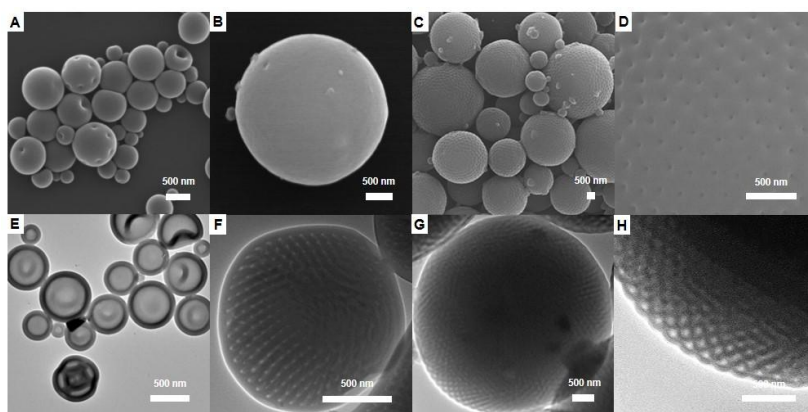


**Figure 2.2** Representative EM images of the self-assembled structures of BCP: a) SEM and e) TEM images of polymersomes of **3** self-assembled by cosolvent method. b) SEM and f) TEM images of polymer hexosomes of **5** self-assembled by solvent diffusion-evaporation self-assembly method. c,d) SEM and g,h) TEM images of polymer cubosomes of **4** self-assembled by solvent diffusion-evaporation self-assembly method.

### 2.3.3. Self-Assembly of Binary Blends of H-BCP **3** and L-BCP **6**

A series of the binary blends of H-BCP **3** self-assembling to polymer vesicles and L-BCP **6** forming spherical micelles were prepared by dissolving the BCPs in

dioxane (1 wt%, 1 mL) (Figure 2.20).<sup>[20]</sup> The composition of 6 was varied from 5% to 30%. To ensure the coassembly, water was slowly added to the dioxane solution of the BCP blend at  $0.25 \text{ mL h}^{-1}$  until the volume fraction of water reached 50%. After removing dioxane by dialysis against water, the resulting suspensions of the H-BCP/L-BCP (3/6) blends were analyzed using TEM and SEM (Figure 2.3). The morphology of the self-assembled structures of 3/6 blends transformed from polymersomes and sponge phase particles to cylindrical micelles tethered to flat lamellae as the content of 6 increased (Figure 2.3a-c,e-g). Interestingly, the cylindrical micelles exhibited Y-junctions when the length of the micelles was long. Eventually, the 3/6 (70:30 w/w) blend self-assembled into spherical micelles (Figure 2.3d,h). Further increasing the content of 6 did not alter the morphology of the self-assembled structures.

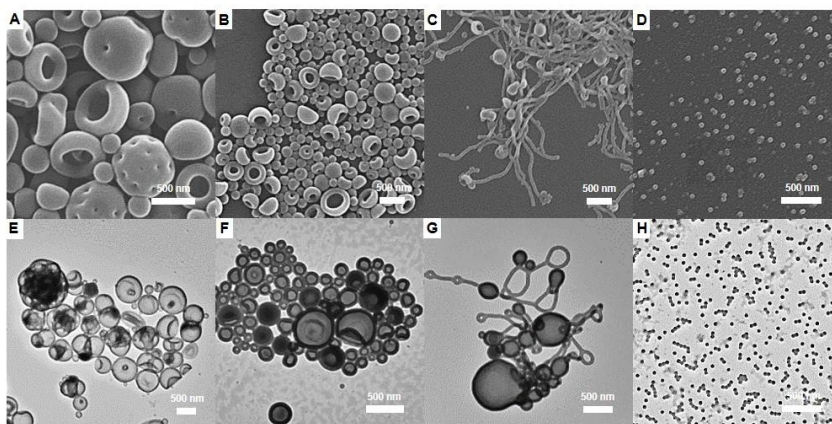


**Figure 2.3** a–d) Representative SEM and e–h) TEM images of the self-assembled structures of BCP 3/6 blends: a,e) Polymersomes and sponge-phase particles (95:5 w/w). b,f) Polymersomes (85:15 w/w). c,g) Cylindrical micelles tethered to flat lamellae (80:20 w/w). d,h) Spherical micelles (70:30 w/w).

### 2.3.4. Self-Assembly of Binary Blends Containing H-BCPs

After confirming that the presence of L-BCP in the blend transformed the morphology of self-assembled structures mainly composed of H-BCPs, the self-assembly of the 4/6 blend was investigated by gradually increasing the content of 6 from 5% to 50% (Figure 2.4). The morphology of the 4/6 (95:5 w/w) blend transformed from smaller cubosomes (average diameter = 1.7  $\mu\text{m}$ ) (Figure 2.4a,e) to entangled networks of branched wormlike micelles. This surprising morphology appeared from the disintegration of polymer cubosomes into Y-junctioned worm-like micelles, as estimated from the TEM and SEM images of the self-assembled structure of 4/6 (90:10 w/w) blend (Figure 2.4b,f). The disintegration of polymer cubosomes into entangled cylindrical micelles was more pronounced when the composition of 6 in the blend was increased to 15% and 20%. At 25% composition, the entangled worm-like micelles were unwound to micellar networks. The length of the micelles and the degree of branching (the density of Y-junction) gradually decreased to form shorter Y-junctioned worm-like micelles as the content of 6 increased (Figure 2.4c,g). The morphology finally changed to small vesicular structures in 4/6 (50:50 w/w) blend (Figure 2.4d,h). These results were in striking contrast to similar binary blends of L-BCPs, which exhibited morphological transition from bicontinuous mesophases to flat lamellar and vesicular structures, and worm-like and spherical micelles as the composition of the BCP possessing a greater block ratio.<sup>[20]</sup> Particularly, the gradual disintegration of inverse bicontinuous mesophase particles, such as cubosomes into entangled worm-like micelles without passing the bilayer-rich phases has not been previously observed in the BCP self-assembly. The presence of Y-junctions in the worm-like micelles indicated that these

unusual morphologies may have resulted from the nonergodic behavior of H-BCP during the self-assembly,<sup>[12]</sup> which was promoted by the presence of L-BCP acting as a diluent to enhance the H-BCP mobility.

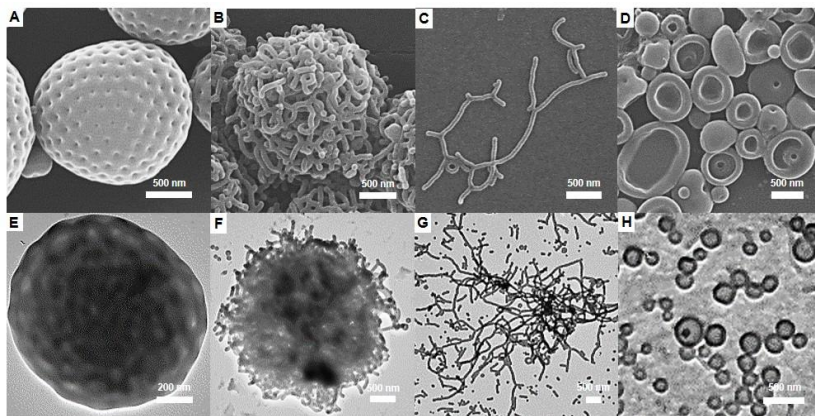


**Figure 2.4** a–d) Representative SEM and e–h) TEM images of the self-assembled structures of BCP 4/6 blends: a,e) Smaller cubosomes (95:5 w/w). b,f) Spherically entangled worm-like micelles (90:10 w/w). c,g) Worm-like micelles (75:25 w/w). d,h) Small vesicular structures (50:50 w/w).

The morphological transition of the series of blends of H-BCP 5 forming hexosomes and L-BCP 6 was investigated by gradually increasing the content of 6 in the blends (Figure 2.5). The hexosomes of H-BCP 5 transformed into cubosomes when the 5/6 (95:5 w/w) blend was self-assembled in solution (Figure 2.5a,f). The cubosomes exhibited regularly arranged well-defined surface pores. The internal order of the cubosomes was confirmed by the TEM analysis. With the increased content of 6, the 5/6 (90:10 w/w) blend formed ill-defined cubosome-like microparticles (Figure 2.5b,g). The diameters of these particles were reduced to  $\approx 2$   $\mu\text{m}$  and the internal order, as examined using TEM, was deteriorated. Furthermore,

partially degraded polymer cubosomes started to appear. Self-assembly of the 5/6 blend (85:15 w/w) resulted in the complete disintegration of cubosomes into spherical particles composed of entangled worm-like micelles (Figure 2.5c,h). The spherical morphology of these particles strongly suggested that the entanglement of worm-like micelles originated from the direct decomposition of bicontinuous mesophases composed of cubosomes into worm-like micelles. The TEM images of these particles revealed that the internal structures were only composed of entangled worm-like micelles without any bilayer structures. The entanglement was further confirmed using confocal laser scanning microscopy (CLSM) by encapsulating Nile red in the hydrophobic interior of worm-like micelles (Figure 2.6). The increase of the content of 6% to 20% in the 5/6 (80:20 w/w) blend resulted in the unwinding of the entanglements, producing interesting fragments of Y-junctioned worm-like micelles and their 3D structures (Figure 2.5d,i). Further increase in the content of 6 in the 5/6 blend (70:30 w/w) led to a complete unwinding of the structures into short worm-like micelles (Figure 2.5e,j). These results strongly indicate the non-ergodic behavior of HBCPs during the self-assembly of H-BCP/L-BCP blends and the role of L-BCP as a diluent when the BCP blend was coassembled into nanostructures.

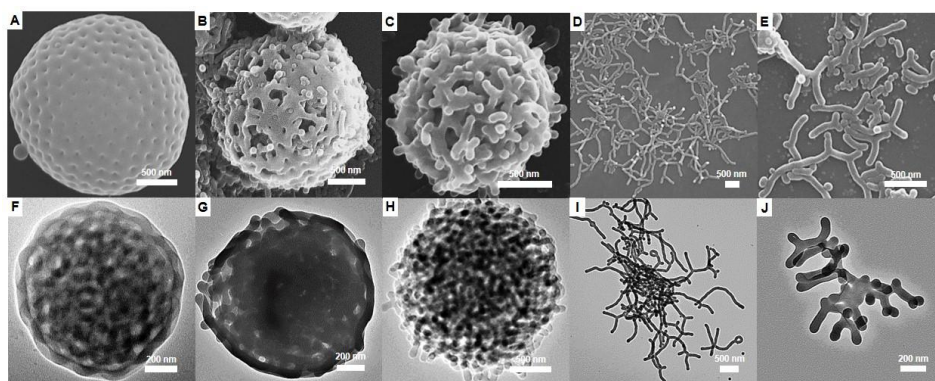


**Figure 2.5** Representative SEM and TEM images of the self-assembled structures of BCP 5/6 blends: a,f) Polymer cubosomes (95:5 w/w). b,g) Ill-defined cubosomes-like particles (90:10 w/w). c,h) Spherically entangled worm-like micelles (85:15 w/w). d,i) Unwinding of the entanglement of worm-like micelles (80:20 w/w). e,j) Short worm-like micelles (70:30 w/w).

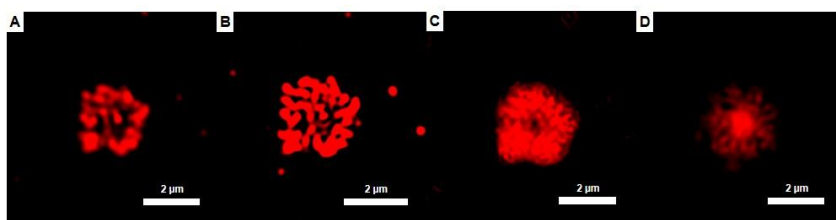


**Figure 2.6** SIM image of the BCP 5/6 blends: Nile red-labeled Spherically entangled worm-like micelles (80:20 w/w). a–d) Cross-sectional CLSM images of Nile red-labeled spherically entangled worm-like micelles at different focal planes along the *z*-axis.

### 2.3.5. Characterization of Entangled Structures of Y-Junctioned Worm-Like Micelles

The morphology of the self-assembled structures of a series of H-BCP/L-BCP blends was examined by changing the molecular weight of the PS block in the H-BCP. The results indicated that the presence of Y-junctioned worm-like micelles was critically affected by the molecular weight of the PS block. In case of forming the blends with L-BCP 6, the critical DP of the PS block of H-BCP was estimated to be

$\approx 1800$ . The presence of L-BCP was assumed to promote the formation of worm-like micelles and Y-junctioned micelles concentrating this higher block ratio BCP at the hemispherical end caps and Y-junctions where the interfacial energy should be higher than other parts of the micelles.<sup>[34–38]</sup> This assumption was partially justified by the observation of the increase in the degree of Y-junctions in the 5/6 blend with increasing content of 6 from 20% to  $\approx 28\%$  at an increment of 1%. Moreover, the length of the worm-like micelles in the 5/6 blend gradually decreased as the content of 6 increased from 30% to 50% (Figure 2.7a–j). These changes increased the number of hemispherical end caps and Y-junctions of worm-like micelles, which thereby increased the interfacial area to be stabilized by the preferential presence of L-BCP. To prove this assumption, L-BCP 7 having branched alkyne terminated PEG blocks was synthesized (Figures 2.21 and 2.22)<sup>[39]</sup> by covalently connecting the branched alkyne-terminated PEG block to the triarm PS block ( $M_n = 21.7 \text{ kg mol}^{-1}$ ,  $D = 1.12$ ,  $f_{\text{PEG}} = 27.6\%$ ). The terminal alkynes of the PEG block could be used for locating the L-BCP 7 in the self-assembled structure. Additionally, the reduced PS length of the triarm hydrophobic block with a similar block ratio as that of L-BCP 6 could facilitate the local movement of L-BCP 7 during the coassembly with H-BCP by avoiding the entanglement with long PS chains (Scheme 2.5, Table 2.3, Figures 2.23 and 2.24).<sup>[40,41]</sup> Therefore, a series of 4/7 blends with varied content of L-BCP 7 from 10% to 25% were self-assembled in solution. The 4/7 blend having 25% L-BCP 7 self-assembled into Y-junctioned worm-like micelles, which were labeled with N<sub>3</sub>-functionalized gold nanoparticles (AuNPs) (Figures 2.26–2.28).<sup>[42–44]</sup> The click reaction of N<sub>3</sub>-functionalized AuNPs (5 or 25 nm) with Y-junctioned micelles of the 4/7 blend positioned the AuNPs in the L-BCP 7 populated regions of the



micelles. The TEM images of the AuNP-labeled micelles suggested that the L-BCP with a higher block ratio than H-BCP was distributed on the water micelle interface of the micelles (Figure 2.8b,c). However, the analysis of the TEM images did not give a conclusive result to support the assumption that the L-BCP 7 could be concentrated at the regions of the micelles where the interfacial energy was higher.

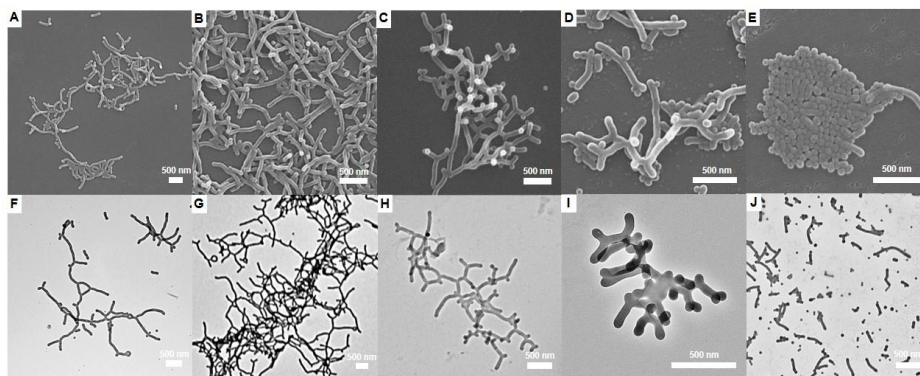


**Figure 2.7.** Representative SEM and TEM images of the self-assembled structures of BCP 5/6 blends: a,f) The composition of 6 is 22% (78:22 w/w). b,g) 25% (75:25 w/w). c,h) 28% (72:28 w/w). d,i) 30% (70:30 w/w). e,j) 50% (50:50 w/w).

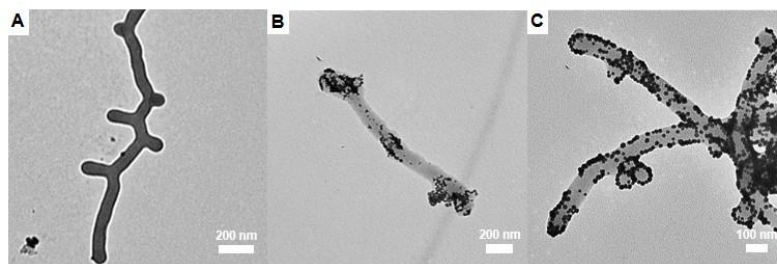


**Figure 2.8.** TEM images of structures of BCP 4/7 blends (75:25 w/w): a) purified Y-junctioned micelles after the mixing with AuNPs (25nm) without click reaction. b,c) Purified the micelles after click reaction with AuNPs (5, 25 nm), respectively.

## 2.4 Conclusion

To summarize, nonergodic behavior of the binary blends in the solution self-assembly was studied. The blends were composed of branched-linear BCPs with similar chemistries of both polymer blocks but different molecular weights. In particular, the self-assembled structures of H-BCP that did not reach time-averaged equilibrium and settled prematurely at local energy minima, resulting in the emergence of interesting morphologies. A gradual transition of morphologies from polymer vesicles, hexosomes, and cubosomes into 3D micellar networks, short cylinders, and spherical micelles was observed with increasing content of LBCP in the binary blend. The L-BCP could accelerate the formation of worm-like micelles and Y-junctioned micelles due to its concentration at the hemispherical end caps and Y-junctions where the interfacial energy should be higher than other parts of micelles. This was proven by synthesizing an L-BCP with alkyne-terminated PEG blocks for locating the L-BCP in the self-assembled structures. The L-BCP concentration at the hemispherical end caps and Y-junctions was easily observed by attaching  $N_3$ -functionalized AuNPs via click reaction.

## 2.5 Experimental

### *Synthesis*

***Self-Assembly of Block Copolymer Blends by Cosolvent Methods:*** The stock solutions of two block copolymers having a concentration of  $10 \text{ mg mL}^{-1}$  in 1,4-dioxane were prepared. According to a ratio, each stock solution was added to the capped vial and resulting solution of BCP blend (total  $5 \text{ mg/1 mL}$ , 1 wt%) was stirred for 24 h at room temperature for the homogeneous mixing. 1 mL of water was added at a constant rate ( $0.25 \text{ mL h}^{-1}$ ) to the solution of BCP blend using a syringe pump with vigorous stirring. After self-assembly, the organic solvent in the resulting

suspension was removed by dialysis (molecular weight cutoff (MWCO) = 12–14 kDa, SpectraPor) against water for 1 d.

***N<sub>3</sub>-Au Nanoparticles Labeling via Click Reaction:*** Azide-functionalized gold nanoparticles (5 nm, 25 nm) were attached to the surface of the self-assembled structure via a click reaction. CuSO<sub>4</sub>, sodium ascorbate and AuNPs were added to the aqueous solution of polymer structures and stirred for about 2 h.<sup>[45]</sup> The precipitate obtained through 30 min centrifugation at rpm 2500–3000. The AuNPs need to be centrifuged at about 10000 rpm for 2 h to sink, so it was confirmed that the AuNPs with the submerged polymer were attached through click reaction.

### **2.5.1 Materials**

All reagents and chemicals were used as received from Sigma Aldrich, Alfa Aesar and TCI. Styrene monomer was purified by using basic alumina column before use. Dichloromethane (MC) was dried over CaH<sub>2</sub> under N<sub>2</sub> and Tetrahydrofuran (THF) was refluxed over a mixture of Na and benzophenone under N<sub>2</sub> and distilled before use. All reactions were performed under N<sub>2</sub> unless otherwise note.

### **2.5.2 Techniques**

<sup>1</sup>H NMR spectra was recorded at 400 MHz and 500 MHz, respectively on an Agilent 400-MR DD2 spectrometer and a Bruker DRX (500 MHz) NMR spectrometer. All NMR spectra were measured at 25 °C in the indicated deuterated solvents. CD<sub>2</sub>Cl<sub>2</sub> was used as standard solution in <sup>1</sup>H NMR spectra. The average molecular weights and molecular dispersity of block copolymers were measured by Agilent 1260 Infinity GPC system, comprising a PL gel 5 μm mixed D column (Agilent Technologies) and differential refractive index detectors using THF as an eluent at 35°C with a flow rate of 1 mL min<sup>-1</sup>. The polymer sample in THF was filtered by

using PTFE filter before injection. For the calibration of GPC system, a PS standard (Agilent Technologies) was used.

#### **2.5.2.1 Matrix-Assisted Laser Desorption/Ionization Time of Flight (MALDI-TOF)**

Matrix-assisted laser desorption ionization time-of-flight mass spectroscopy (MALDI-TOF MS) was performed using a Bruker Ultra flex III TOF-TOF mass spectrometer equipped with a nitrogen laser (335nm). The experimental sample was prepared by mixing block copolymers dissolved in THF (5mg mL<sup>-1</sup>) and matrix solution (sinapic acid or dithranol in THF, 30mg mL<sup>-1</sup>). The prepared sample was dropped onto the MALDI plate and dries at room temperature before measurement.

#### **2.5.2.2 Scanning Electron Microscopy (SEM)**

Scanning electron microscopy (SEM) was performed on Hitachi S-4300 at an acceleration voltage of 15kV. Sample was prepared by dropping the self-assembled solution onto a slide glass and drying at room temperature. The prepared by sample was coated with Pt by using Hitachi E-1030 ion sputter (20mA, 60s).

#### **2.5.2.3 Transmission Electron Microscopy (TEM)**

Transmission electron microscopy (TEM) images were obtained on JEOL JEM-2100 microscope at 200kV and Hitachi 7600 at 100kV. Specimens were prepared by adding a drop of the suspension of self-assembled structures onto a carbon-coated Cu grid (200 mesh, EM science). After 30 min, remaining solution on a grid was removed with a filter paper, and the grid was air-dried at room temperature overnight.

#### **2.5.2.4 Small-Angle X-ray Scattering (SAXS)**

Synchrotron small angle X-ray scattering data were obtained on the SAXS beam line (PLS-II 6D, 11.18 keV, 6.5m) at Pohang acceleration laboratory (Pohang, Korea). The concentrated suspension of the polymer structures was dried for 2 days in freeze

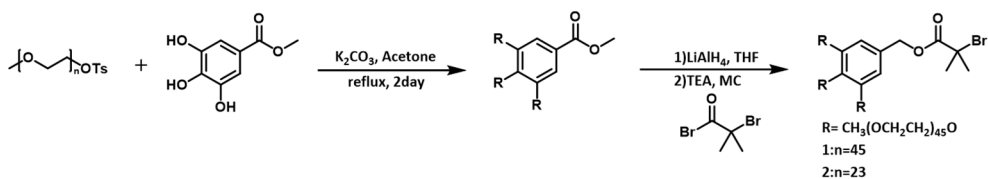
dryer. The resulting power was placed on a customized holder. Ti-SBA standard was used and X-ray irradiation time was 2~10 seconds dependent on the saturation level of the detector.

### 2.5.2.5 Structured Illumination Microscopy (SIM)

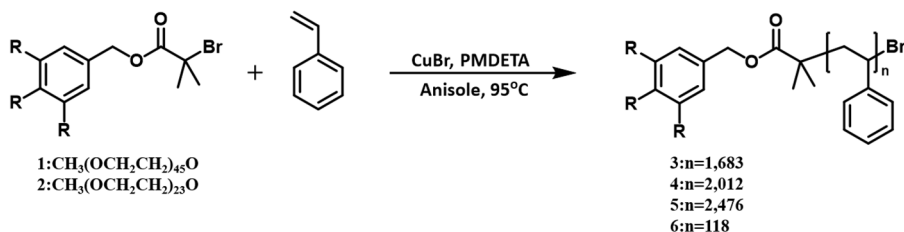
SIM images of cylindrical micelles of BCP labeled with Nile Red (Sigma Aldrich,  $\lambda_{\text{Ex}} = 552 \text{ nm}$ ,  $\lambda_{\text{Em}} = 636 \text{ nm}$ ) were obtained using Nikon NSIM Super-Resolution Microscope System. 5-10  $\mu\text{L}$  of concentrated suspension of fluorescently labeled structure was placed on a slide glass and sealed with cover glass. Residual solution was removed by filter paper and cover glass was fixed with sealant.

## 2.5.3 Synthesis

### 2.5.3.1 Preparation of dendritic linear block copolymers



**Scheme 2.1** Preparation of hydrophilic block (1). Dendritic hydrophilic block used in this study was synthesized as previously reported.<sup>[29]</sup>

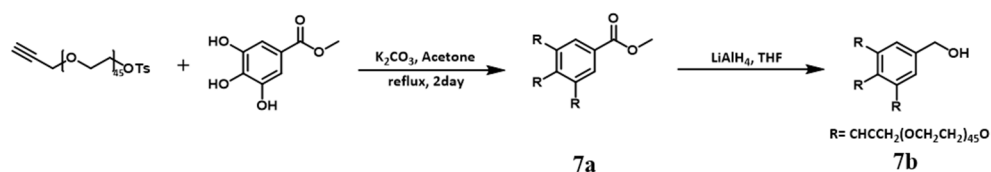


**Scheme 2.2** Preparation of amphiphilic block copolymers (3)-(6).

**Atom transfer radical polymerization (ATRP).**

CuBr(1.3eq) and N,N,N',N'',N'''-pentamethyldiethylenetriamine (PMDETA)(2.6eq) were mixed with anisole in a Schlenk flask with a magnetic bar. The mixture was bubbled with N<sub>2</sub> for 15 min. Then, the solution of macroinitiator 1 or 2(1eq) and styrene monomer(2500eq) was added into the mixture. The flask was immersed in a preheated oil bath (95-100 °C). The Mn of the BCP was adjusted by controlling the duration of the polymerization reaction. The ATRP of styrene resulted in the formation of BCPs with a significantly broad molecular weight distribution ( $D > 1.5$ ), as monitored by GPC. The BCP was purified by precipitation in MeOH and by performing the gradient chromatography on SiO<sub>2</sub> with a CH<sub>2</sub>Cl<sub>2</sub>/MeOH mixture (100:0 to 96:4 v/v) as an eluent utilizing the marked difference of the affinity of PEG and PS blocks toward silica (Figure 2.12). The gradient chromatography of the precipitated polymers yielded homo-PS as the first fraction using CH<sub>2</sub>Cl<sub>2</sub> as an eluent, and, then, the desired BCP as the second fraction eluted with a mixed solvent of MC/MeOH 4%.<sup>[31]</sup>

### 2.5.3.2 Preparation of alkyne-dendritic branched block copolymers

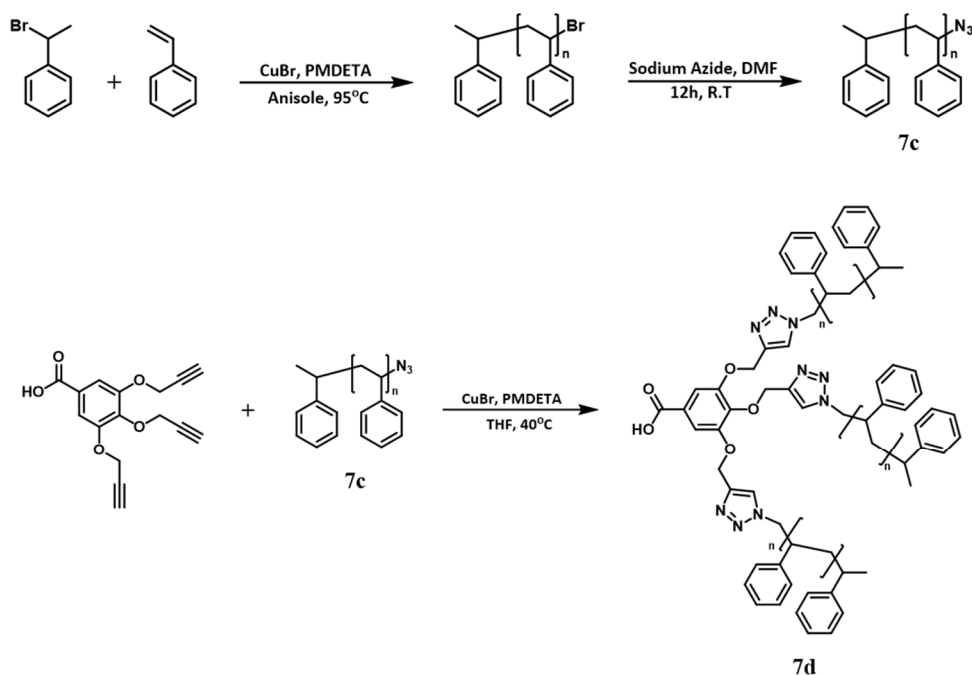


**Scheme 2.3** Preparation of hydrophilic block.

**(7a).** To an acetone solution (250mL) of methyl 3,4,5-trihydroxybenzoate 1 g and poly(ethylene glycol)propargyl ether tosylate 40 g were added K<sub>2</sub>CO<sub>3</sub> 6.75 g and KI 0.2 g. The reaction mixture was stirred at 80 °C for 48 h under N<sub>2</sub> atmosphere. Then

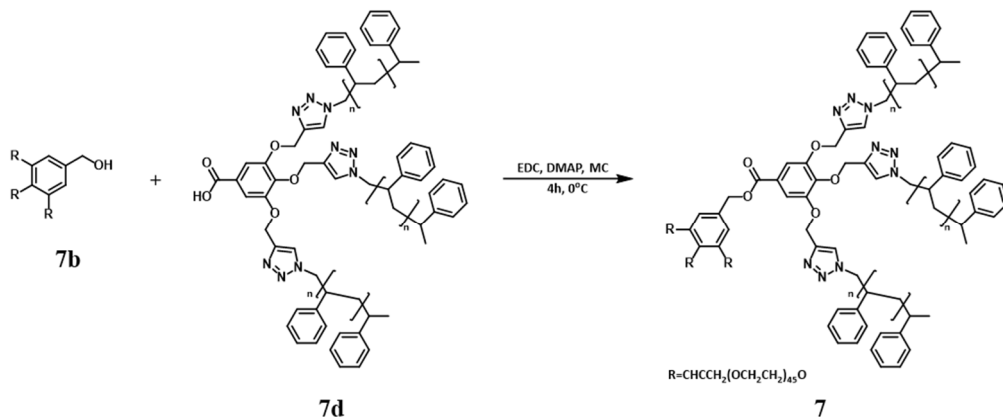
the reaction mixture was concentrated under reduced pressure. After then reaction mixture was poured into 100 mL water and extracted with 3\*100 mL of MC. An Organic layer was washed with brine and dried over MgSO<sub>4</sub>. Then the organic layer was concentrated under reduced pressure. The crude product was purified by column chromatography on silica gel with a mobile phase of MC/MeOH 5~10% to yield compound 7a.<sup>[39]</sup>

**(7b).** To a THF solution (250 mL) of compound 7a 3 g was added LiAlH<sub>4</sub> 0.1g at 0°C. The reaction mixture was stirred for 4 h under N<sub>2</sub> atmosphere. The reaction mixture was quenched with D.I water on an ice-bath. After then reaction mixture was filtered and concentrated under reduced pressure. The crude was extracted with 3\*100 mL of MC. An organic layer was dried over MgSO<sub>4</sub> and concentrated under vacuum condition to yield compound 7b.



**Scheme 2.4** Preparation of hydrophobic block.

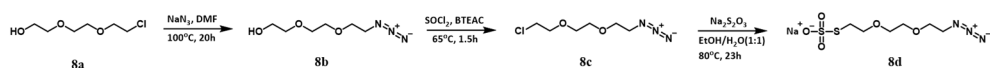
(7c) and (7d). Detailed synthetic procedures were reported previously.<sup>[46]</sup>



**Scheme 2.5** Preparation of amphiphilic block copolymers.

(7). 7b 1.5g and 7d 1.8g were dissolved in dry MC, and the mixture was cooled to 0 °C on an ice bath. To the 4-(dimethylamino)pyridine 0.01g and 1-(3-dimethylaminopropyl)- 3- ethylcarbodiimide hydrochloride 0.07g were added in to the mixture of 7b and 7d. The reaction mixture was stirred overnight at room temperature. Then the reaction mixture was washed with water and brine. The combined organic layer was dried over MgSO<sub>4</sub>, and concentrated under reduced pressure. The crude product was purified by automated column chromatography with a mobile phase of MC/MeOH 5~10% to yield compound 7.

### 2.5.3.3 Preparation of gold nanoparticles (AuNPs)



**Scheme 2.6** Preparation of azide functionalized Bunte Salt.



**1-azido-2-(2-(2-chloroethoxy)ethoxy)ethane (8b).**

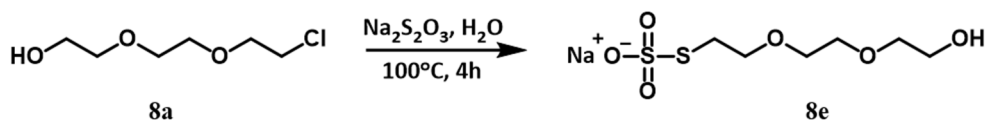
2-(2-(2-chloroethoxy)-ethoxy)ethanol (8a) 4g was dissolved in anhydrous DMF under N<sub>2</sub>. NaN<sub>3</sub> 3.1 g was added in to DMF solution. The mixture was heated to 100 °C and stirring for 20 h. Then mixture was cooled to r.t. and concentrated under reduced pressure. The crude was condensed over NaOH pellets to trap any HN<sub>3</sub> potentially produced and suspended in diethyl ether (100 mL). Then the crude was filtered concentrated in vacuo to yield 8b.<sup>[42]</sup>

**1-azido-2-(2-(2-chloroethoxy)ethoxy)ethane (8c).**

A mixture of 8b 3.50 g and benzyl triethyl ammonium chloride (BTEAC) 0.15 g was heated to 65 °C. Thionyl chloride 5 g was added dropwise and the reaction mixture was stirred at 65 °C for 1.5 h under N<sub>2</sub>. The mixture was cooled to r.t. and excess thionyl chloride was removed by rotary evaporation. The crude product was suspended in phosphate buffer 50 mM (pH = 7.0, 15 mL) and extracted with EtOAc/hexane. The organic layer was washed with phosphate buffer 4 times, dried with Na<sub>2</sub>SO<sub>4</sub>, filtered and concentrated in vacuo to yield 8c.

**S-(2-(2-(2-azidoethoxy)ethoxy)ethyl)sulfothioate (8d).**

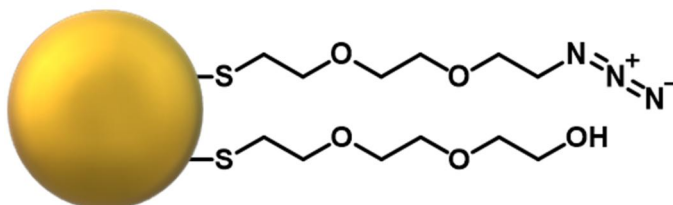
Chloro compound 8c 2.5 g was dissolved in EtOH/H<sub>2</sub>O = (4:3), 70 mL total. Anhydrous sodium thiosulfate 2.5 g was added over ~ 2 min. The resulting mixture was heated to 80 °C for 23 h. Upon letting cool to r.t., EtOH and H<sub>2</sub>O were removed by rotary evaporation. The crude was dissolved in CH<sub>3</sub>CN to precipitate salts that were subsequently removed by filtering. CH<sub>3</sub>CN was removed by rotary evaporation. Then the crude was redissolved in D.I water to separate starting material. The water solution was decanted and filtered to remove residual starting material. Concentration in vacuo produced 8d.



**Scheme 2.7** Preparation of Bunte Salt.

### 2-(2-(2-chloroethoxy)-ethoxy)ethanol (8e)

2-(2-(2-chloroethoxy)-ethoxy)ethanol (8a) 2g was combined with 1.5g of sodium thiosulfate in 150 mL of D.I water and heated to 100°C for 4 h. The reaction mixture was cooled to r.t. and concentrated by rotary evaporation. The crude was dried overnight in vacuo. The crude product was purified by dissolving in ethanol and removing the sodium chloride side product by filtration. The product was concentrated in vacuo to yield 8e.<sup>[47]</sup>



**Scheme 2.8** Preparation of azide-functionalized AuNPs.<sup>[48]</sup>

## 2.5.4 Preparation of Self-assembly structures

### 2.5.4.1 Solution self-assembly of block copolymers by co-solvent methods

For BCPs, 10mg of the amphiphilic block copolymer was dissolved in 2 mL of 1,4-dioxane (1 wt %) in a capped vial, and the solution was stirred for 1 h at room temperature. 2 mL of D.I water was added at a controlled rate (0.5 mL h<sup>-1</sup>) to the solution via a syringe pump with vigorous stirring. The resulting solution was

dialyzed (molecular weight cutoff (MWCO) = 12-14 kDa, SpectraPor) against water for 1 day.

### 2.5.4.2 Solvent diffusion-evaporation self-assembly (SDEMS) of block copolymers

For H-BCPs, 10 mg of the block copolymer was dissolved in 1,4-dioxane (990 mg) in a 4 mL vial and stirred for 3 h at room temperature. A sealed humidity chamber was prepared by mixing 20 mL of 1,4-dioxane and 20 mL of water in a 100 mL vial including cylindrical column to put a glass substrate. 0.4 mL of the polymer solution was cast on the  $2 \times 2 \text{ cm}^2$  glass substrate on the column in the humidity chamber. Then the humidity chamber was sealed. After 4 h, the glass substrate was immersed into excess water. The self-assembly structures were collected after removing 1,4-dioxane by solvent exchange in water.

### 2.5.5 Characterization

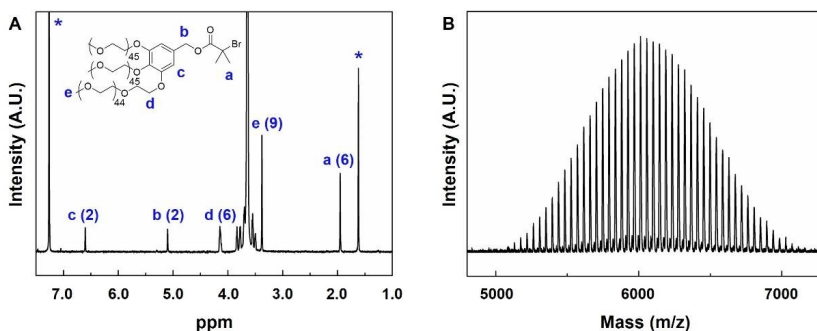


**Figure 2.9** a)  $^1\text{H}$  NMR spectrum of the macroinitiator PEG2000<sub>3</sub>-Br, 1. b) MALDI-TOF MS spectrum of the precursor of the macroinitiator, PEG2000<sub>3</sub>-OH.

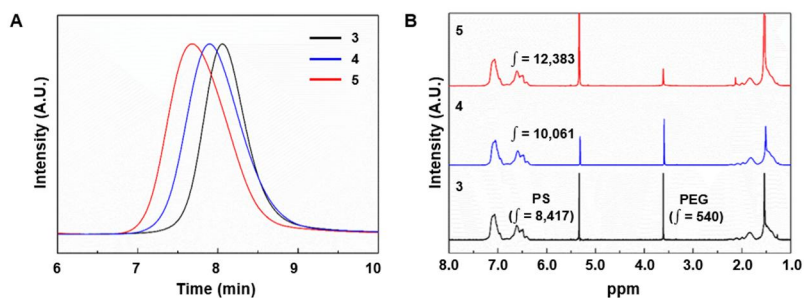


**Figure 2.10** a) GPC elugrams (DMF as an eluent) and b)  $^1\text{H}$  NMR in  $\text{CD}_2\text{Cl}_2$  spectra of BCPs.

**Table 2.1** Characterization of BCPs.

BCP	$M_n$ ( $\text{kg mol}^{-1}$ ) <sup>a</sup>	$\bar{D}$ <sup>a</sup>	$DP_n$ <sup>b</sup>	$M_n$ ( $\text{kg mol}^{-1}$ ) <sup>b</sup>	$f_{\text{PEG}}$ (%) <sup>c</sup>
3	158.7	1.21	1,683	181.2	3.5
4	186.9	1.25	2,012	215.4	3.0
5	245.9	1.26	2,476	263.7	2.4

<sup>a</sup>Determined by GPC using DMF as an eluent. <sup>b</sup>Calculated by  $^1\text{H}$  NMR integration assuming the  $M_n$  of PEG chains of 6,000 g/mol. <sup>c</sup>Calculated by  $f_{\text{PEG}} = (M_n \text{ of PEG} / M_n \text{ of a BCP})$ .

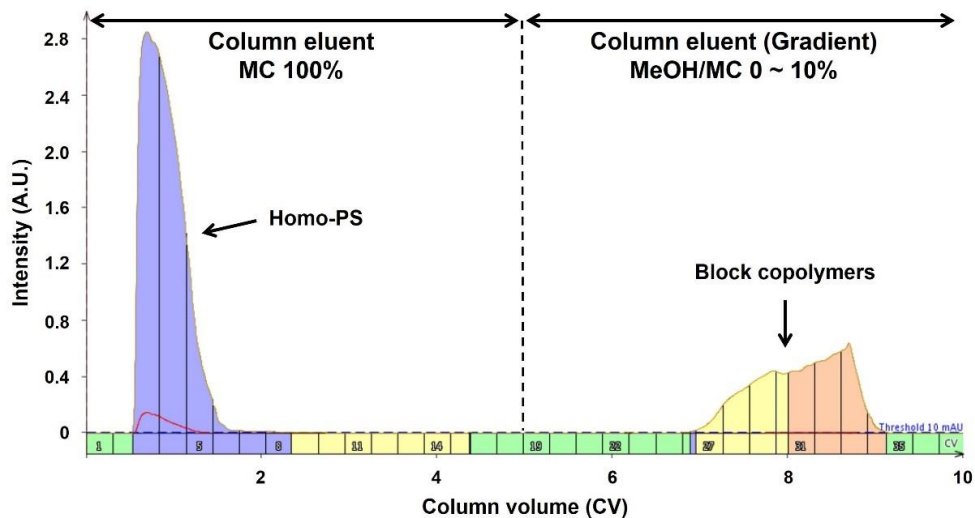


**Figure 2.11** Plot of column volume vs intensity of the entire absorbance of gradient column chromatography by Isolera™ Specktra system showing a successful separation of homo-PS. The yield of block copolymers was ~17%.

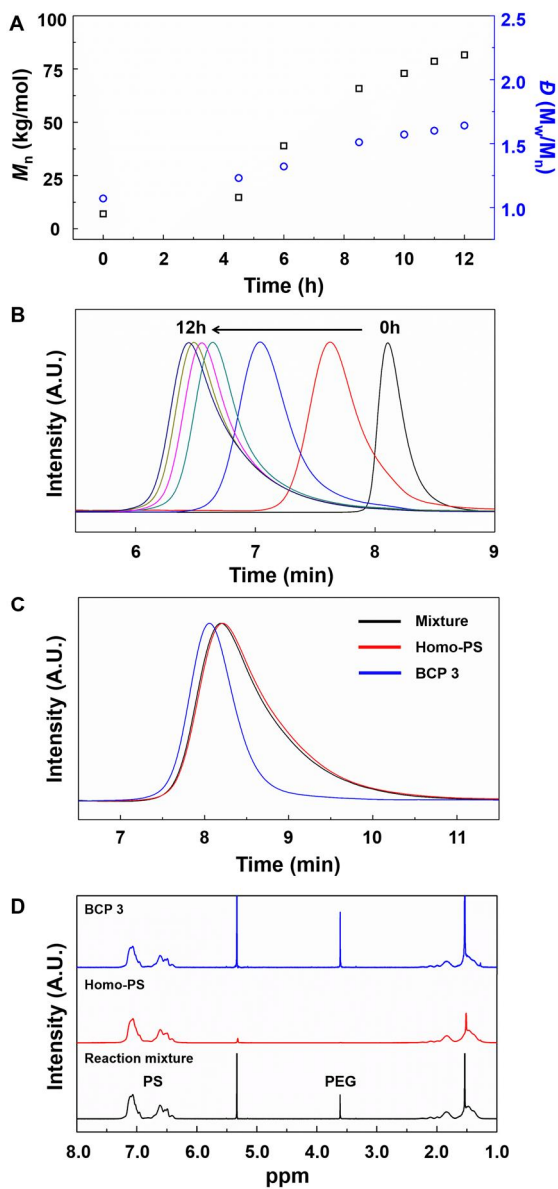


**Figure 2.12** a) Plot of polymerization time vs the number average of molecular weight ( $M_n$ ) and molecular dispersity ( $D$ ) for 3. ( $M_n = 81,700 \text{ g mol}^{-1}$ ,  $D = 1.65$ ) b) GPC (THF as an eluent) results showing the progress during the polymerization time for 3. c) GPC (DMF as an eluent) and d)  $^1\text{H}$  NMR spectra showing the reaction mixture before purification process (black), the homo-PS separated as a first fraction of the gradient chromatography (red), and 3 separated as the second fraction (blue).

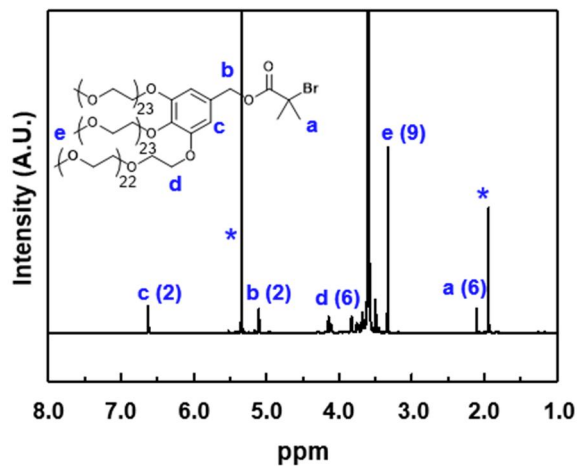


**Figure 2.13**  $^1\text{H}$  NMR in  $\text{CD}_2\text{Cl}_2$  spectrum of the macroinitiator PEG1000<sub>3</sub>-Br, 2.

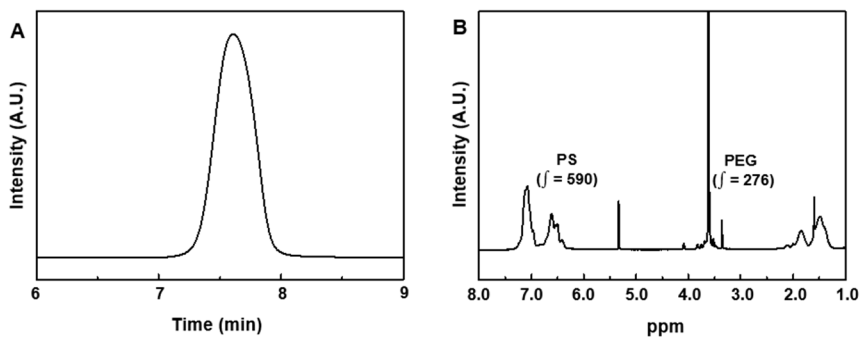


**Figure 2.14** a) GPC elugram (THF as an eluent) and b)  $^1\text{H}$  NMR in  $\text{CD}_2\text{Cl}_2$  spectrum of LBCP 6.

**Table 2.2** Characterization of BCPs.

BCP	$M_n$ ( $\text{kg mol}^{-1}$ ) <sup>a</sup>	$D^a$	$DP_n^b$	$M_n$ ( $\text{kg mol}^{-1}$ ) <sup>b</sup>	$f_{\text{PEG}}$ (%) <sup>c</sup>
6	19	1.09	118	15.7	15.8

<sup>a</sup>Determined by GPC using THF as an eluent. <sup>b</sup>Calculated by  $^1\text{H}$  NMR integration assuming the  $M_n$  of PEG chains of 3,000 g/mol. <sup>c</sup>Calculated by  $f_{\text{PEG}} = (M_n \text{ of PEG} / M_n \text{ of a BCP})$ .

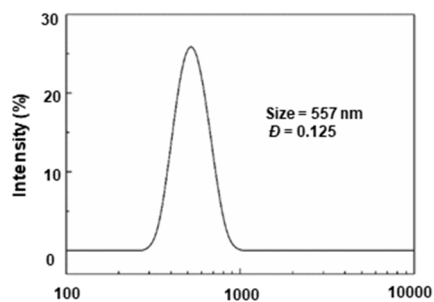


**Figure 2.15** DLS plots of polymersomes of 3 self-assembled by co-solvent method.

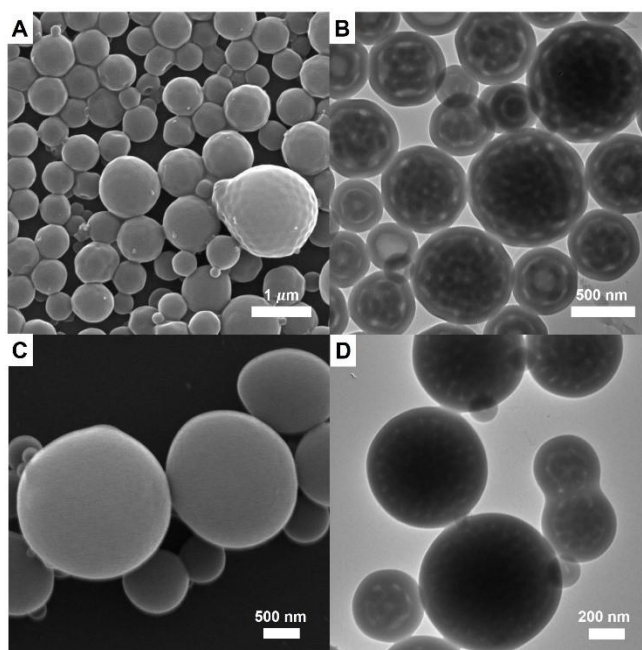


**Figure 2.16** a) SEM and b) TEM images of self-assembled structures of 4 by the co-solvent method. c) SEM and d) TEM images of self-assembled structures of 5 by the co-solvent method.



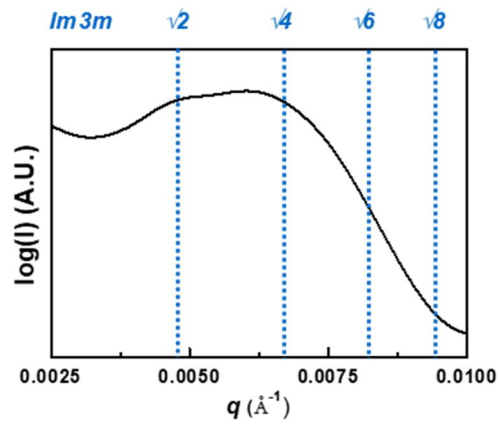


**Figure 2.17** Small-angle x-ray scattering result obtained from the dried polymer cubosomes of 4 ( $Im\bar{3}m$  symmetry,  $a = 190$  nm).

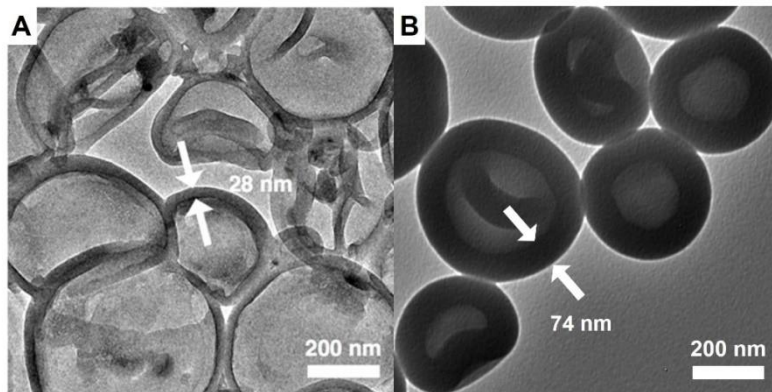


**Figure 2.18** TEM images of the polymersomes of a) PEG2000-PS<sub>228</sub> and b) PEG2000<sub>3</sub>-PS<sub>1683</sub> 3 showing the thickness of the bilayer membrane.

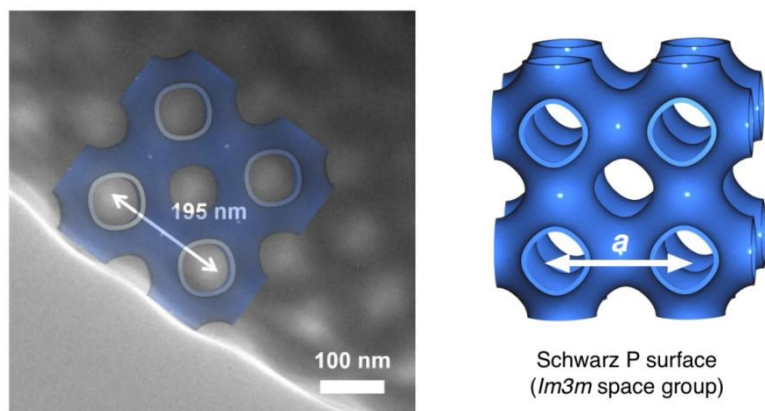


**Figure 2.19** TEM image of the polymer cubosome of 4 by SDEMS method and the representative lattice of Schwarz P surface of BCP bilayers. The computer-generated (100) plane of Schwarz P surface was superimposed on TEM image to indicates the lattice parameter.

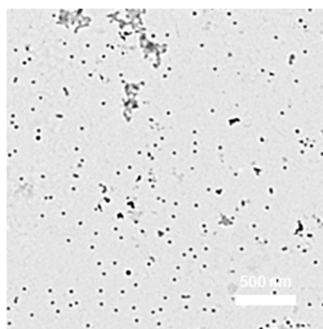


**Figure 2.20** TEM image of the self-assembled spherical micelle structure of the L-BCP6.

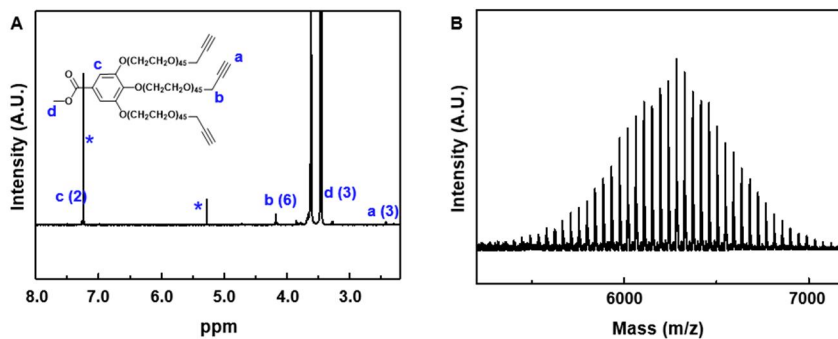


**Figure 2.21** a)  $^1\text{H}$  NMR in  $\text{CDCl}_3$  and b) MALDI spectrum of alkyne functionalized hydrophilic block 7b.

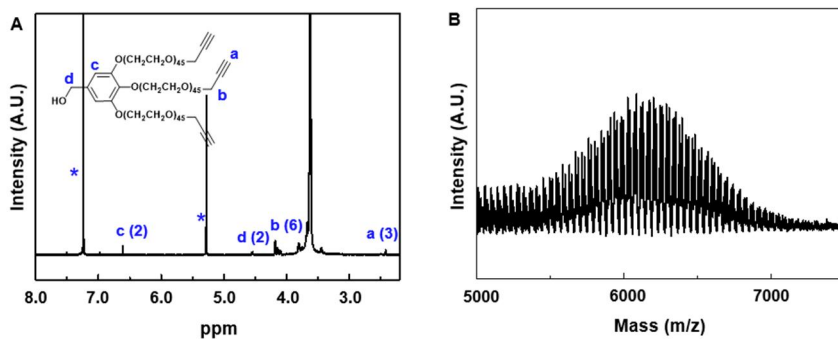


**Figure 2.22** a)  $^1\text{H}$  NMR in  $\text{CDCl}_3$  and b) MALDI spectrum of alkyne functionalized hydrophilic block 7a.

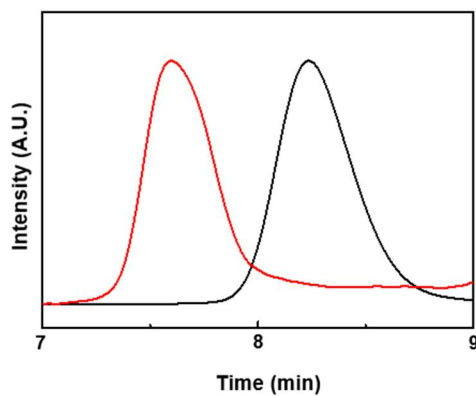


**Figure 2.23** GPC (THF as an eluent) elugrams of hydrophobic block before 7c (black) and after 7d (red) click reaction.

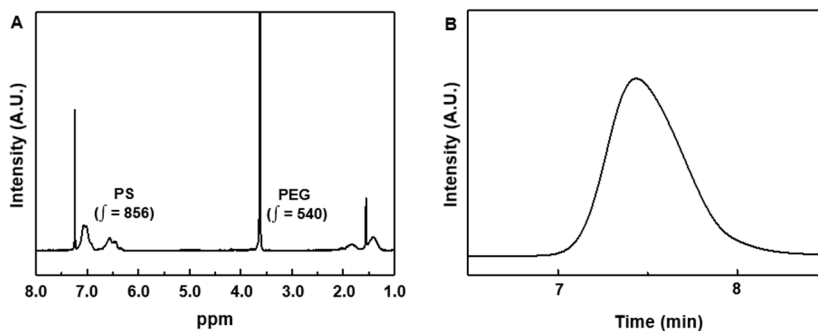


**Figure 2.24** a)  $^1\text{H}$  NMR spectrum and b) GPC elugram of the L-BCP7.

**Table 2.3** Characterization of BCPs.

BCP	$M_n$ ( $\text{kg mol}^{-1}$ ) <sup>a</sup>	$D^a$	$DP_n$	$M_n$ ( $\text{kg mol}^{-1}$ ) <sup>b</sup>	$f_{\text{PEG}}$ (%) <sup>c</sup>
<b>7</b>	21.7	1.12	171 <sup>b</sup>	24.5	27.6
<b>7c</b>	5.4	1.08	50 <sup>a</sup>	-	-
<b>7d</b>	16.8	1.06	156 <sup>a</sup>	-	-

<sup>a</sup>Determined by GPC using THF as an eluent. <sup>b</sup>Calculated by  $^1\text{H}$  NMR integration assuming the  $M_n$  of PEG chains of 6,000  $\text{g/mol}$ . <sup>c</sup>Calculated by  $f_{\text{PEG}} = (M_n \text{ of PEG} / M_n \text{ of a BCP})$ .

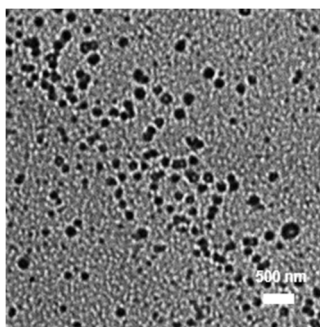


**Figure 2.25** TEM image of the self-assembled spherical micelle structure of the L-BCP7.

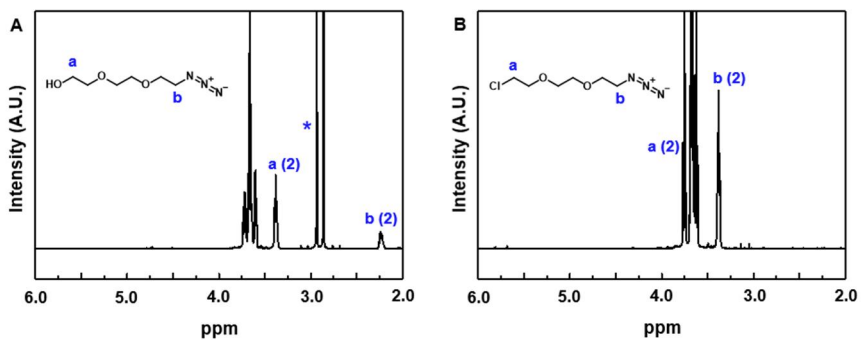


Figure 2.26  $^1\text{H}$  NMR in  $\text{CDCl}_3$  spectrum of (a) 8b and (b) 8c.

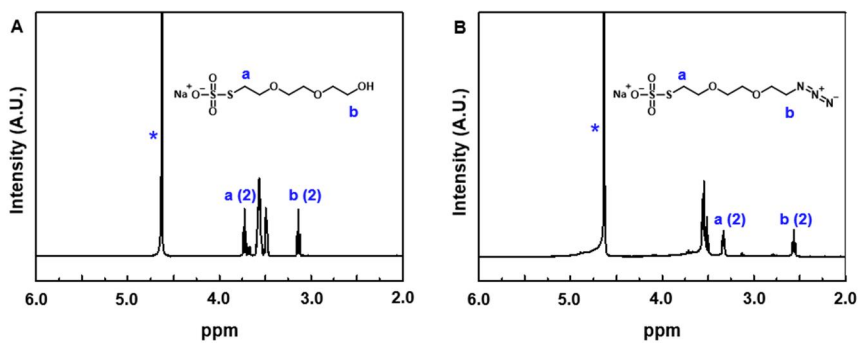
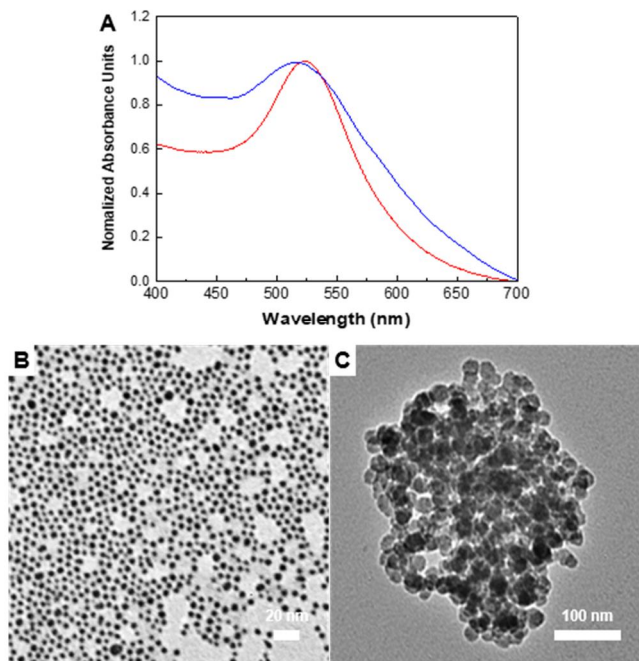


Figure 2.27  $^1\text{H}$  NMR in  $\text{D}_2\text{O}$  spectrum of (a) 8d and (b) 8e.



**Figure 2.28** a) UV-vis spectra of azide-functionalized AuNPs 5nm ( $\lambda_{\text{max}}= 520\text{nm}$ , blue) and 25nm ( $\lambda_{\text{max}}= 525\text{nm}$ , red), respectively. b),c) TEM images of azide-functionalized AuNPs 5nm and 25nm.

## 2.6 Reference

- [1] Hamley, I. W. *Block Copolymers in Solution: Fundamentals and Applications*, Wiley, Chichester **2005**.
- [2] Holder, S. J.; Sommerdijk, N. A. J. M. *Polym. Chem.* **2011**, 2, 1018.
- [3] Deng, Z.; Liu, S. *Polymer* **2020**, 207, 122914.
- [4] Karayianni, M.; Pispas, S. *J. Polym. Sci.* **2021**, 59, 1874.
- [5] Alexandridis, P.; Lindman, B. *Amphiphilic Block Copolymers: Self Assembly and Applications*, Elsevier, Amsterdam **2000**.
- [6] Schacher, F. H.; Rupar, P. A.; Manners, I. *Angew. Chem., Int. Ed.* **2012**, 51, 7898.

- [7] Tritschler, U.; Pearce, S.; Gwyther, J.; Whittell, G. R.; Manners, I. *Macromolecules* **2017**, *50*, 3439.
- [8] Wong, C. K.; Qiang, X.; Müller, A. H. E.; Gröschel, A. H. *Prog. Polym. Sci.* **2020**, *102*, 101211.
- [9] Won, Y.-Y.; Davis, H. T.; Bates, F. S. *Macromolecules* **2003**, *36*, 953.
- [10] Kulkarni, C. V.; Wachter, W.; Iglesias-Salto, G.; Engelskirchen, S.; Ahualli, S. *Phys. Chem. Chem. Phys.* **2011**, *13*, 3004.
- [11] Mai, Y.; Eisenberg, A. *Chem. Soc. Rev.* **2012**, *41*, 5969.
- [12] Jain, S.; Bates, F. S. *Science* **2003**, *300*, 460.
- [13] Jain, S.; Bates, F. S. *Macromolecules* **2004**, *37*, 1511.
- [14] Won, Y.-Y.; Brannan, A. K.; Davis, H. T.; Bates, F. S. *J. Phys. Chem.* **2002**, *106*, 3354.
- [15] He, Y.; Li, Z.; Simone, P.; Lodge, T. P. *J. Am. Chem. Soc.* **2006**, *128*, 2745.
- [16] Zhang, L.; Yu, K.; Eisenberg, A. *Science* **1996**, *272*, 1777.
- [17] Carmean, R. N.; Sims, M. B.; Figg, C. A.; Hurst, P. J.; Patterson, J. P.; Sumerlin, B. S. *ACS Macro Lett.* **2020**, *9*, 613.
- [18] Plucinski, A.; Pavlovic, M.; Clarke, M.; Bhella, D.; Schmidt, B. V. K. J. *Macromol. Rapid Commun.* **2022**, *43*, 2100656.
- [19] Robeson, L. M. *Polym. Eng. Sci.* **1984**, *24*, 587.
- [20] Cho, A.; La, Y.; Jeoung, S.; Moon, H. R.; Ryu, J.H.; Shin, T. J.; Kim, K. T. *Macromolecules* **2017**, *50*, 3234.
- [21] Court, F.; Hashimoto, T. *Macromolecules* **2001**, *34*, 2536.
- [22] Court, F.; Hashimoto, T. *Macromolecules* **2002**, *35*, 2566.
- [23] Chen, F.; Kondo, Y.; Hashimoto, T. *Macromolecules* **2007**, *40*, 3714.

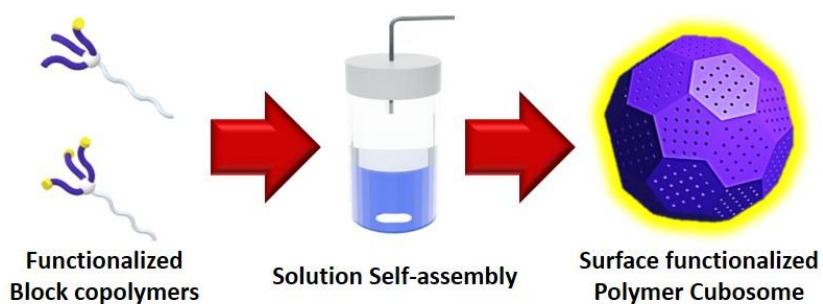
- [24] Qiu, H.; Gao, Y.; Boott, C. E.; Gould, O. E. C.; Harniman, R. L.; Miles, M. J.; Webb, S. E. D.; Winnik, M. A.; Manners, I. *Science* **2016**, *352*, 697.
- [25] Wright, D. B.; Patterson, J. P.; Pitto-Barry, A.; Lu, A.; Kirby, N.; Gianneschi, N. C.; Chassenieux, C.; Colombani, O.; O'reilly, R. K. *Macromolecules* **2015**, *48*, 6516.
- [26] Zhu, J.; Zhang, S.; Zhang, K.; Wang, X.; Mays, J. W.; Wooley, K. L.; Pochan, D. J. *Nat. Commun.* **2013**, *4*, 2291.
- [27] Park, C.; La, Y.; An, T. H.; Jeong, H. Y.; Kang, S.; Joo, S. H.; Ahn, H.; Shin, T. J.; Kim, K. T. *Nat. Commun.* **2015**, *6*, 6392.
- [28] La, Y.; An, T. H.; Shin, T. J.; Park, C.; Kim, K. T. *Angew. Chem., Int. Ed.* **2015**, *54*, 10483.
- [29] An, T. H.; La, Y.; Cho, A.; Jeong, M. G.; Shin, T. J.; Park, C.; Kim, K. T. *ACS Nano* **2015**, *9*, 3084.
- [30] Jeong, M. G.; Kim, K. T. *Macromolecules* **2017**, *50*, 223.
- [31] La, Y.; Song, J.; Jeong, M. G.; Cho, A.; Jin, S. M.; Lee, E.; Kim, K. T. *Nat. Commun.* **2018**, *9*, 5327.
- [32] Shen, H.; Eisenberg, A. *Macromolecules* **2000**, *33*, 2561.
- [33] Terreau, O.; Luo, L.; Eisenberg, A. *Langmuir* **2003**, *19*, 5601.
- [34] Percec, V.; Johansson, G.; Ungar, G.; Zhou, J. *J. Am. Chem. Soc.* **1996**, *118*, 9855.
- [35] In, M.; Aguerre-Chariol, O.; Zana, R. *J. Phys. Chem. B* **1999**, *103*, 7747.
- [36] Cates, M. E.; Candau, S. J. *J. Phys.: Condens. Matter* **1990**, *2*, 6869.
- [37] Petschek, R. G.; Pfeuty, P.; Wheeler, J. C. *Phys. Rev. A* **1986**, *34*, 2391.
- [38] Tlusty, T.; Safran, S. A. *J. Phys.: Condens. Matter* **2000**, *12*, A253.



- [39] Zhang, C. Li, S.; Wu, J. Pang, Y.; Gu, Z. *Adv. Funct. Mater.* **2015**, *25*, 3764.
- [40] Kolb, H. C.; Finn, M. G.; Sharpless, K. B. *Angew. Chem., Int. Ed.* **2001**, *40*, 2004.
- [41] Rostovtsev, V. V.; Green, L. G.; Fokin, V. V.; Sharpless, K. B. *Angew. Chem* **2002**, *114*, 2708.
- [42] Elliott, E. W.; Ginzburg, A. L.; Kennedy, Z. C.; Feng, Z.; Hutchison, J. E. *Langmuir* **2017**, *33*, 5796.
- [43] Amaral, S. P.; Fernandez-Villamarin, M.; Correa, J.; Riguera, R.; Fernandez Megia, E. *Org. Lett.* **2011**, *13*, 4522.
- [44] Elliott, E. W.; Haben, P. M.; Hutchison, J. E. *Langmuir* **2015**, *31*, 11886.
- [45] Sivakumar, K.; Xie, F.; Cash, B. M.; Long, S.; Barnhill, H. N.; Wang, Q. *Org. Lett.* **2004**, *6*, 4603.
- [46] Cho, A.; La, Y.; Shin, T. J.; Park, C.; Kim, K. T. *Macromolecules* **2016**, *49*, 4510–4519.
- [47] Lohse, S. E.; Dahl, J. A.; Hutchison, J. E. *Langmuir* **2010**, *26*, 7504–7511.
- [48] Upadhyay, A. P.; Behara, D. K.; Sharma, G. P.; Bajpai, A.; Sharac, N.; Ragan, R.; Pala, R. G. S.; Sivakumar, S. *ACS Appl. Mater. Interfaces* **2013**, *5*, 9554–9562.

# Chapter 3

## Polymer cubosomes with high-density surface functional groups



### 3.1 Abstract

(This work was collaborated with Arah Cho and Prof. Kyoung Taek Kim)

Polymer cubosome is a highly ordered periodic porous polymer nanostructure with large-pore networks composed of inverse cubic mesophases of block copolymer (BCP) bilayers. Due to its large surface area, it has a potential to be used in separation, catalysis, drug delivery and nanotemplating by the introduction of desired functional groups on its surface. The structural requirements for preferential self-assembly of block copolymers into polymer cubosomes requires the hydrophilic block to have a branched architecture. Herein, we describe the synthesis of branched-linear block copolymers having hydrophilic blocks composed of three poly(ethylene glycol)s with an alkyne end group. These block copolymers self-assemble in aqueous solution to provide well-defined polymer cubosomes with densely populated surface functional groups. To utilize the large surface area of functionalized polymer cubosomes as nanoreactor, we introduced the L-proline moieties to the acetylene groups at the surface of polymer cubosomes by CuAAC click chemistry. The resulting polymer cubosomes were examined as a nanoreactor in which the asymmetric aldol reaction of 4-nitrobenzaldehyde and acetone to yield (R)-4-hydroxy-4-(4-nitrophenyl)butan-2-one takes place.

### **3.2 Introduction**

A nanoreactor provides a nanoscale porous cage that is separated from the surrounding environment. This chemical reactor can control the selectivity and rate of the catalytic reaction by limiting the diffusion of reagents.<sup>[1-4]</sup> This nanoreactor has the advantage of increasing the stability of catalysts that are unstable in the external bulk environment, increasing reaction efficiency, and enabling reuse of catalysts. In particular, mesoporous materials have been spotlighted as promising

support materials for nanoreactors containing small-sized catalysts.<sup>[5-7]</sup>

Mesoporous materials are a class of porous materials with well-defined nanochannels and with a pore size of 2-50 nm.<sup>[8]</sup> These mesoporous materials contain highly ordered mesostructures and have size-controllable pores, large surface areas, and pore volumes. Due to these characteristics, it has the advantage of smooth diffusion of substrate molecules. Based on these points, mesoporous materials are expected to be applied in various fields such as catalysts, adsorption, membranes, separations, and sensors.<sup>[8,9]</sup> These mesoporous materials are composed of various materials such as silica, alumina, carbon, frameworks, zeolites and polymers.<sup>[10]</sup> Recently, among these materials, research on mesoporous materials based on inexpensive and durable polymers has been actively studied. Representatively, there is a polymer cubosome reported by Kim's group.<sup>[11]</sup>

Polymer cubosomes contain pores with diameters ranging from 37 to 50 nm on the surface and have highly ordered periodic porous polymer nanostructures inside. These polymeric cubosomes are composed of inverse cubic mesophases of block copolymer bilayers and internalize networks of two non-intersecting nanochannels arranged in cubic crystal order. In addition, since the hydrophobic block is composed of polystyrene chains, it has a relatively robust structure with a high glass transition temperature ( $T_g$ ) and high surface-area-to-volume ratios.<sup>[12]</sup> In particular, based on the advantage of having a large surface area, polymer cubosomes have the potential to be used as scaffolds for nanotemplating, drug delivery, separation, catalysis and chemical reactors.<sup>[4,13,14]</sup> In order to realize these applications, it is very important to modify the properties of the mesopore surface or to give functional groups.<sup>[11]</sup>

However, realizing a mesoporous polymer structure containing high-density

functional groups on the surface still remains challenges. In previous studies<sup>[15]</sup>, when surface functional groups were imparted through block copolymer binary blending method, there was a problem in that morphology transitions occurred from inverse bicontinuous structures to other phases when the blending ratio exceeded a certain ratio.

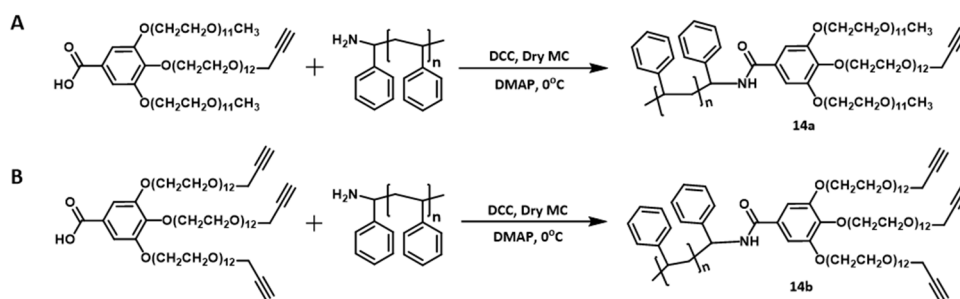
Herein, we report polymer cubosomes with high-density surface functional groups. We synthesized branched-linear block copolymers having hydrophilic blocks composed of three poly(ethylene glycol)s (PEGs) with an alkyne end group. In order to compare the difference according to the density of high-density functional groups present on the surface of the structure, hydrophilic blocks made of PEGs were synthesized to have one and three alkyne groups at the ends, respectively. Hydrophobic block was synthesized through atom transfer radical polymerization (ATRP) of styrene (Sty), and block copolymer was prepared through *N,N'*-Dicyclohexylcarbodiimide (DCC) coupling of hydrophilic block and hydrophobic block. Solution self-assembly of these block copolymers (BCPs) revealed the well-defined polymer cubosomes with densely populated surface functional groups.

### **3.3 Results and discussion**

#### **3.3.1 Synthesis of block copolymers containing alkyne groups**

According to previous studies, preferential self-assembly of block copolymers (BCPs) into polymer cubosome requires the hydrophilic block to have a branched architecture.<sup>[11,12,16]</sup> Therefore, to obtain high density surface-functionalized polymer cubosomes, we synthesized branched-linear block copolymers having hydrophilic blocks composed of three poly(ethyleneglycol)s (PEGs) with an alkyne end group. And to realize robust self-assembled structures, polystyrene (PS) with a high glass

transition temperature ( $T_g$ ) was used for the hydrophobic block. Each of two blocks were combined by a reaction using N,N'-Dicyclohexylcarbodiimide (DCC) after terminal modification. Two types of polymers were synthesized, one containing single acetylene group and the other containing three acetylene groups (Scheme 3.1).<sup>[17-22]</sup> This strategy was introduced to compare the efficiency of different surface functional group densities after becoming polymer cubosomes with high density of functional groups. These two types of BCPs were characterized by <sup>1</sup>H NMR and GPC (Fig. 3.15a-d)



**Scheme 3.1** Chemical structure of branched-linear block copolymer containing functional groups: a) one acetylene group; b) three acetylene groups.

The BCPs were self-assembled under standard conditions.<sup>[23]</sup> The BCP self-assembled into polymer cubosomes with one alkyne functional group (14a), of which the average diameter was 2-5 $\mu$ m, as analyzed in SEM and TEM images (Figure 3.1a-d). Nano scale pores on the surface and regular channels on the inside, which are typical characteristics of polymer cubosomes, were also observed. The Small angle X-ray scattering (SAXS) results for dried polymer cubosomes of the BCPs (14a) denote a set of peaks corresponding to the Schwarz minimal D surface ( $Pn\bar{3}m$  symmetry, lattice constant ( $a$ ) = 50.3 nm) (Figure 3.1e).

### 3.3.2 Synthesis of polymer cubosome with high density functional groups

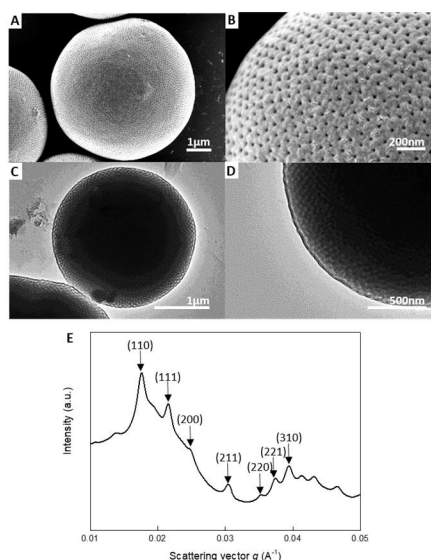


**Figure 3.1** Characterization of polymer cubosomes containing one acetylene group (14a): a),b) SEM images of surface mesopores and c),d) TEM images of internal structures. e) The peaks of polymer cubosomes corresponding to  $Pn\bar{3}m$  symmetry analyzed by SAXS (lattice constant  $a=50.3$  nm).

Similarly, BCPs (14b) with three alkyne functional groups became a polymer cubosomes through solution self-assembly, and SEM and TEM images showed that it had an average diameter of about 2  $\mu\text{m}$ , micropores on the surface, and internal channels (Figure 3.2a-d). In addition, the SAXS results also revealed the set of peaks corresponding to the Schwarz minimal D surface ( $Pn\bar{3}m$  symmetry, lattice constant ( $a$ ) = 37.2 nm) (Figure 3.2e). As a result, polymer cubosomes with high density alkyne groups were well synthesized in standard self-assembly condition.

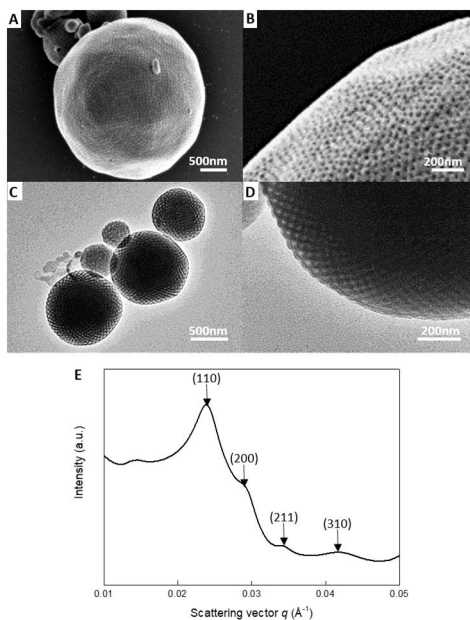
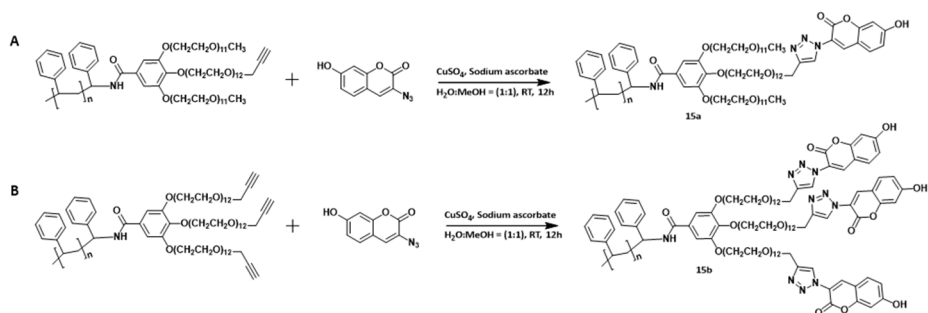


**Figure 3.2** Characterization of polymer cubosomes containing three acetylene groups (14b): a),b) SEM images of surface mesopores and c),d) TEM images of internal structures. e) The peaks of polymer cubosomes corresponding to  $Pn\bar{3}m$  symmetry analyzed by SAXS (lattice constant  $a=37.2$  nm).

### 3.3.3 Click reaction on the surface of polymer cubosomes

Click chemistry was introduced to confirm that the alkyne functional groups are well located on the surface of the polymer cubosomes and that these functional groups react well.<sup>[24]</sup> We synthesized a coumarin dye containing an azide functional group. Synthesized 3-azidocoumarin was analyzed by  $^1\text{H}$  NMR (Figure 3.16).<sup>[24,25]</sup> Coumarin was attached to the surface of polymer cubosomes dispersed in water using Copper (I)-catalyzed azide-alkyne cycloadditions (CuAAC) (Scheme 3.2).<sup>[26,27]</sup>





**Scheme 3.2** Scheme for Copper (I)-catalyzed azide-alkyne cycloadditions (CuAAC) of polymers with alkyne groups and azido coumarin in water condition.

Through surface and internal structure analysis by SEM and TEM images, no morphological transition and damages of self-assembled structure were observed in both polymers even after the click reaction (Figure 3.3a-d). After cycloaddition by injecting an excess amount of 3-azidocoumarin, the binding of the coumarin dye showed blue luminescence ( $\lambda_{\text{Ex}} = 404 \text{ nm}$ ,  $\lambda_{\text{Em}} = 477 \text{ nm}$ ) was analyzed through confocal laser scanning microscopy (CLSM) without any purification (Figure 3.3e, f). According to previous studies,<sup>[26,27]</sup> azido-coumarin dyes have been reported to exhibit luminescent properties only when they contain triazole moieties through click chemistry.

Therefore, the set of peaks corresponding to SAXS data after the CuAAC remained unchanged. This result also provided evidence that the self-assembled structure was intact and that each polymer cubosomes exhibited the Schwarz minimal D surface ( $Pn\bar{3}m$  symmetry, lattice constant ( $a$ ) = 53.1 nm, 52.8 nm) (Figure 3.3g, h). These results suggest that the alkyne functional groups of polymer cubosomes are well exposed to the surface and the movement and diffusion of coumarin dye and reagents into the channel are smooth.

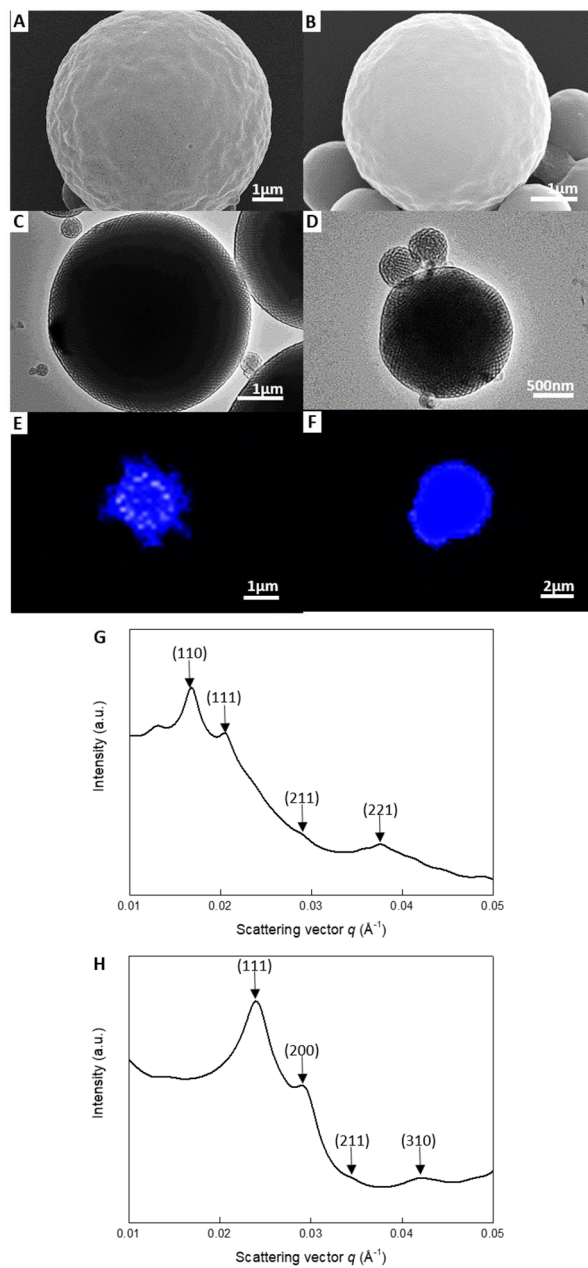


**Figure 3.3** Characterization of polymer cubosomes after CuAAC (15a and 15b): SEM image of a) 15a and b) 15b. TEM image of c) 15a and d) 15b. Blue luminescence of e) 15a and f) 15b analysed by CLSM images ( $\lambda_{\text{Ex}} = 404 \text{ nm}$ ,  $\lambda_{\text{Em}} = 477 \text{ nm}$ ). The SAXS spectra for g) 15a ( $a = 53.1 \text{ nm}$ ) and h) 15b ( $a = 52.8 \text{ nm}$ ).

### 3.4 Conclusion

In summary, we report high density surface-functionalized polymer cubosomes by synthesizing branched-linear block copolymers having hydrophilic blocks composed of three poly(ethyleneglycol)s (PEGs) with an alkyne end group. And click chemistry was performed on the surface of the functionalized polymer cubosomes to show that post modification of the surface is possible. Then, based on this report, polymer cubosomes with high-density surface alkyne groups can be used as nanoreactors for an asymmetric aldol reaction by introducing L-proline into the surface using click chemistry.<sup>[4,28]</sup> These will be performed as high efficiency materials for nanoreactor attributed to its large surface area.

### 3.5 Experimental

#### 3.5.1 Materials

All reagents were obtained from commercial sources and used without purification unless otherwise stated. CH<sub>2</sub>Cl<sub>2</sub> (MC) was dried over CaH<sub>2</sub> and freshly distilled before use. DMF was kept over molecular sieves prior to use. THF was distilled over Na/benzophenone immediately before use. Solvents and reagents were deoxygenated when necessary by purging with nitrogen.

#### 3.5.2 Techniques

<sup>1</sup>H NMR spectra was recorded at 400 MHz and 500 MHz, respectively on an Agilent 400-MR DD2 spectrometer and a Bruker DRX (500 MHz) NMR spectrometer. All NMR spectra were measured at 25 °C in the indicated deuterated solvents. Residual protic solvent of CDCl<sub>3</sub> (<sup>1</sup>H, δ 7.26 ppm) or CD<sub>2</sub>Cl<sub>2</sub> (<sup>1</sup>H, δ 5.30 ppm) and tetramethylsilane (TMS) were used as the internal reference in the <sup>1</sup>H-NMR spectra.

### **3.5.2.1 Matrix-Assisted Laser Desorption/Ionization Time of Flight (MALDI-TOF)**

Matrix-assisted laser desorption ionization time-of-flight mass spectroscopy (MALDI-TOF MS) was performed using a Bruker Ultra flex III TOF-TOF mass spectrometer equipped with a nitrogen laser (335nm). The experimental sample was prepared by mixing block copolymers dissolved in THF (5mg mL<sup>-1</sup>) and matrix solution (sinapic acid or dithranol in THF, 30mg mL<sup>-1</sup>). The prepared sample was dropped onto the MALDI plate and dries at room temperature before measurement.

### **3.5.2.2 Scanning Electron Microscopy (SEM)**

Scanning electron microscopy (SEM) was performed on Hitachi S-4300 at an acceleration voltage of 15kV. Sample was prepared by dropping the self-assembled solution onto a slide glass and drying at room temperature. The prepared by sample was coated with Pt by using Hitachi E-1030 ion sputter (20mA, 60s).

### **3.5.2.3 Field-Emission Scanning Electron Microscope (FE SEM)**

Field-Emission Scanning electron microscopy (FE-SEM) was performed on Carl Zeiss SUPRA 55VP at an acceleration voltage of 15kV. Sample was prepared by dropping the self-assembled solution onto a slide glass and drying at room temperature. The prepared by sample was coated with Pt by using Hitachi E-1030 ion sputter (20mA, 60s).

### **3.5.2.4 Transmission Electron Microscopy (TEM)**

Transmission electron microscopy (TEM) images were obtained on JEOL JEM-2100 microscope at 200kV and Hitachi 7600 at 100kV. Specimens were prepared by adding a drop of the suspension of self-assembled structures onto a carbon-coated Cu grid (200 mesh, EM science). After 30 min, remaining solution on a grid was removed with a filter paper, and the grid was air-dried at room temperature overnight.

### 3.5.2.5 Small-Angle X-ray Scattering (SAXS)

Synchrotron small angle X-ray scattering data were obtained on the SAXS beam line (PLS-II 6D, 11.18 keV, 6.5m) at Pohang acceleration laboratory (Pohang, Korea). The concentrated suspension of the polymer structures was dried for 2 days in freeze dryer. The resulting power was placed on a customized holder. Ti-SBA standard was used and X-ray irradiation time was 2~10 seconds dependent on the saturation level of the detector.

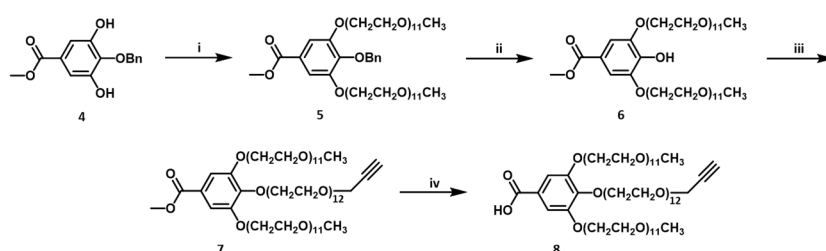
### 3.5.2.6 Confocal Laser Scanning Microscope (+Super-resolution) (CLSM)

CLSM images of cylindrical micelles of BCP labeled with azido-Coumarin (Sigma Aldrich,  $\lambda_{\text{Ex}} = 404 \text{ nm}$ ,  $\lambda_{\text{Em}} = 477 \text{ nm}$ ) were obtained using Leica, SP8 X. 5-10  $\mu\text{L}$  of concentrated suspension of fluorescently labeled structure was placed on a slide glass and sealed with cover glass. Residual solution was removed by filter paper and cover glass was fixed with sealant.

## 3.5.3 Synthesis

Tosyl terminated PEGs used in this study were synthesized as previously reported. [18,29]

### 3.5.3.1 Preparation of hydrophilic blocks with alkyne groups



**Scheme 3.3** Reaction conditions for each step: (i)  $\text{CH}_3(\text{OCH}_2\text{CH}_2)_{11}\text{OTs}$ ,  $\text{K}_2\text{CO}$ ,  $\text{KI}$ , Acetone,  $80 \text{ }^\circ\text{C}$ ; (ii)  $\text{Pd/C}$  (5%), Dry MeOH,  $55 \text{ }^\circ\text{C}$ , reflux; (iii)  $\text{HCCCH}_2(\text{OCH}_2\text{CH}_2)_{12}\text{OTs}$ ,  $\text{K}_2\text{CO}_3$ ,  $\text{KI}$ , Acetone,  $80 \text{ }^\circ\text{C}$ ; (iv)  $\text{KOH}$ , EtOH, reflux.<sup>[17]</sup>

(4). 3g of Methyl 3,4,5-trihydroxybenzoate, 2.2mL of benzyl bromide 5g of  $K_2CO_3$  and 0.02g of KI were dissolved in Acetone (50mL) and stirred for 8h at 80°C. Then reaction mixture was cool to room temperature and was poured in MC (100mL). The organic mixture was quenched with 1M HCl and washed with Brine for 3 times. The combined organic layer was dried over  $MgSO_4$  and filtered. The crude was concentrated under reduced pressure and the residue was purified by column chromatography with a mobile phase of EA /n-Hexane 5~10%. After that product was recrystallized in EA/n-Hexane.<sup>[30]</sup>

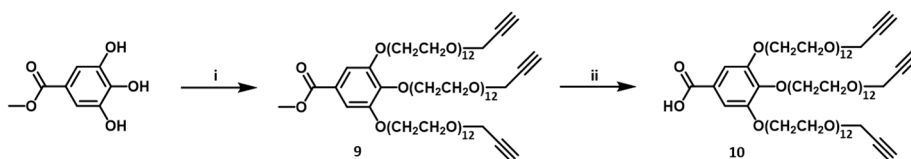
(5). 0.5g of **4**, 6g of poly(ethylene glycol) monomethyl ether tosylate, 3g of  $K_2CO_3$  and 0.2g of KI were dissolved in Acetone (100mL) and stirred for 3days at 80°C under  $N_2$ . Thereafter, the reaction mixture was quenched with 100 mL of D.I water and the mixture was extracted with MC for three times. An organic layer was dried over  $MgSO_4$  and filtered. The crude was concentrated by rotary evaporator. Then residue was purified by column chromatography with a mobile phase of MC/MeOH 5%.

(6). 3g of **5** and 0.05g of palladium on activated carbon 5% was added into 100mL Dry MeOH. The mixture was bubbling with  $H_2$  for 1h and then stirred at 55 °C for 12 h under  $H_2$ . Then the mixture was cool to room temperature and filtered through Celite®. The filtrate was concentrated to dryness.

(7). 2g of **6**, 5g of  $HCCCH_2(OCH_2CH_2)_{12}OTs$ , 3g of  $K_2CO_3$  and 0.2g of KI were added in Acetone(100mL). The mixture was stirred at 80 °C for 3ays under  $N_2$ . Then, the reaction mixture was quenched with 1m HCl and the mixture was poured into 200 mL of MC. The organic layer was washed with Brine for 3 times and dried over  $MgSO_4$ . The crude was concentrated by rotary evaporator. The residue was purified

by column chromatography with a mobile phase of MC/MeOH 5%.

**(8).** 1g of **7** and 1.5g of KOH was added into 50mL EtOH. The mixture was stirred at 85 °C for 12 h under N<sub>2</sub>. After cooling to room temperature, 1M HCl was added until pH = 1 at 0 °C. Then the reaction mixture was extracted with MC. The organic layer was dried over MgSO<sub>4</sub> and filtered. The filtrate was evaporated under reduced pressure.

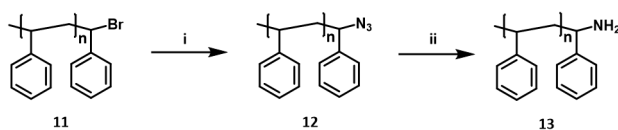


**Scheme 3.4** Reaction conditions for each step: (i) HCCCH<sub>2</sub>(OCH<sub>2</sub>CH<sub>2</sub>)<sub>12</sub>OTs, K<sub>2</sub>CO<sub>3</sub>, KI, Acetone, 80 °C; (ii) KOH, EtOH, reflux.<sup>[18]</sup>

**(9).** 0.3g of Methyl 3,4,5-trihydroxybenzoate and 6g of HCCCH<sub>2</sub>(OCH<sub>2</sub>CH<sub>2</sub>)<sub>12</sub>OTs, 3g of K<sub>2</sub>CO<sub>3</sub> and 0.02g of KI were dissolved in 100mL of Acetone. The mixture was stirred at 80 °C for 3days under N<sub>2</sub>. After that reaction mixture was cool to room temperature and was quenched with 1M HCl. The mixture was extracted with MC and the organic layer was dried over MgSO<sub>4</sub>. The crude was concentrated by rotary evaporator. The residue was purified by column chromatography MC/MeOH 5%.

**(10).** 1g of **9** and 1.5g of KOH was added into 50mL EtOH. The mixture was stirred at 85 °C for 12 h under N<sub>2</sub>. After cooling to room temperature, 1M HCl was added until pH = 1 at 0 °C. Then the reaction mixture was extracted with MC. The organic layer was dried over MgSO<sub>4</sub> and filtered. The filtrate was evaporated under reduced pressure.

### 3.5.3.2 Preparation of hydrophobic blocks with amino group



**Scheme 3.5** Reaction conditions for each step: (i) DMF,  $\text{NaN}_3$ , R.T, 12h; (ii) Dry THF,  $\text{LiAlH}_4$ ,  $70^\circ\text{C}$ , 3h.<sup>[19-21]</sup>

**(11).** Polymerization of styrene was performed under a standard ATRP condition. 15mg of  $\text{CuBr}$  and 30mL of  $\text{N,N,N',N'',N''}$ -pentamethyldiethylenetriamine (PMDETA) were mixed with 1mL of anisole in a Schlenk flask with a magnetic bar. The mixture was stirred for 15min under  $\text{N}_2$ . To this solution, the mixture of styrene monomer (70mL) and 10mg of 1-Bromoethylbenzene was added via syringe. The green solution was degassed by bubbling  $\text{N}_2$  for 15min. After degassing, the flask was immersed in a preheated oil bath ( $95^\circ\text{C}$ ). The progress of polymerization was monitored by taking GPC at an interval of 1h. When the molecular weight of the polymer reached to the desired value, the reaction was quenched with  $\text{CHCl}_3$  and cooling in a freezer. The cooled solution was filtered through a pack of aluminium oxide(basic) with  $\text{CHCl}_3$  to remove the  $\text{Cu}^{2+}$ . The filtrate was concentrated on a rotary evaporator, and the resulting residue was diluted with MC. The solution was precipitated into MeOH. White powder was collected by vacuum filtration and dried in vacuo.<sup>[19]</sup>

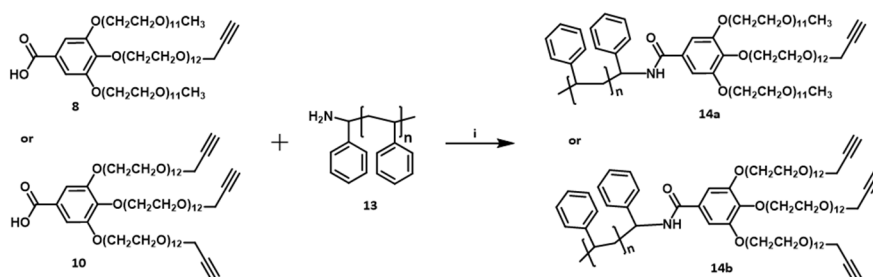
**(12).** 1g of brominated polystyrene (Br-PS) and 0.3g of sodium azide were dissolved in DMF (100mL) stirring at room temperature. After 12h, DMF was removed by a rotary evaporator and precipitated into MeOH several times. The azido polystyrene ( $\text{N}_3$ -PS) was dried under reduced pressure.<sup>[20]</sup>

**(13).** 1g of azido polystyrene( $\text{N}_3$ -PS) was added to THF (200mL) solution of  $\text{LiAlH}_4$



(0.01g) at 0 °C under N<sub>2</sub>. The mixture was stirred at 70 °C for 3h. The mixture was quenched with the water. Then 1M NaOH aqueous solution was added. When the reaction mixture was turned into a clear solution with a gray precipitate. The solution was filtered and the filtrate was poured into MeOH. Then the amine terminated polystyrene (NH<sub>2</sub>-PS) was collected by vacuum filtration and dried in vacuo.<sup>[21]</sup>

### 3.5.3.3 Preparation of block copolymers



**Scheme 3.6** Reaction conditions: (i) Dry MC, DCC, DMAP, 0 °C.<sup>[17,22]</sup>

**(14a).** 0.1g of **8**, 0.02g of N,N'-dicyclohexylcarbodiimide(DCC) and 0.002g of 4-dimethylaminopyridine(DMAP) were dissolved in Dry MC (1mL) . The mixture was stirred for 30min under N<sub>2</sub>. To this solution, a Dry MC (5mL) solution of **13** (3g) was added by canula at 0 °C. The reaction mixture was stirred for 3h and concentrated by rotary evaporator. The residue was diluted with MC and precipitated into MeOH. White powder was collected by vacuum filtration and dried in vacuo. The residue was purified by column chromatography with a mobile phase of MC/MeOH 5%.

**(14b).** 0.1g of **10**, 0.02g of N,N'-dicyclohexylcarbodiimide(DCC) and 0.002g of 4-dimethylaminopyridine(DMAP) were dissolved in Dry MC (1mL) . The mixture was stirred for 30min under N<sub>2</sub>. To this solution, a Dry MC (5mL) solution of **13** (3g)

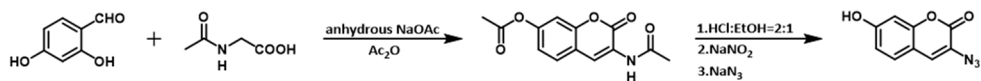
was added by canula at 0 °C. The reaction mixture was stirred for 3h and concentrated by rotary evaporator. The residue was diluted with MC and precipitated into MeOH. White powder was collected by vacuum filtration and dried in vacuo. The residue was purified by column chromatography with a mobile phase of MC/MeOH 5%.

**Table 3.1** Characterization of polymers.

BCP	$M_n$ (kg mol <sup>-1</sup> ) <sup>a</sup>	$\mathcal{D}^a$
<b>13a</b>	19.4	1.08
<b>13b</b>	23.8	1.05
<b>14a</b>	22.5	1.07
<b>14b</b>	28.2	1.03

<sup>a</sup>Determined by GPC using THF as an eluent.

### 3.5.3.4 Preparation of 3-azidocoumarin



**Scheme 3.7** Synthetic procedure for 3-Azidocoumarin.<sup>[25,26]</sup>

**3-Azidocoumarin.** 3g of 2,4-dihydroxy benzaldehyde, 2.5g of *N*-acetylglycine, 5.3g of anhydrous sodium acetate were dissolved in acetic anhydride (100 ml) and refluxed under stirring for 4 h. The reaction mixture was poured onto ice to give a yellow precipitate. After filtration, the yellow solid was washed with ice D.I water. Then the yellow solid was refluxed in a solution of conc. HCl and EtOH (2:1, 30 mL) for 1 hour. The reaction mixture was added to 40mL of ice D.I water. The diluted solution was cooled in an ice bath and 3g of NaNO<sub>2</sub> was added. Then the mixture

was stirred for 10 minutes and 4.3g of  $\text{NaN}_3$  was added in portions. The reaction mixture was stirred 15min, resulting precipitate was filtered off and washed with D.I water. The product was dried in vacuo to yield a brown solid.

### **3.5.4 Preparation of polymer cubosome**

#### **3.5.4.1 Solution self-assembly of block copolymers.**

For BCPs, 10mg of the amphiphilic block copolymer was dissolved in 2 mL of 1,4-dioxane or Acetone (1 wt %) in a capped vial, and the solution was stirred for 15 minutes at room temperature. 2 mL of D.I water was added at a controlled rate ( $0.5 \text{ mL h}^{-1}$ ) to the solution via a syringe pump with vigorous stirring. The resulting solution was dialyzed (molecular weight cutoff (MWCO) = 12-14 kDa, SpectraPor) against water for 1 day.<sup>[23]</sup>

#### **3.5.4.2 Copper (I) catalyzed azide-alkyne cycloaddition of block copolymers.**

10mg of block copolymers and 10mg of 3-azidocoumarin were dissolved in solution of MeOH and D.I water (1:1, 20mL) in capped vial. To this mixture,  $3\mu\text{L}$  of 0.1M  $\text{CuSO}_4$  aqueous solution and 0.05mL of 0.1M NaAsc aqueous solution were added and mixed using shaker for 12h at room temperature. Then the residue was dialyzed (molecular weight cutoff (MWCO) = 12-14 kDa, SpectraPor) against water for 1 day.<sup>[26]</sup>

### **3.5.5 Characterization**

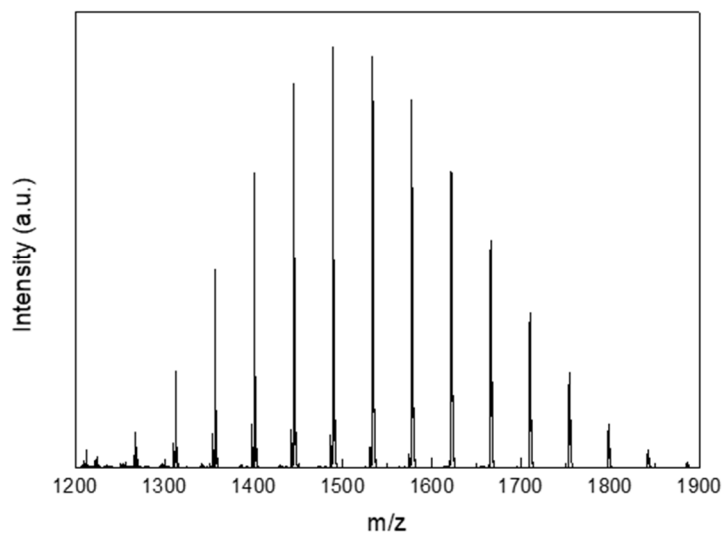


**Figure 3.4** MALDI-TOF mass spectrum of compound **5** (MW= 1,489.75 g mol<sup>-1</sup>).

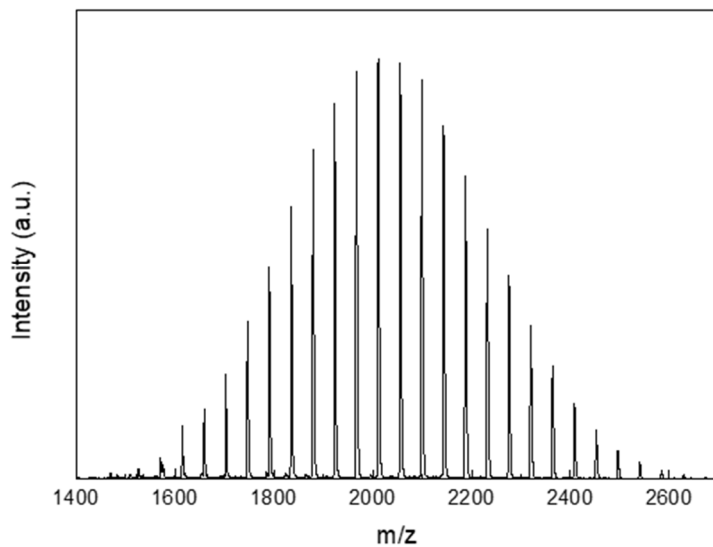


**Figure 3.5** MALDI-TOF mass spectrum of compound **7** (MW= 2,011.76 g mol<sup>-1</sup>).

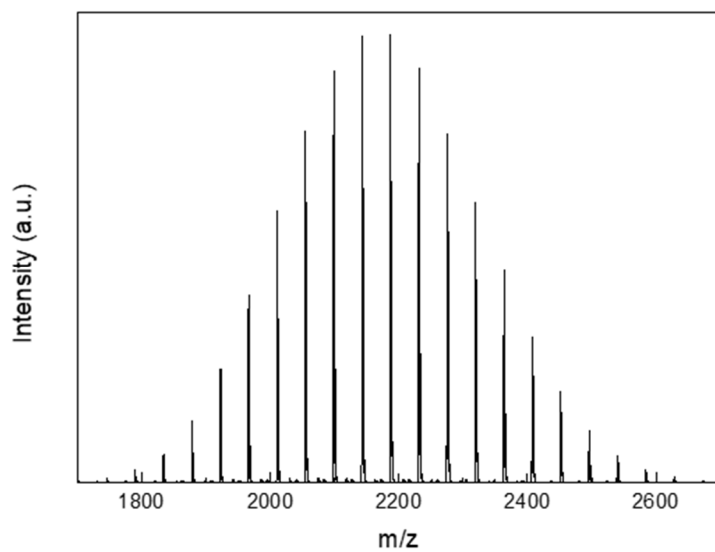


**Figure 3.6** MALDI-TOF mass spectrum of compound **9** (MW= 2,186.16 g mol<sup>-1</sup>).

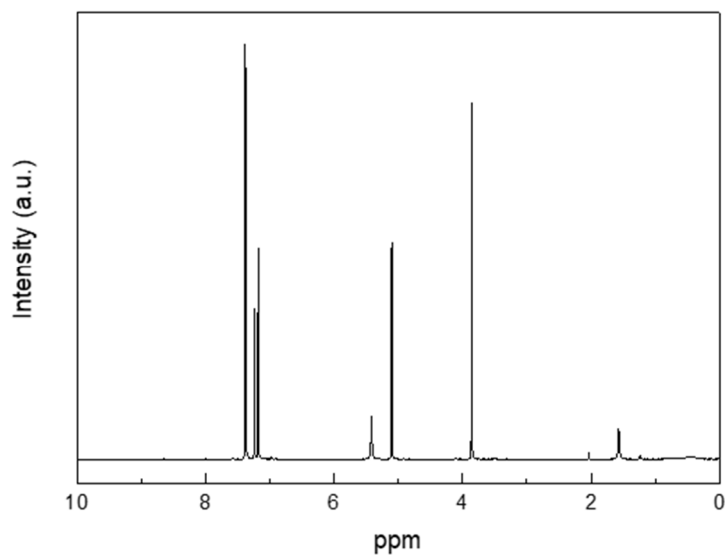


**Figure 3.7** <sup>1</sup>H NMR spectrum of compound **4**.

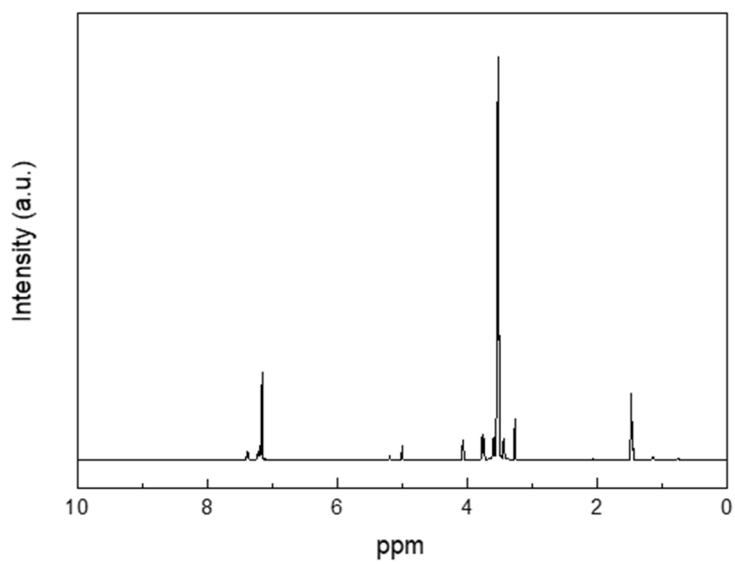


**Figure 3.8**  $^1\text{H}$  NMR spectrum of compound **5**.

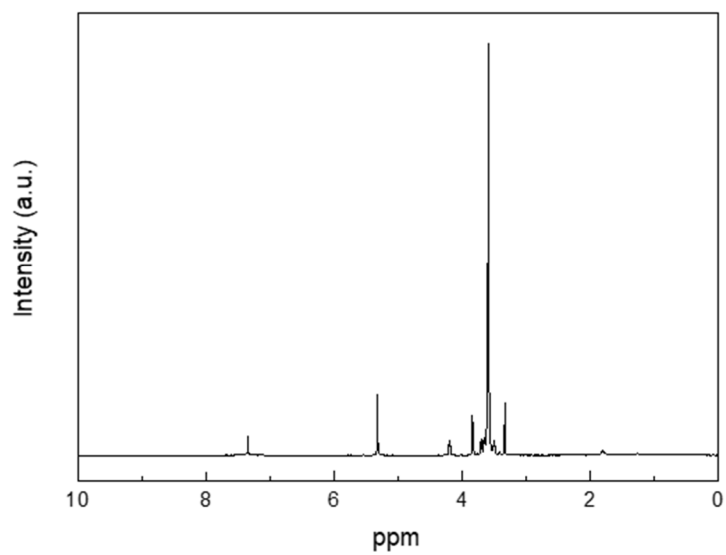


**Figure 3.9**  $^1\text{H}$  NMR spectrum of compound **6**.

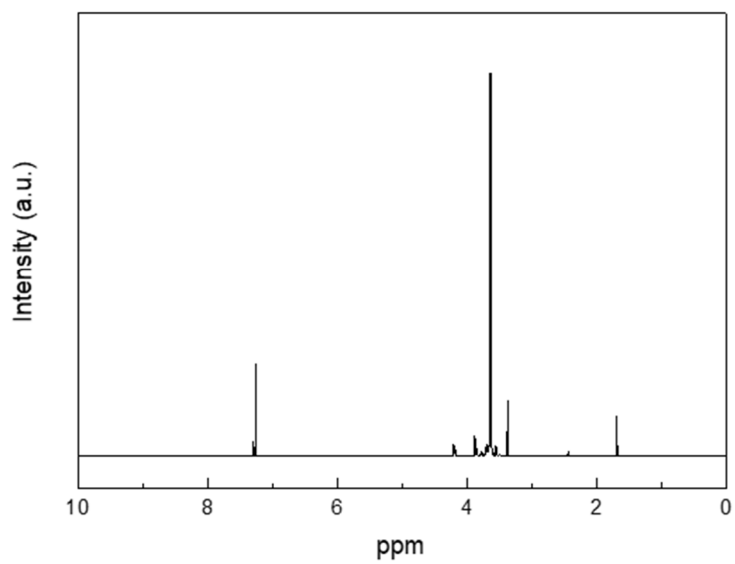


**Figure 3.10**  $^1\text{H}$  NMR spectrum of compound 7.

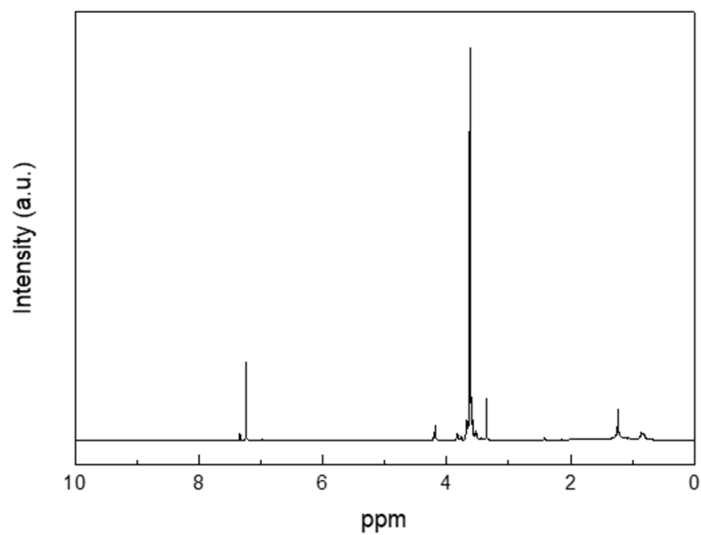


**Figure 3.11**  $^1\text{H}$  NMR spectrum of compound 8.

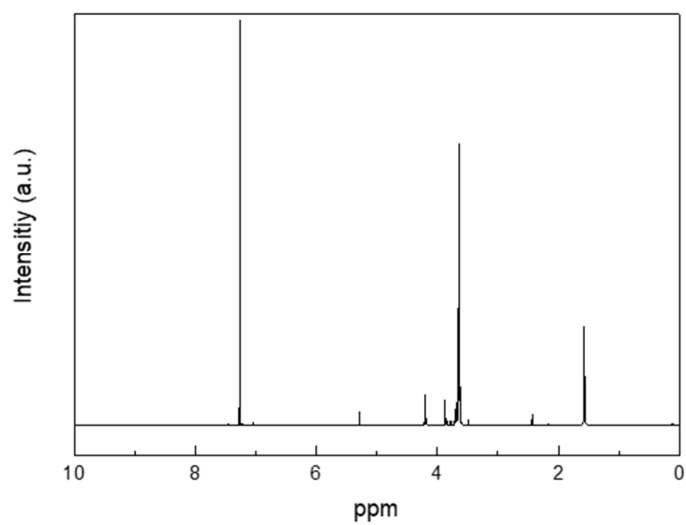


**Figure 3.12** <sup>1</sup>H NMR spectrum of compound **9**.

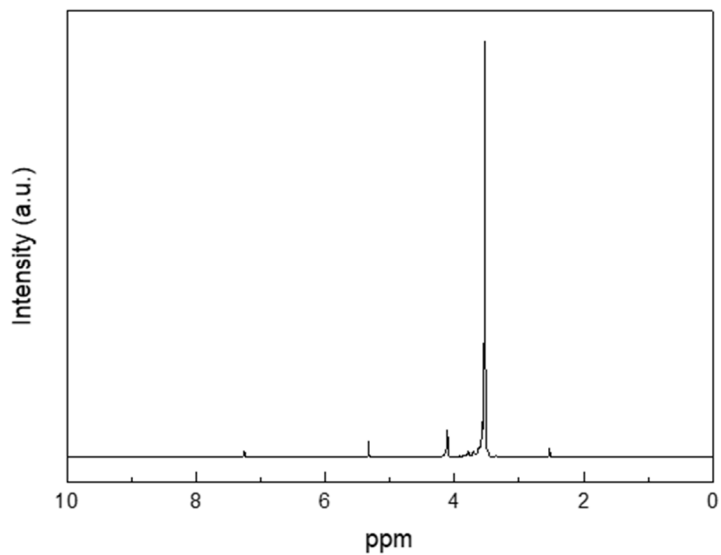


**Figure 3.13** <sup>1</sup>H NMR spectrum of compound **10**.



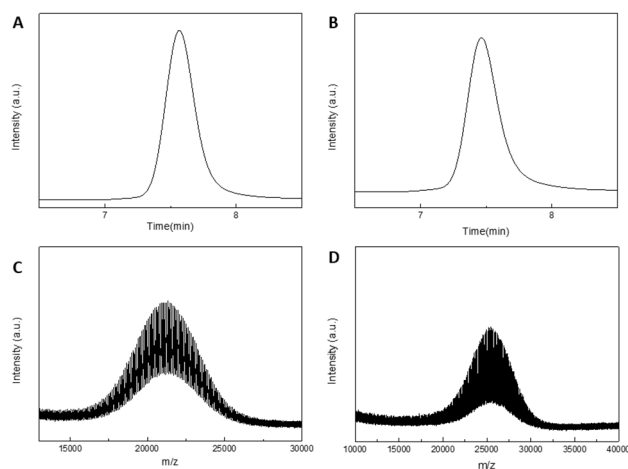


**Figure 3.14** Characterization of amine terminated polystyrene ( $\text{NH}_2\text{-PS}$ ):  $^1\text{H}$  NMR spectrum of a) **13a** ( $M_n = 19,439 \text{ g mol}^{-1}$ ,  $D = 1.0759$ ) and b) **13b** ( $M_n = 23,785 \text{ g mol}^{-1}$ ,  $D = 1.0548$ ). MALDI-TOF mass spectrum of c) **13a** ( $MW = 21,235.53 \text{ g mol}^{-1}$ ) and d) **13b** ( $MW = 25,406.96 \text{ g mol}^{-1}$ ).

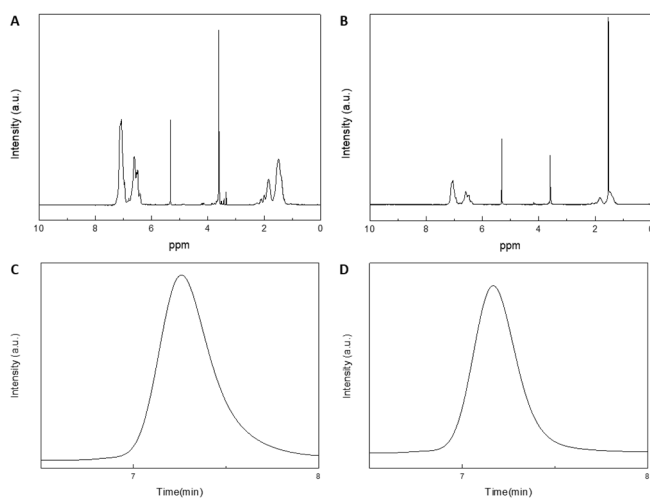


**Figure 3.15** Characterization of block copolymers:  $^1\text{H}$  NMR spectrum of a) **14a** and b) **14b**. THF GPC spectrum of c) **14a** ( $M_n = 22,511 \text{ g mol}^{-1}$ ,  $D = 1.0739$ ) and d) **14b** ( $M_n = 28,164 \text{ g mol}^{-1}$ ,  $D = 1.0301$ ).

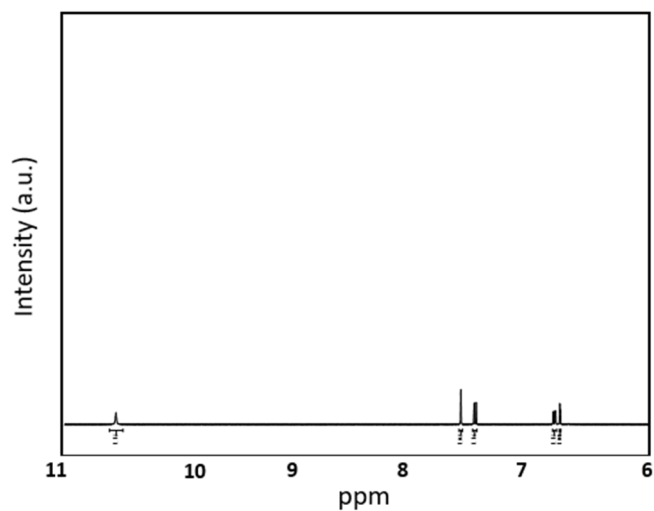


**Figure 3.16**  $^1\text{H}$  NMR spectrum of 3-azidocoumarin.

### 3.6 Reference

- [1] Palivan, C. G; Fischer-Onaca, O.; Delcea, M.; IteI, F.; Meier, W. *Chem. Soc. Rev.* **2012**, *41*, 2800–2823.
- [2] Wang, X.; Feng, J.; Bai, Y.; Zhang, Q.; Yin, Y. *Chem. Rev.* **2016**, *116*, 10983–11060.
- [3] Vázquez-González, M.; Wang, C.; Willner, I. *Nat. Catal.* **2020**, *3*, 256–273.
- [4] Kwon, J. H.; Kim, J.; Kim, K. T. *Polym. Chem.* **2021**, *12*, 2701.
- [5] Petrosko, S. H.; Johnson, R.; White, H.; Mirkin, C. A. *J. Am. Chem. Soc.* **2016**, *138*, 7443–7445.
- [6] Swisher, J. H.; Jibril, L.; Petrosko, S. H.; Mirkin, C. A. *Nat. Rev. Mater.* **2022**, *7*, 428–448.
- [7] Syah, R.; Zahar, M.; Kianfar, E. *Int. J. Chem. React. Eng.* **2021**, *19*, 981–1007.
- [8] Lan, K.; Zhao, D. *Nano Lett.* **2022**, *22*, 3177–3179.
- [9] Liu, Y.; Ohnishi, K.; Sugimoto, S.; Okuhara, K.; Maeda, R.; Nabae, Y.; Kakimoto,

- M.; Wang, X.; Hayakawa, T. *Polym. Chem.* **2014**, *5*, 6452.
- [10] Verma, P.; Kuwahara, Y.; Mori, K.; Raja, R.; Yamashita, H. *Nanoscale*, **2020**, *12*, 11333.
- [11] La, Y.; Park, C.; Shin, T. J.; Joo, S. H.; Kang, S.; Kim, K. T. *Nat. Chem.* **2014**, *6*, 534–541.
- [12] Ha, S.; La, Y.; Kim, K. T. *Acc. Chem. Res.* **2020**, *53*, 620–631.
- [13] Lee, H.; Kim, D.; Ma, H.; Kim, K. T. *Chem. Commun.* **2020**, *56*, 14059–14062.
- [14] Song, J.; Choi, S.; Lim, J.; Kim, K. T. *RSC Adv.* **2022**, *12*, 8429–8434.
- [15] Cho, A.; La, Y.; Jeoung, S.; Moon, H. R.; Ryu, J.H.; Shin, T. J.; Kim, K. T. *Macromolecules* **2017**, *50*, 3234.
- [16] An, T. H.; La, Y.; Cho, A.; Jeong, M. G.; Shin, T. J.; Park, C.; Kim, K. T. *ACS Nano* **2015**, *9*, 3084.
- [17] Zhang, S.; Xiao, Q.; Sherman, S. E.; Muncan, A.; Vicente, A. D. M. R.; Wang, Z.; Hammer, D. A.; Williams, D.; Chen, Y.; Pochan, D. J.; Vértessy, S.; André, S.; Klein, M. L.; Gabius, H. J.; Percec, V. *J. Am. Chem. Soc.* **2015**, *137*, 13334–13344.
- [18] Li, C.; Zhang, S.; Pang, J.; Wu, Y.; Gu, Z. *Adv. Funct. Mater.* **2015**, *25*, 3764–3774.
- [19] Jeong, M. G.; van Hest, J. C. M.; Kim, K. T. *Chem. Commun.* **2012**, *48*, 3590–3592.
- [20] Cho, A.; La, Y.; Shin, T. J.; Park, C.; Kim, K. T. *Macromolecules* **2016**, *49*, 4510–4519.
- [21] Matyjaszewski, K.; Nakagawa, Y.; Gaynor, S. G. *Macromol. Rapid Commun.* **1997**, *18*, 1057–1064.
- [22] Percec, V.; Wilson, D. A.; Leowanawat, P.; Wilson, C. J.; Hughes, A. D.;

Kaucher, M. S.; Hammer, D. A.; Levine, D. H.; Kim, A. J.; Bates, F. S.; Davis, K. P.; Lodge, T. P.; Klein, M. L.; DeVane, R. H.; Aqad, E.; Rosen, B. M.; Argintaru, A. O.; Sienkowska, M. J.; Rissanen, K.; Nummelin, S.; Ropponen, J. *Science* **2010**, *328*, 1009–1014.

[23] An, T. H.; La, Y.; Cho, A.; Jeong, M. G.; Shin, T. J.; Park, C.; Kim, K. T. *ACS Nano* **2015**, *9*, 3084.

[24] Kolb, H. C.; Finn, M. G.; Sharpless, K. B. *Angew. Chem., Int. Ed.* **2001**, *40*, 2004–2021.

[25] Ngororabanga, J. M. V.; Okerio, J.; Mama, N. S. *Afr. J. Chem.* **2017**, *70*, 89–93.

[26] Sivakumar, K.; Xie, F.; Cash, B. M.; Long, S.; Barnhill, H. N.; Wang, Q. *Org. Lett.* **2004**, *6*, 4603–4606.

[27] Schiedel, M. S.; Briehn, C. A.; Bauerle, P. *Angew. Chem. Int. Ed.* **2001**, *40*, 4677–4680.

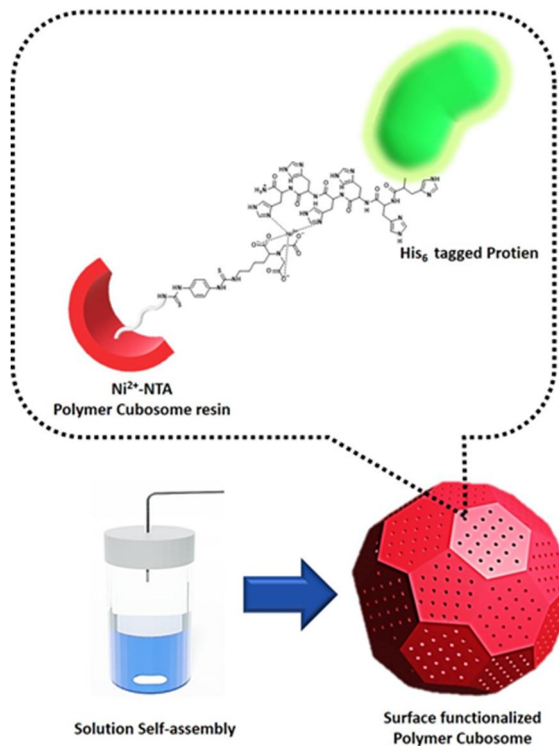
[28] Ayats, A.; Henseler, A. H.; Pericàs, M. A. *ChemSusChem* **2012**, *5*, 320–325.

[29] Pawlak, M.; Mistlberger, G.; Bakker, E.; *J. Mater. Chem.* **2012**, *22*, 12796–12801.

[30] Pearson, A. J.; Bruhn, P. R. *J. Org. Chem.* **1991**, *56*, 7092–7097.

# Chapter 4

## Polymer cubosomes as a stationary phase for affinity chromatography of proteins



## **4.1 Abstract**

(This work was collaborated with Prof. Kyoung Taek Kim)

Solution self-assembly is one of the good tools to create various microstructures. Among various structures, polymer cubosome is highly ordered periodic nanostructures composed of the triply periodic minimal surfaces with inverse bicontinuous cubic (IBC) mesophases. In addition, it has a large surface area due to its meoporous structure, so it is a visionary material that can be applied in various fields by introducing functional groups to the surface. In this report, we suggest polymer cubosomes having high-density amine groups on the surface. To utilize the large surface area of functionalized polymer cubosomes as affinity-based separation of biomolecules, we introduced the Ni-NTA complex to the amine groups at the surface of polymer cubosomes. The resulting polymer cubosomes were examined as a highly efficient stationary phase for the immobilized metal ion affinity chromatography to separate the His-tagged protein.

## **4.2 Introduction**

In the post-genomic era, with the development of molecular biology, efforts have been made to understand the vast amount of biological genetic information at the molecular level.<sup>[1]</sup> In particular, since gene products and proteins are indispensable to each other, studies have emerged to artificially produce and analyze recombinant proteins with desired functions and characteristics.<sup>[2]</sup> In order to accurately analyze the synthesized proteins, a technology to separate them purely was required. As a result, purification methods that can selectively separate proteins have emerged one by one. These strategies used properties such as solubility, charge, size, shape, and hydrophobicity of proteins. Representative methods include precipitation, phase

partitioning, and chromatography.<sup>[3]</sup> Various methods have been developed, but among them, Immobilized-Metal Affinity Chromatography (IMAC), which utilizes the selective affinity between a transition metal ion ( $\text{Ni}^{2+}$ ,  $\text{Fe}^{2+}$ ,  $\text{Ca}^{2+}$ ,  $\text{Co}^{2+}$ ,  $\text{Cu}^{2+}$ ,  $\text{Zn}^{2+}$ ) immobilized on an insoluble resin and a specific functional group of an amino acid, has been used as a powerful tool to facilitate protein purification.<sup>[4]</sup>

IMAC was reported by Porath et al. in 1975 as a method of strongly immobilizing metal ions in a stationary phase such as agarose gel based on the affinity between the transition metal and histidine or cysteine in solution. This method has advantages such as specific binding, mild elution conditions and the ability to control selectivity by including low concentrations of imidazole in chromatography buffers. And various types of materials were intended to be used as stationary phase resins for immobilization, high loading capacity, and easy separation and purification. For example, agarose gel, beads, nanoparticles, etc. have attached metal ions.<sup>[4,5]</sup>

Nickelated nitrilotriacetic acid (Ni-NTA) is one of the metal-affinity coordination methodologies and metal chelator complexes used in IMAC along with Nickelated iminodiacetic acid (Ni-IDA) to purify His-tag proteins.<sup>[6]</sup> Nitrogen of imidazole present in histidine acts as an electron donor, and chelated  $\text{Ni}^{2+}$  acts as an electron acceptor, showing high affinity.<sup>[5]</sup> In addition, these metal chelator complexes have been widely used by being attached to stationary phases such as gold nanoparticles, magnetic beads, and polymer microspheres. Recently, research on improving purification efficiency by using a stationary phase having a large surface area, such as mesoporous silica, has been reported.<sup>[7-10]</sup>

Polymer cubosomes reported in previous studies are produced through solution self-assembly of amphiphilic block copolymers (BCPs) composed of

Poly(ethyleneglycol)-*co*-Polystyrene (PEG-*co*-PS). It is a highly ordered periodic porous nanostructure containing large-pore networks composed of an inverse bicontinuous cubic (IBC) mesophase of a block copolymer bilayer inside.<sup>[11-13]</sup> This polymer cubosome has a large surface area and is robust due to the high glass transition temperature ( $T_g$ ) of polystyrene constituting the hydrophobic block. It is attracting attention as a material with various potential applications such as drug delivery and nanotemplating. It is attracting great attention as a material with various application possibilities such as drug delivery and nanotemplates.<sup>[14]</sup> The surface of polymer cubosomes could be easily functionalized with high-density functional groups through modifications to the ends of hydrophilic blocks composed of PEGs.

In this article, we report that polymer cubosomes containing high-density functional groups on the surface were shown via solution self-assembly of a block copolymer containing three amine groups at the end of a hydrophilic block and used as an IMAC resin that can selectively purify Histidine-tagged proteins by adding NTA ligand to the surface functional groups.

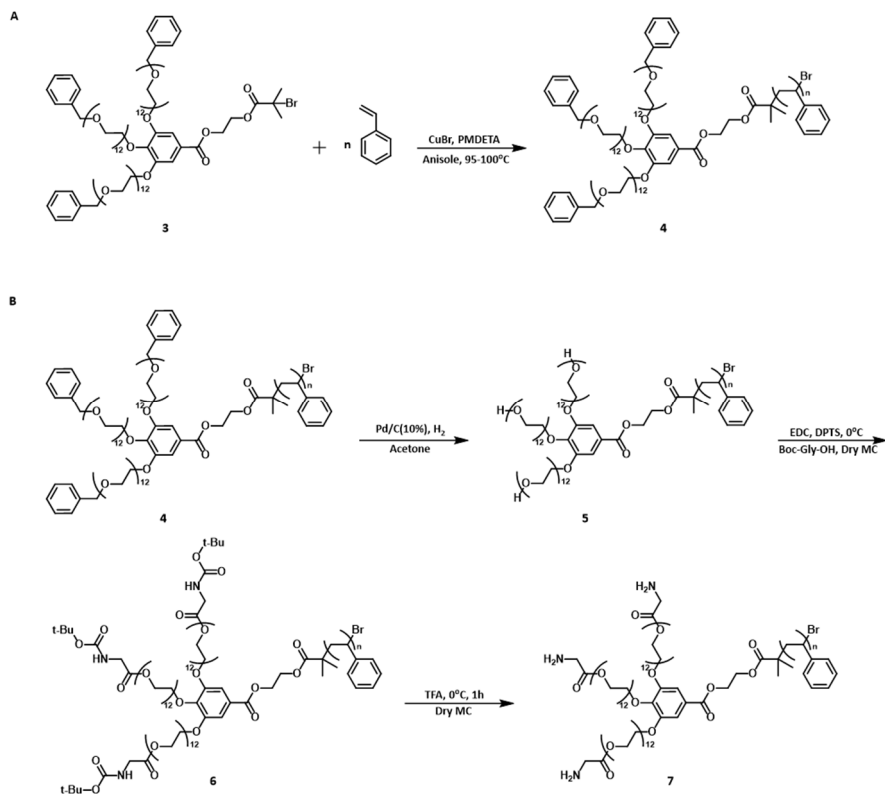
## **4.3 Results and discussion**

### **4.3.1 Synthesis of functionalized block copolymer**

The structure produced as a result of solution self-assembly of amphiphilic BCP is closely related to the chemical structure. Based on the critical packing parameter (P, defined as  $P = v/a_0l_c$ , where  $v$  is the volume of the hydrophobic part,  $a_0$  is the molecular area per amphiphile, and  $l_c$  is the critical length of the hydrophobic part) in our previous study, the branched architecture of the hydrophilic block played a crucial role in the forming the preferred self-assembly structure of branched-linear BCPs.<sup>[5]</sup> Here, a macroinitiator with a branched hydrophilic block composed of three



benzyl protected poly(ethylene glycols) was synthesized to obtain polymer cubosomes, and a branched linear BCP was produced through atom transfer radical polymerization (ATRP) using styrene as a monomer (Scheme 4.1a). As a result, the BCPs synthesized in the molecular weight range assembled into an inverse bicontinuous structure were analyzed by GPC (Figure 4.14a, b). The synthesized BCPs containing hydrophilic block end-protected with benzyl groups were modified into amine groups through a post-modification process (Scheme 4.1b). In the first step, the terminals were converted to hydroxy groups through hydrogenation followed by modification of (*tert*-butoxycarbonyl)glycine (t-Boc-glycine) via esterification. In the last step, t-Boc is eliminated through a simple deprotection process using acid to finally obtain BCPs with amine end groups.<sup>[16-18]</sup> All of these products were analyzed by <sup>1</sup>H NMR and GPC (Figure 4.13a-d and Figure 4.14c-d).



**Scheme 4.1** a) Synthesis of BCPs via ATRP. b) Post-modification process of BCPs.

### 4.3.2 Solution self-assembly of block copolymers

A series of BCPs in the process of post-modification (Table 4.1) was self-assembled under standard conditions by dissolving the BCPs in Acetone or 1,4-dioxane (1 wt%, 2mL).<sup>[19]</sup> Each self-assembled structure was analyzed by SEM. (Figure 4.1) First, in the case of Bn-PEG3-co-PS (**4a**), polymer cubosomes appeared in acetone, but only a few filled-cubosomes were observed in 1,4-dioxane. (Figure 4.1a, e) During the solution self-assembly process, it was observed that the polymers were not well dispersed in the solvent and agglomerated. We inferred that this phenomenon was caused by the increase in hydrophobicity due to the benzyl group located at the end

of the hydrophilic block, which made it difficult to dissolve in 1,4-dioxane. And in the case of OH-PEG<sub>3</sub>-co-PS (**5a**), hexosomes were formed as a result of assembly in acetone and dioxane. (Figure 4.1b, f) In acetone, t-Boc-PEG<sub>3</sub>-co-PS (**6a**) was observed as a structure in which flat tubes were tethered to particles with micropores in the core. Then hexosomes were observed in 1,4-dioxane. (Figure 4.1c, g) When all terminals became amine groups, NH<sub>2</sub>-PEG<sub>3</sub>-co-PS (**7a**) became spherical micelles in acetone and vesicles in 1,4-dioxane. (Figure 4.1d, g)

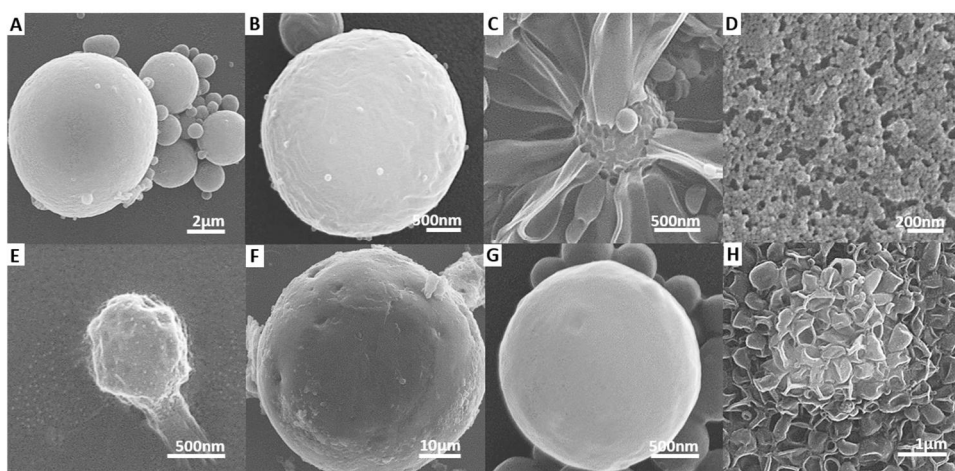


**Figure 4.1** SEM images of self-assembly structures in acetone: a) polymer cubosomes of **4a**, b) hexosome of **5a**, c) flat tubes were tethered to particles with micropores in the core of **6a**, d) spherical micelles of **7a**; In 1,4-dioxane e) filled-polymer cubosomes of **4a**, f), g) hexosome of **5a** and **6a**, h) vesicles of **7a**.

In addition, when the molecular weight of BCPs was slightly higher, Bn-PEG<sub>3</sub>-co-PS (**4b**) showed the form of cubosomes in acetone and filled-cubosomes in 1,4-dioxane, respectively. (Figure 4.2a, e) And in the case of OH-PEG<sub>3</sub>-co-PS (**5b**), vesicles appeared in acetone, but hexosomes were observed in 1,4-dioxane. (Figure 4.2b, f) Then, t-Boc-PEG<sub>3</sub>-co-PS (**6b**) produced vesicles from acetone and

hexosomes from dioxane, (Figure 4.2c, g) and vesicles were observed from both solvents in the case of  $\text{NH}_2\text{-PEG}_3\text{-}co\text{-PS}$  (**7b**). (Figure 4.2d, h) The amine groups formed a good hydrogen bond with the solvent, and as a result, the hydrophilicity increases, resulting in the same effect as relatively increasing the  $a_0$  value.<sup>[20]</sup>

We post-modify the ends of a batch of polymers sequentially and found that the structures resulting from solution self-assembly in each modification step show morphological transitions under the influence of terminal functional groups. This is in line with the results of previous studies, and we believe that using this strategy will help to easily obtain various microstructures in the future.

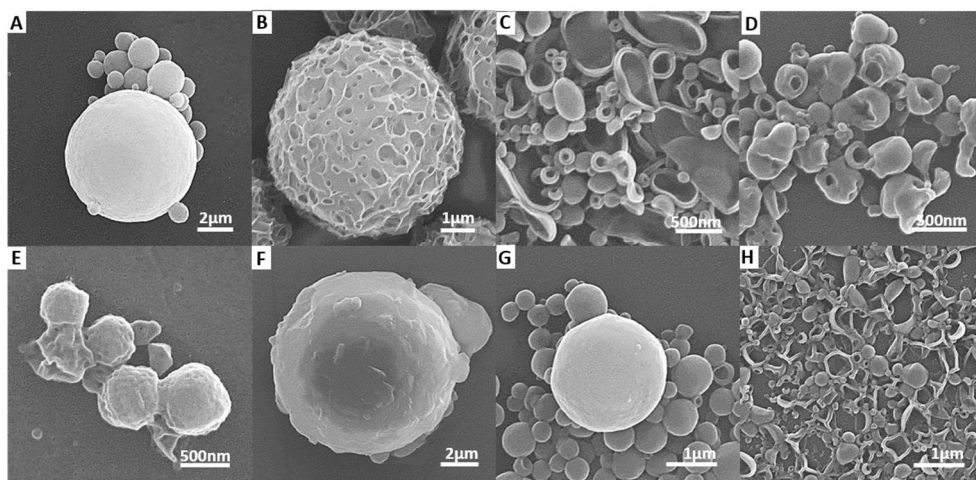


**Figure 4.2** SEM images of self-assembly structures in acetone: a) polymer cubosomes of **4b**, b) sponge structure of **5b**, c), d) vesicles of **6b** and **7b**; In 1,4-dioxane e) filled-polymer cubosomes of **4b**, f), g) hexosome of **5b** and **6b**, h) vesicles of **7b**.

### 4.3.3 Protonation of block copolymers containing amine end groups

As mentioned above, the desired structure of polymer cubosomes could not be obtained due to the high hydrophilicity of the amine groups. To obtain polymer cubosomes, we tried new strategies to relatively reduce the hydrophilicity by protonating the amine groups. The first attempt was to precipitate BCPs containing amine groups in a mixed solution of methanol and 10 mM HCl, dry the precipitates, and proceed with self-assembly in the same manner as before. As a result, in the case of **7a**, a unique structure was observed in acetone. (Figure 4.3a, b) The particles about 2  $\mu\text{m}$  in size were covered with a smooth surface without pores on one side and tethered with very small vesicular petals on the other side. In the case of **7b**, fine vesicles and some particles with a broken surface structure were observed. (Figure 4.4a, b) On the other hand, in 1,4-dioxane, small vesicles and polymer cubosomes were mixed in the case of **7a**, (Figure 4.3c, d) and cylindrical micelles and particles having multiple layers with a diameter close to 10  $\mu\text{m}$  were mixed in the case of **7b**. (Figure 4.4c, d) We reasoned that these structures are a kind of defect during self-assembly because the amine group was not sufficiently protonated during the precipitation process. So, as a second strategy, 2mL of 10mM HCl was used instead of D.I water in the self-assembly process. As a result, particles in which fine vesicular petals were tethered appeared in both **7a** and **7b** in acetone. (Figure 4.3e, f and Figure 4.4e, f) However, in 1,4-dioxane, well-defined polymer cubosomes were observed in both polymers. (Figure 4.3g, h and Figure4.4g, h) In addition, using TEM, it was analyzed that these cubosomes have regular channels inside. (Figure 4.5a-d)

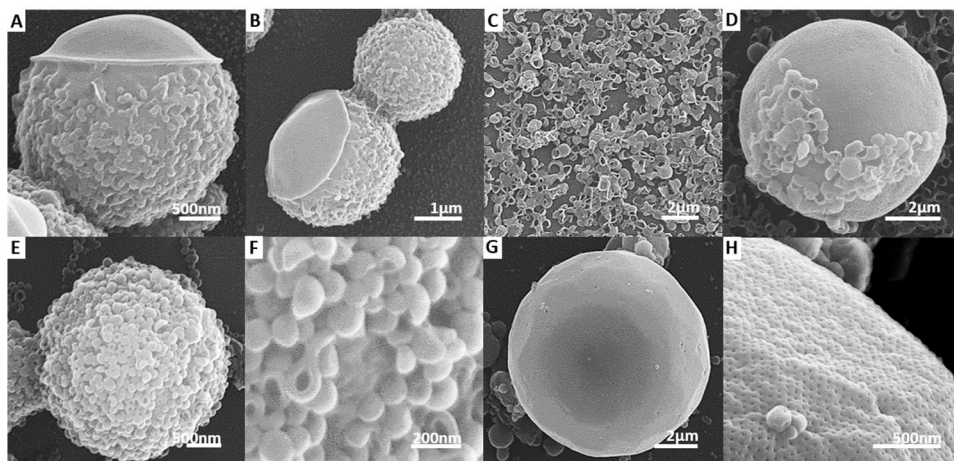


**Figure 4.3** SEM images of self-assembly structures of **7a**: the case of **7a** precipitated in mixed solution of MeOH and 10 mM HCl a), b) in acetone, the particles covered with a smooth surface without pores on one side and tethered with very small vesicular petals on the other side and c), d) in 1,4-dioxane, small vesicles and polymer cubosomes.; the case of self-assembly with 10mM HCl e), f) in acetone, particles in which fine vesicular petals were tethered and g), h) in 1,4-dioxane, well-defined polymer cubosomes.

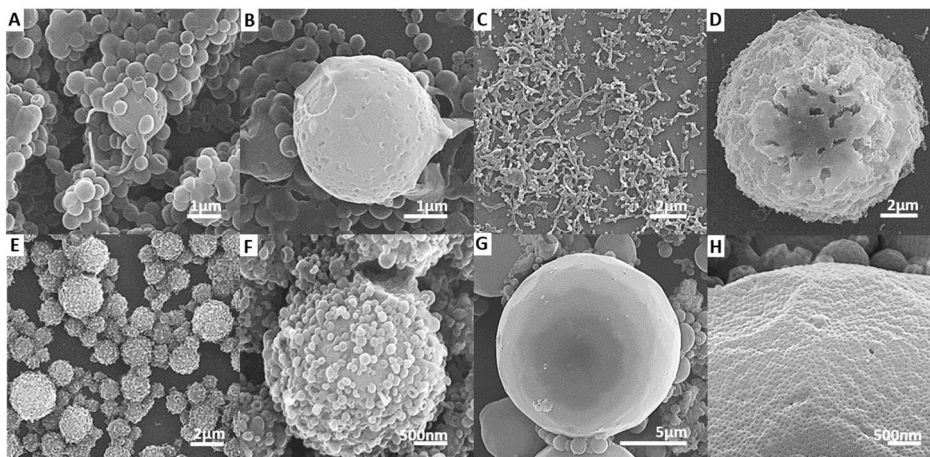


**Figure 4.4** SEM images of self-assembly structures of **7b**: the case of **7b** precipitated in mixed solution of MeOH and 10 mM HCl a), b) in acetone, fine vesicles and some particles with a broken surface structure and c), d) in 1,4-dioxane, cylindrical micelles and particles having multiple layers.; the case of self-assembly with 10mM HCl e), f) in acetone, particles in which fine vesicular petals were tethered and g), h) in 1,4-dioxane, well-defined polymer cubosomes.

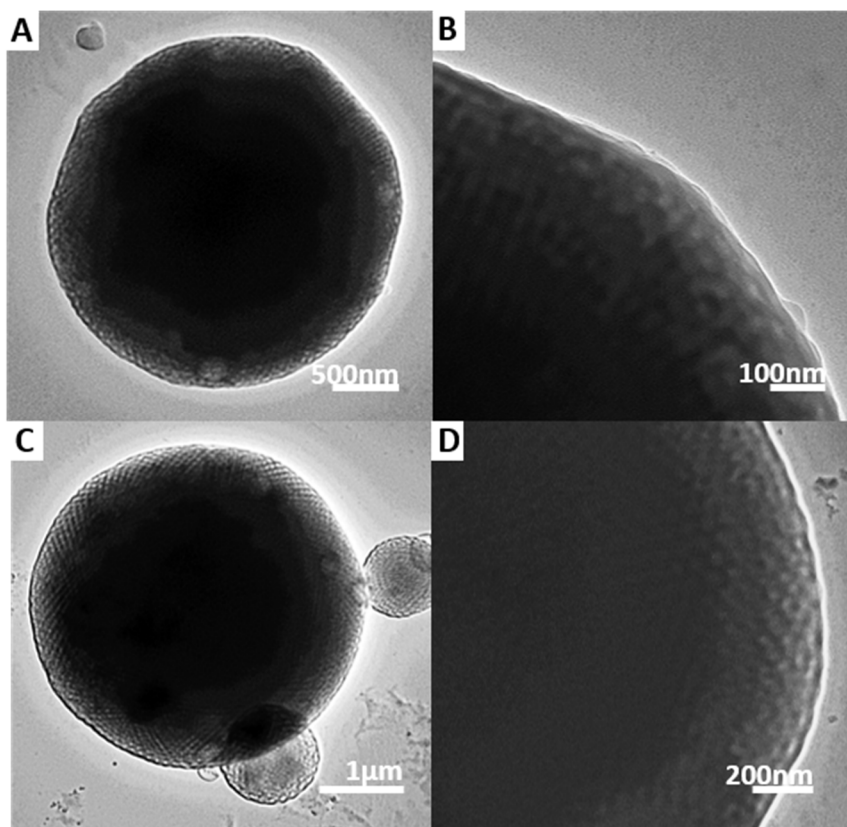


**Figure 4.5** TEM image of the structures self-assembled with 10mM HCl: a), b) polymer cubosome internal channels of **7a** and c), d) polymer cubosome internal channels of **7b**.

#### 4.3.4 Synthesis of Ni-NTA polymer cubosome resin

We tried to introduce the Nickel-Nitrilotriacetic acid (Ni-NTA) complex to use the previously implemented polymer cubosome containing high-density amine functional groups on the surface as a stationary phase for immobilized metal ion affinity chromatography. The NTA ligands were attached to the surface of the cubosome using *p*-Phenylene diisothiocyanate, which has high reactivity with the amine group. (Figure 4.6)<sup>[21]</sup> Besides, Ni<sup>2+</sup> ions were coordinatively combined with



NTA ligands to synthesize high-efficiency Histidine-tagged protein purification resins.<sup>[22]</sup>

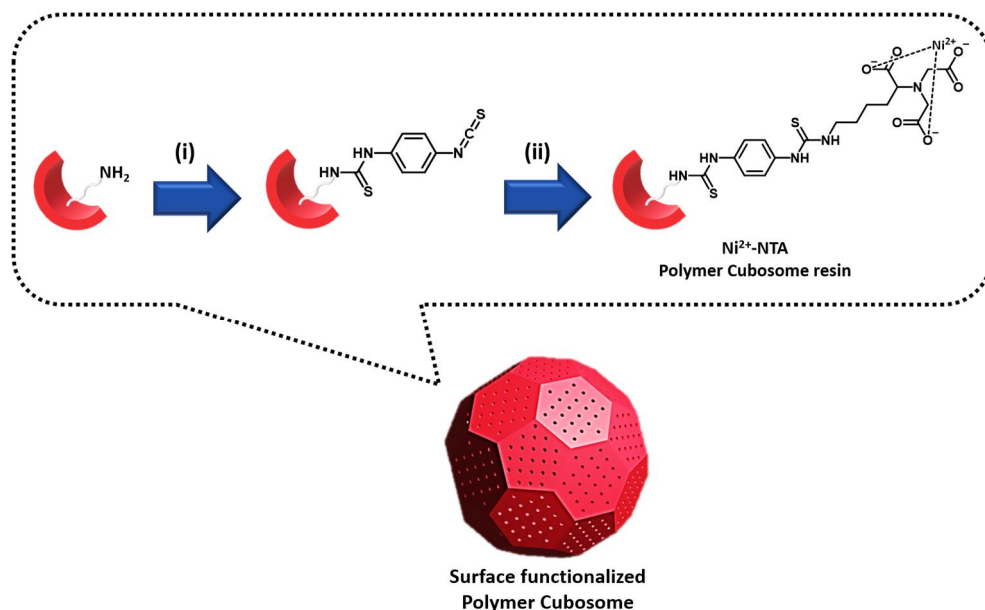


**Figure 4.6** Schematic illustration of introducing the Ni-NTA complex to polymer cubosome surface with high density amine groups. Reaction conditions for each step:

(i) *p*-Phenylene diisothiocyanate, MeOH, 40°C; (ii) NTA, water, NiSO<sub>4</sub>.

## 4.4 Conclusion

In summary, we synthesized branched-linear block copolymers containing functional groups at the end of the hydrophilic block and obtained polymer cubosomes with high-density amine functional groups on the surface through solution self-assembly. In the process of synthesizing polymer cubosomes, morphological transitions of structures resulting from self-assembly were also observed under the influence of the polymer chain terminal functional groups. These

phenomena are expected to be of great help in making various microstructures easily in the future. Then, we introduced Ni-NTA complex to the functional groups at the surface of polymer cubosomes using *p*-Phenylene diisothiocyanate. As a result, polymer cubosomes containing high density surface functional groups can be used as a stationary phase for the immobilized metal ion affinity chromatography to separate the His-tagged green fluorescent protein.

## **4.5 Experimental**

### **4.5.1 Materials**

All reagents were obtained from commercial sources and used without purification unless otherwise stated. CH<sub>2</sub>Cl<sub>2</sub> (MC) was dried over CaH<sub>2</sub> and freshly distilled before use. DMF was kept over molecular sieves prior to use. THF was distilled over Na/benzophenone immediately before use. Solvents and reagents were deoxygenated when necessary by purging with nitrogen.

### **4.5.2 Techniques**

<sup>1</sup>H NMR spectra was recorded at 400 MHz and 500 MHz, respectively on an Agilent 400-MR DD2 spectrometer and a Bruker DRX (500 MHz) NMR spectrometer. All NMR spectra were measured at 25 °C in the indicated deuterated solvents. Residual protic solvent of CD<sub>2</sub>Cl<sub>2</sub> (<sup>1</sup>H,  $\delta$  5.32 ppm; <sup>13</sup>C,  $\delta$  54.00 ppm (central resonance of the quintet)), and tetramethylsilane (TMS) were used as the internal reference in the <sup>1</sup>H- and <sup>13</sup>C-NMR spectra.

#### **4.5.2.1 Matrix-Assisted Laser Desorption/Ionization Time of Flight (MALDI-TOF)**

Matrix-assisted laser desorption ionization time-of-flight mass spectroscopy (MALDI-TOF MS) was performed using a Bruker Ultra flex III TOF-TOF mass spectrometer equipped with a nitrogen laser (335nm). The experimental sample was

prepared by mixing block copolymers dissolved in THF ( $5\text{mg mL}^{-1}$ ) and matrix solution (sinapic acid or dithranol in THF,  $30\text{mg mL}^{-1}$ ). The prepared sample was dropped onto the MALDI plate and dries at room temperature before measurement.

#### 4.5.2.2 Scanning Electron Microscopy (SEM)

Scanning electron microscopy (SEM) was performed on Hitachi S-4300 at an acceleration voltage of 15kV. Sample was prepared by dropping the self-assembled solution onto a slide glass and drying at room temperature. The prepared by sample was coated with Pt by using Hitachi E-1030 ion sputter (20mA, 60s).

#### 4.5.2.3 Transmission Electron Microscopy (TEM)

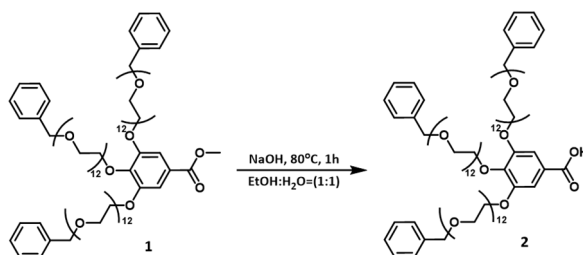
Transmission electron microscopy (TEM) images were obtained on JEOL JEM-2100 microscope at 200kV and Hitachi 7600 at 100kV. Specimens were prepared by adding a drop of the suspension of self-assembled structures onto a carbon-coated Cu grid (200 mesh, EM science). After 30 min, remaining solution on a grid was removed with a filter paper, and the grid was air-dried at room temperature overnight.

### 4.5.3 Synthesis

Tosyl terminated PEGs used in this study were synthesized as previously reported.

[11,23]

#### 4.5.3.1 Preparation of block copolymers

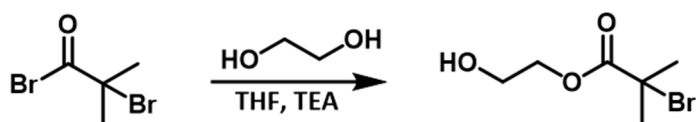


**Scheme 4.2** Synthesis of dendritic hydrophilic block.<sup>[24]</sup>

(1). 0.3g of Methyl 3,4,5-trihydroxybenzoate and 6g of  $\text{C}_6\text{H}_5\text{CH}_2(\text{OCH}_2\text{CH}_2)_{12}\text{OTs}$ ,

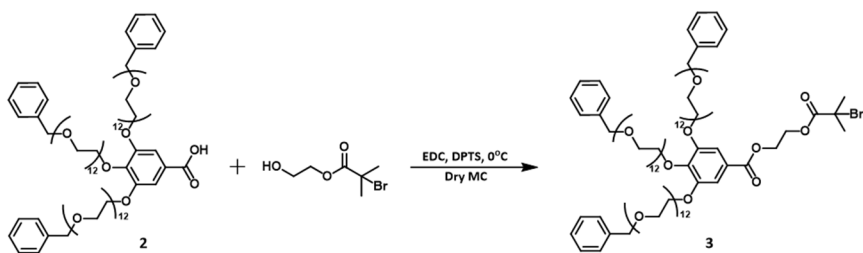
3g of  $K_2CO_3$  and 0.02g of KI were dissolved in 100mL of Acetone. The mixture was stirred at 80 °C for 3days under  $N_2$ . After that reaction mixture was cool to room temperature and was quenched with 1M HCl. The mixture was extracted with MC and the organic layer was dried over  $MgSO_4$ . The crude was concentrated by rotary evaporator. The residue was purified by column chromatography with a mobile phase of MC/MeOH 5%.

(2). 1g of **1** and 1.5g of NaOH was added into the mixture of EtOH and D.I water (1:1, 50mL). The mixture was stirred at 80 °C for 1 h under  $N_2$ . After cooling to room temperature, 1M HCl was added until pH = 1 at 0 °C. Then the reaction mixture was extracted with MC. The organic layer was dried over  $MgSO_4$  and filtered. The filtrate was evaporated under reduced pressure.



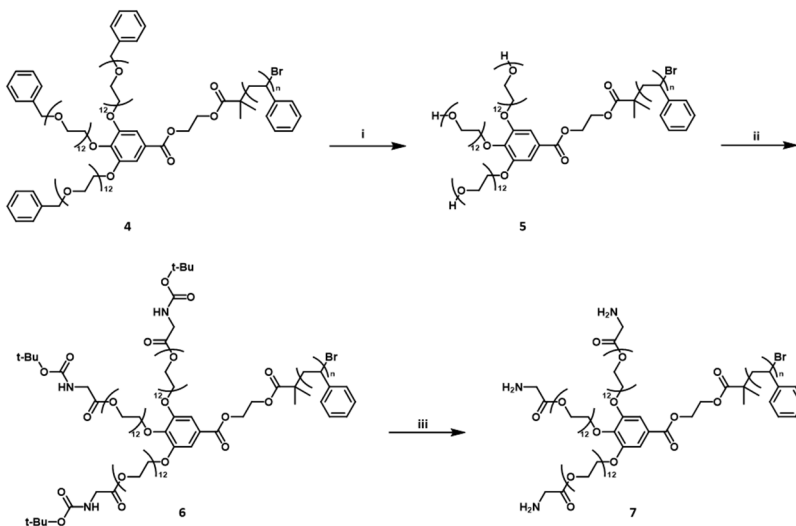
**Scheme 4.3** Synthesis of 2-hydroxyethyl 2-bromoisobutyrate.<sup>[25]</sup>

**2-hydroxyethyl 2-bromoisobutyrate.** 68g of ethylene glycol and 4.5g of TEA were dissolved in 25 mL of dry THF stirred in an ice bath. 5g of  $\alpha$ -Bromoisobutyl bromide was injected dropwise over 10 minutes and mixture was stirred under  $N_2$  at ambient temperature for 16 h. The reaction mixture was poured into 180 mL of D.I water and extracted with MC. The organic layer was washed with 1 M HCl and dried over  $MgSO_4$ . The residue was concentrated under reduced pressure.



**Scheme 4.4** Synthesis of ATRP macroinitiator.

(3). 0.5g of **2** and 0.5g of 2-hydroxyethyl 2-bromoisobutyrate were added into 3mL of Dry MC. The mixture was cooled to 0 °C on an ice bath. 0.3g of 1-Ethyl-3-(3-dimethylaminopropyl)carbodiimide (EDC) and 0.1g of 1,4-Dimethylpyridinium *p*-toluene sulfonate (DPTS) were added to the mixture. The reaction mixture was stirred for 2-3h. Then the reaction mixture was washed with D.I water and brine. The combined organic layer was dried over MgSO<sub>4</sub>, and concentrated by vacuum rotary. The crude was purified by automated column chromatography with a mobile phase of MC/MeOH 10% to yield macro initiator.<sup>[17]</sup>



**Scheme 4.5** Reaction conditions for each step: (i) Pd/C (10%), Acetone, H<sub>2</sub>; (ii) t-Boc-glycine, dryMC, EDC, DPTS, 0 °C; (iii) TFA, Dry MC, R.T, 1h.<sup>[16-19]</sup>

(4). Polymerization was performed under a standard ATRP condition. 7mg of CuBr and 15mL of N,N,N',N'',N'''-pentamethyldiethylenetriamine (PMDETA) were mixed with 10mL of anisole in a Schlenk flask with a magnetic bar. The mixture was stirred for 15min under N<sub>2</sub>. To this solution, the mixture of styrene monomer (20mL) and 500mg of **3** was added via syringe. The green solution was degassed by bubbling N<sub>2</sub> for 15min. After degassing, the flask was immersed in a preheated oil bath (95 °C). The progress of polymerization was monitored by taking GPC at an interval of 1h. When the molecular weight of the polymer reached to the desired value, the reaction was quenched with CHCl<sub>3</sub> and cooling in a freezer. The cooled solution was precipitated into MeOH. The precipitate was collected by vacuum filtration and purified by automated column chromatography with a mobile phase of EA100% and MC/MeOH 10%. The product was concentrated under reduced pressure.<sup>[19]</sup>

(5). 1g of **4** was added in 100ml schlenk flask with acetone (50mL) and 0.1g of Pd/C (10%). Vacuum the flask 2s for several times. A balloon of H<sub>2</sub> gas was injected into the vacuumed flask to purge. After that bubbling the H<sub>2</sub> gas for 2h with stirring. Then the reaction mixture was filtered with filter paper and washed with Acetone. The organic layers concentrated by rotary evaporator to **5**.<sup>[16]</sup>

(6). 0.5g of **5** and 0.06g of t-Boc-glycine were added into 3mL of Dry MC. The mixture was cooled to 0 °C on an ice bath. 0.04g of 1-Ethyl-3-(3-dimethylaminopropyl)carbodiimide (EDC) and 0.01g of 1,4-Dimethylpyridinium *p*-toluene sulfonate (DPTS) were added to the mixture. The reaction mixture was stirred for 2-3h. The crude was precipitated into MeOH several times. The precipitate was collected by vacuum filtration to yield **6**.<sup>[17]</sup>

(7). 0.5g of **6** was added in 100ml schlenk flask with dry MC (50mL) and cooled to

0 °C on an ice bath. 0.1mL of TFA was injected into the reaction mixture dropwise. After that the mixture was stirred for 2h under N<sub>2</sub>. The crude was precipitated into MeOH several times. The precipitate was collected by vacuum filtration to yield **7**.<sup>[18]</sup>

**Table 4.1** Characterization of BCPs.

BCP	$M_n$ (kg mol <sup>-1</sup> ) <sup>a</sup>	$\bar{D}$ <sup>a</sup>	$DP_n^b$	$M_n$ (kg mol <sup>-1</sup> ) <sup>b</sup>	$f_{PEG}$ (%) <sup>c</sup>
<b>4a</b>	22.3	1.08	215.4	24.7	9.0
<b>4b</b>	23.4	1.10	181.2	21.1	10.5
<b>5a</b>	17.1	1.18	208	23.6	8.3
<b>5b</b>	18.1	1.16	204	23.2	8.4
<b>6a</b>	-	-	211	24.4	9.9
<b>6b</b>	-	-	208	24.1	10.1
<b>7a</b>	18.0	1.06	217	24.7	8.6
<b>7b</b>	18.8	1.09	225	25.6	8.3

<sup>a</sup>Determined by GPC using THF or DMF as an eluent. <sup>b</sup>Calculated by <sup>1</sup>H NMR integration assuming the  $M_n$  of PEG chains of 2,000 g/mol. <sup>c</sup>Calculated by  $f_{PEG} = (M_n \text{ of PEG} / M_n \text{ of a BCP})$ .

#### 4.5.4 Preparation of polymer cubosome

##### 4.5.4.1 Solution self-assembly of block copolymers.<sup>[19]</sup>

For BCPs, 10mg of the amphiphilic block copolymer was dissolved in 2 mL of 1,4-dioxane or Acetone (1 wt %) in a capped vial, and the solution was stirred for 15 minutes at room temperature. 2 mL of D.I water or 10mM HCl was added at a controlled rate (0.5 mL h<sup>-1</sup>) to the solution via a syringe pump with vigorous stirring. The resulting solution was dialyzed (molecular weight cutoff (MWCO) = 12-14 kDa, SpectraPor) against water for 1 day.

## 4.5.5 Characterization

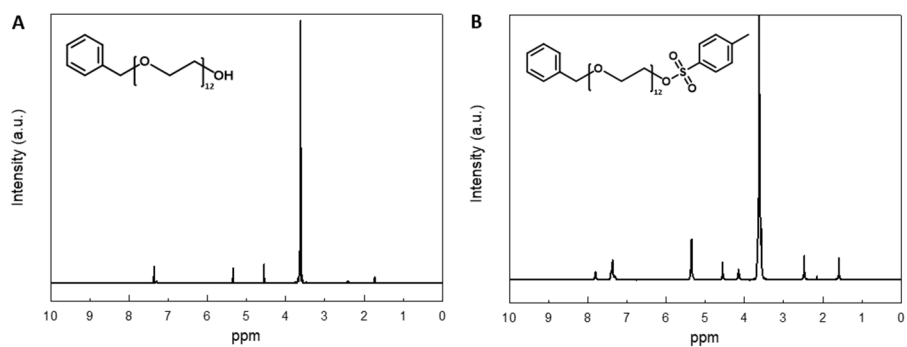


**Figure 4.7** a), b)  $^1\text{H}$  NMR spectra of PEGs.

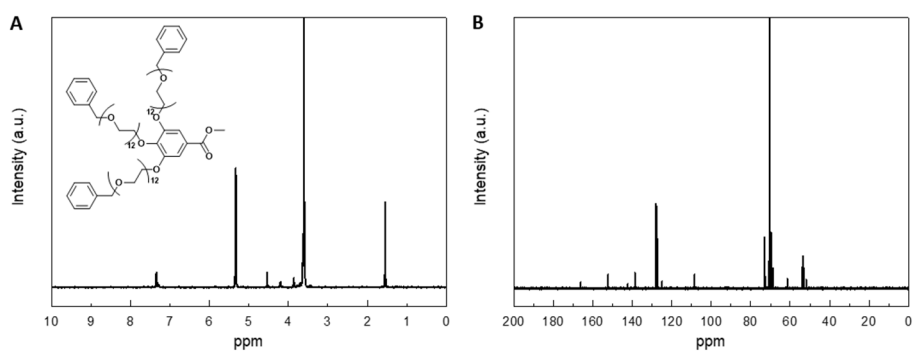


**Figure 4.8** a)  $^1\text{H}$  and b)  $^{13}\text{C}$  NMR spectra of compound 1.



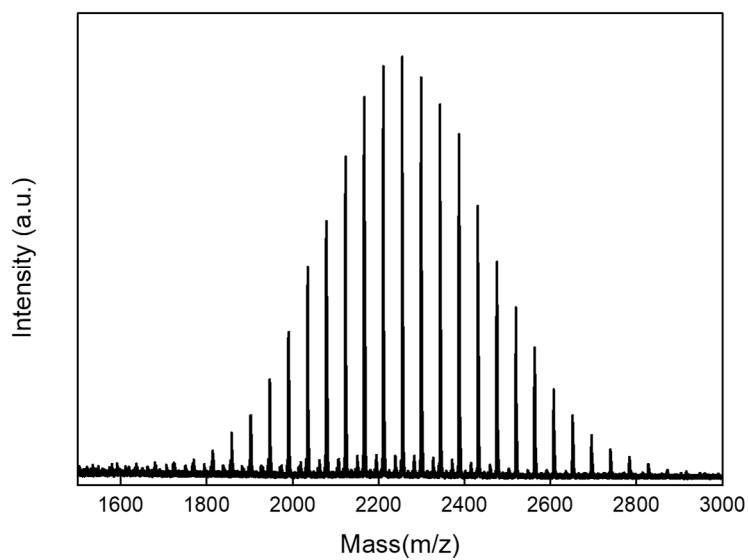


**Figure 4.9** MALDI-TOF mass spectrum of compound **1** (MW= 2,257.79 g mol<sup>-1</sup>).

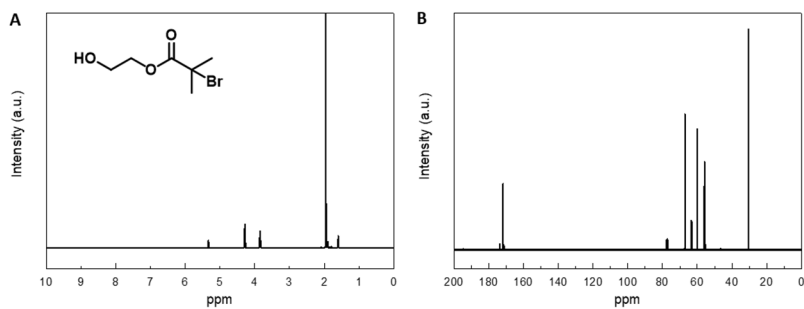


**Figure 4.10** a) <sup>1</sup>H and b) <sup>13</sup>C NMR spectrum of 2-hydroxyethyl 2-bromoisobutyrate.

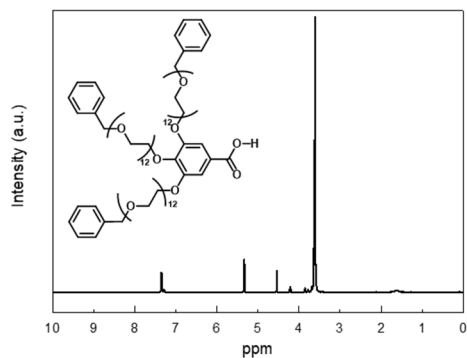


**Figure 4.11**  $^1\text{H}$  NMR spectrum of compound 2.

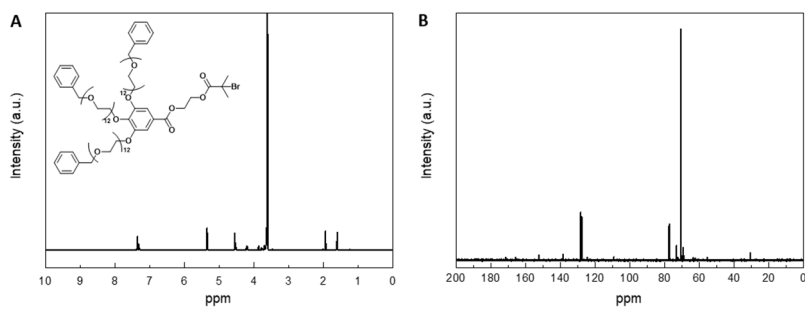


**Figure 4.12** a)  $^1\text{H}$  and b)  $^{13}\text{C}$  NMR spectra of compound 3.

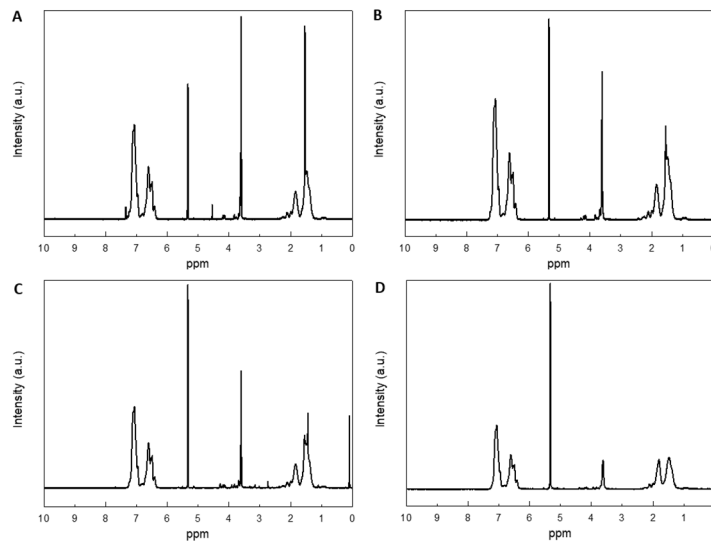


**Figure 4.13**  $^1\text{H}$  NMR spectra of compound a) **4a**, b) **5a**, c) **6a**, d) **7a**.

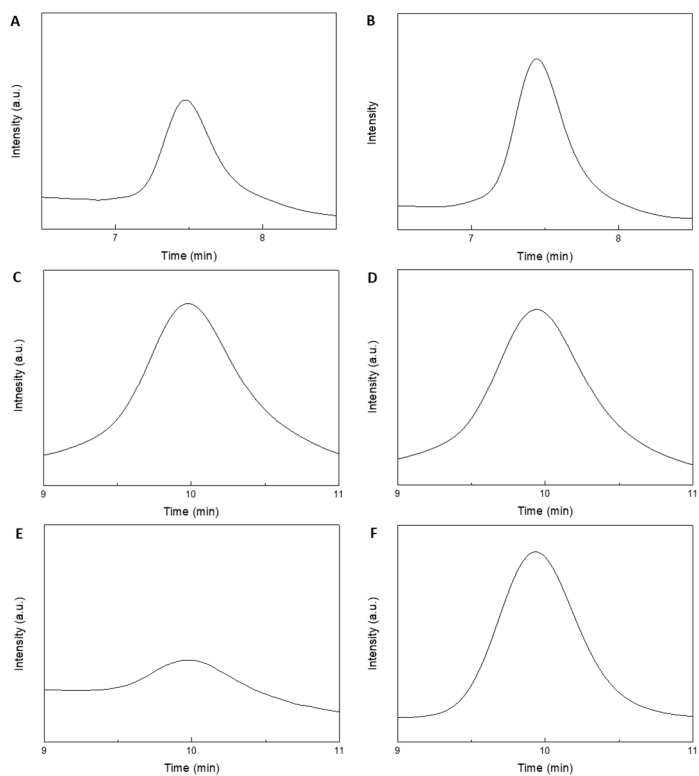


**Figure 4.14** THF GPC spectra of a) **4a** ( $M_n = 22,274 \text{ g mol}^{-1}$ ,  $D = 1.0832$ ), b) **4b**

(Mn= 23,408 g mol<sup>-1</sup>, *D* =1.1022) and DMF GPC spectra of c) **5a** (Mn= 17,055 g mol<sup>-1</sup>, *D* =1.1812), d) **5b** (Mn= 18,118 g mol<sup>-1</sup>, *D* =1.1620) and e) **7a** (Mn= 18,044 g mol<sup>-1</sup>, *D* =1.062), f) **7b** (Mn= 18,776 g mol<sup>-1</sup>, *D* =1.0931).

## 4.6 Reference

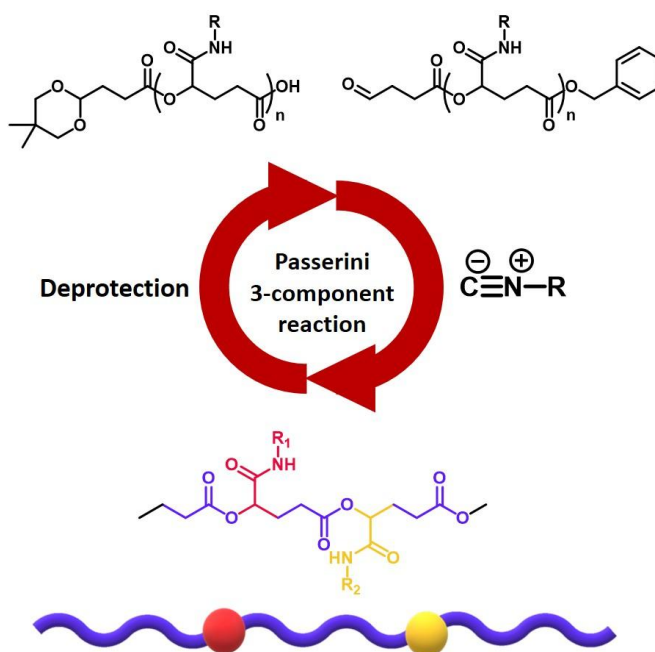
- [1] Hunt, I. *Protein Expr. Purif.* **2005**, *40*, 1–22.
- [2]. Wingfield, P. T. *Proteins. Curr. Protoc. Protein Sci.* **2015**, *80*, 6.1.1–6.1.35.
- [3] Labrou, N. E. *Protein Downstream Processing Design, Development and Application of High and Low-Resolution Methods*, Humana press, London, **2014**.
- [4] Block, H.; Maertens, B.; Spriestersbach, A.; Brinker, N.; Kubicek, J.; Fabis, R.; Labahn, J.; Schäfer, F. *Methods Enzymol.* **2009**, *463*, 439–473.
- [5] Gutiérrez, R.; Valle, E. M. M.; Galán, M. A. *Sep. Purif. Rev.* **2007**, *36*, 71–111.
- [6] Rigüero, V.; Clifford, R.; Dawley, M.; Dickson, M.; Gastfriend, B.; Thompson, C.; Wang, S. C.; O'Connor, E. *J. Chromatogr. A* **2020**, *1629*, 461505.
- [7] Xu, C.; Xu, K.; Gu, H.; Zhong, X.; Guo, Z.; Zheng, R.; Zhang, X.; Xu, B. *J. Am. Chem. Soc.* **2004**, *126*, 3392–3393.
- [8] Hainfeld, J. F.; Liu, W.; Halsey, C. M. R.; Freimuth, P.; Powell, R. D. *J. Struct. Biol.* **1999**, *127*, 185–198.
- [9] Tran, Q. T.; Sanoit, J.; Pierre, S.; Arnault, J. C.; Bergonzo, P. *Electrochim. Acta* **2014**, *136*, 430–434.
- [10] Lin, Y. C.; Liang, M. R.; Lin, Y. C.; Chen, C. T. *Chem. Eur. J.* **2011**, *17*, 13059–13067.
- [11] La, Y.; Park, C.; Shin, T. J.; Joo, S. H.; Kang, S.; Kim, K. T. *Nat. Chem.* **2014**, *6*, 534–541.

- [12] An, T. H.; La, Y.; Cho, A.; Jeong, M. G.; Shin, T. J.; Park, C.; Kim, K. T. *ACS Nano* **2015**, *9*, 3084.
- [13] Cho, A.; La, Y.; Shin, T. J.; Park, C.; Kim, K. T. *Macromolecules* **2016**, *49*, 4510–4519.
- [14] Ha, S.; La, Y.; Kim, K. T. *Acc. Chem. Res.* **2020**, *53*, 620–631.
- [15] Karayianni, M.; Pispas, S. J. *Polym. Sci.* **2021**, *59*, 1874–1898.
- [16] Hashimoto, H.; Ishimoto, T.; Konishi, H.; Hirokane, T.; Wakamori, S.; Ikeuchi, K.; Yamada, H. *Org. Lett.* **2020**, *22*, 6729–6733.
- [17] Percec, V.; Wilson, D. A.; Leowanawat, P.; Wilson, C. J.; Hughes, A. D.; Kaucher, M. S.; Hammer, D. A.; Levine, D. H.; Kim, A. J.; Bates, F. S.; Davis, K. P.; Lodge, T. P.; Klein, M. L.; DeVane, R. H.; Aqad, E.; Rosen, B. M.; Argintaru, A. O.; Sienkowska, M. J.; Rissanen, K.; Nummelin, S.; Ropponen, J. *Science* **2010**, *328*, 1009–1014.
- [18] Lei, M.; Zhang, H.; Miao, H.; Du, X.; Zhou, H.; Wang, J.; Wang, X.; Feng, H.; Shi, J.; Liu, Z.; Shen, J.; Zhu, Y. *Bioorg. Med. Chem.* **2019**, *27*, 4151–4162.
- [19] Jeong, M. G.; van Hest, J. C. M.; Kim, K. T. *Chem. Commun.* **2012**, *48*, 3590–3592.
- [20] Ha, S.; Kim, K. T. *RSC Adv.* **2022**, *12*, 7446.
- [21] Phuong, T.; Minh, T. K.; Ha, N. T. V.; Phuong, H. T. N. *Bioorg. Med. Chem. Lett.* **2004**, *14*, 653–656.
- [22] Lu, L.; Zhang, L.; Yuan, L.; Zhu, T.; Chen, W.; Wang, G.; Wang, Q. *ChemBioChem* **2019**, *20*, 1394–1399.
- [23] Li, Y.; Mullen, K. M.; Claridge, T. D. W.; Costa, P. J.; Felix, V.; Beer, P. D. *Chem. Commun.* **2009**, 7134–7136.

- [24] Zhang, S.; Xiao, Q.; Sherman, S. E.; Muncan, A.; Vicente, A. D. M. R.; Wang, Z.; Hammer, D. A.; Williams, D.; Chen, Y.; Pochan, D. J.; Vértesy, S.; André, S.; Klein, M. L.; Gabius, H. J.; Percec, V. *J. Am. Chem. Soc.* **2015**, *137*, 13334–13344.
- [25] Edwards, S. E.; Flynn, S.; Hobson, J. J.; Chambon, P.; Cauldbeck, H.; Rannard, S. P. *RSC Adv.* **2020**, *10*, 30463–30475.

# Chapter 5

## Synthesis of Sequence defined polymer using Passerini 3-component reaction



## 5.1 Abstract

(This work was collaborated with Mo Beom Koo and Prof. Kyoung Taek Kim)

The synthesis of sequence-defined polymer plays an important role in polymer chemistry field due to the possibility for developing materials with tunable functions and properties. In the previous studies, the various researches on synthesizing discrete polymers with defined sequences were reported. In this study, we suggest new method to synthesize sequence-defined polymer more efficiently via Passerini 3-component reaction. This multi-component reaction involves an isocyanide, an aldehyde and a carboxylic acid to offer the product. The sequence-defined polymers were synthesized by adding a monomer containing an isocyanide group in this research. As a result, we expected that the synthesizing polymers will become a material having various properties by containing functional groups or side chains at desired location.

## 5.2 Introduction

Multicomponent reaction (MCR) is a reaction in which two or more starting compounds react to form a product in such a way that most atoms of the starting material can be found in the product. In the 20th century, as interest in biomolecules increased, MCRs began to be widely used to easily synthesize libraries of various small molecules. Since then, simpler and more economical chemical reactions have emerged and a variety of starting materials have been created. The first MCRs appeared unofficially in 1838, when hydro-benzamide was synthesized in the process of leaving ammonia in bitter almond oil for a long time by French chemists Gerhard and Laurent.<sup>[1]</sup> After that, in 1850, as the process was generalized by Strecker et al, several MCRs began to be described. Since then, various MCRs have



appeared, and these discoveries have led to an improvement in the technology of the experiment. Among these various MCRs, in particular, Isonitrile-based MCRs have received more attention for being useful. For example, there are Passerini 3component reaction (CR) and Ugi 4 CR. The passerini 3CR was discovered by Mario Passerini in 1927 and includes isocyanides, aldehydes (or ketones) and carboxylic acids to form  $\alpha$ -acyloxy amides. Also, the Ugi 4CR was described by Ivar Karl Ugi in 1959 and contains ketones or aldehydes, amines, isocyanides and carboxylic acids to form bis-amides.<sup>[1-3]</sup>

The advantages of MCRs are high convergence, efficient synthesis of complex products, and economical chemical reaction in a double sense. On the other hand, the low diversity of molecular scaffolds remains challenges for improvement. Although it is possible to build a variety of molecules, it does not create a dramatically different molecular scaffold. So, to overcome this limitation, methods have been developed to post-modify MCRs and increase the types of components participating in the reaction.<sup>[1]</sup>

The synthesis of sequence-defined polymers is expected as one of the methods for developing materials having desired functions and properties.<sup>[4]</sup> In particular, many studies have been reported to completely control the function of polymer materials by reducing the dispersion of molecular weight.<sup>[4-6]</sup> In previous studies, there were various researches on methods for synthesizing discrete polymers with defined sequences.<sup>[7]</sup> In recent years, Kim's group has synthesized sequence-defined discrete polymers using a cross-convergent strategy.<sup>[8]</sup> In addition, these studies were reported on introducing a semi-automated system capable of mass synthesis by introducing flow chemistry and applying it as an information storage.<sup>[9]</sup> The cross-

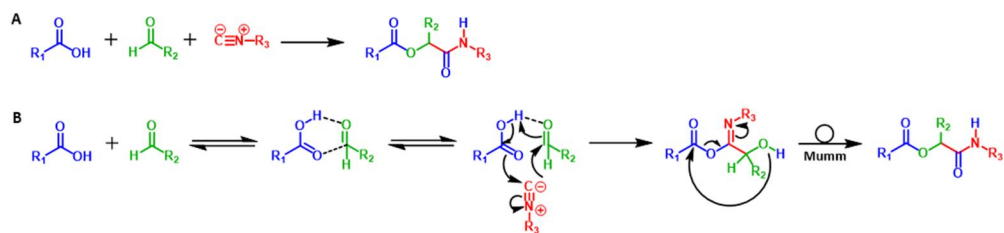
convergent synthesis is a faster, cheaper, and more efficient way than solid-phase synthesis to synthesize various sequence-defined polymers using simple monomers. In this study, L-lactic acid and glycolic acid were used as monomers representing 0 and 1 of the binary code, respectively, and the synthesized poly(L-lactic acid-co-glycolic acid) (PLGA) could store 1 bit per mass of 60 Da. This is a theoretically sequence-defined PLGA 2g with twice the density of DNA, which has been applied for research as an information storage medium, and can store all information (~2500 exabytes) currently stored in data centers around the world.<sup>[10]</sup> They used flow-chemistry to more easily reduce encoding time, cost and synthesized binary codes up to 256 bits in length through large-scale parallel work. As a result, it was shown that the bitmap image (896bit) can be encoded and decoded in the PLGA chain in which 14 types of sequences are defined.<sup>[9]</sup>

In this study, we report the efficient synthesis of sequence-defined discrete polymers via 3-component Passerini reaction. Based on 4-pentenoic acid, two types of monomers containing a carboxylic acid functional group and an aldehyde functional group were synthesized, respectively. Then a benzyl group and an acetal group were introduced as protecting groups for carboxylic acid and aldehyde. In addition, a third type of monomer containing an isocyanide functional group was introduced to synthesize a discrete polymer containing various functional groups and having a defined sequence.

### **5.3 Results and discussion**

### 5.3.1 Mechanism of Passerini 3-component reaction

Passerini 3-component reaction is the first isocyanide based multicomponent reaction which plays an important role in industry in these days and was discovered by Mario Passerini in 1921 in Florence, Italy.<sup>[11,12]</sup> It involves an isocyanide, an aldehyde (or ketone) and a carboxylic acid to form an  $\alpha$ -acyloxy amide (Scheme 5.1a). Several mechanisms of this reaction have been proposed, but the most widely accepted is the process reported by Ugi. This process forms an imidate intermediate through the sequential nucleophilic addition of a carboxylic acid, aldehyde and isocyanide. Afterwards, the product is provided through the Mumm rearrangement process (Scheme 5.1b).<sup>[11]</sup>

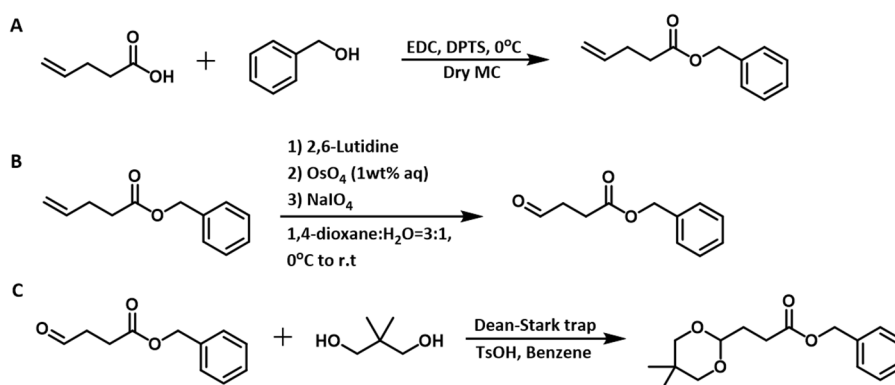


**Scheme 5.1** a) Passerini 3-component reaction. b) Concerted mechanism of Passerini 3-component reaction.

### 5.3.2 Synthesis of monomers having orthogonal protecting group

The modification process of monomers consists of three steps. In first step, a carboxylic acid group in 4-pentenoic acid was protected with benzyl alcohol through Steglich-type esterification (Scheme 5.2a) and benzyl 4-pentenoate was oxidized into benzyl 4-oxobutanoate through Lemieux–Johnson oxidation which makes an olefin undergoes oxidative cleavage to an aldehyde or ketone (Scheme 5.2b).<sup>[13,14]</sup> Finally, an AB type monomer was synthesized which having carboxylic acid and

aldehyde groups protected with orthogonal protection group, respectively. An aldehyde group was protected with neopentyl glycol using Dean-Stark method, as otherwise the aldehydes will deteriorate due to their highly reactive and unstable properties in the air (Scheme 2.2c).<sup>[9,15]</sup> Aldehydes have a polar carbon to oxygen double bond, and in particular, the oxygen atom attracts the bonding electron pair better than the carbon atom, resulting in charge separation within the molecule and causing dipole-dipole interaction. Due to this, aldehyde readily reacts with oxygen in the air to form carboxylic acid. Through thin-layer chromatography analysis, it was found that various damages occur even when the monomers were stored at -20°C without functional group protection. The resulting monomers were characterized by <sup>1</sup>H NMR. The black spots in the spectra are mark of NMR solvent peaks (Figure 5.1-5.3).



**Scheme 5.2** The monomer modification processes: a) Steglich-type esterification of 4-pentenoic acid and benzyl alcohol. b) Lemieux–Johnson oxidation of benzyl 4-pentenoate. c) Protection of aldehyde groups with neopentyl glycols using Dean-Stark method to prepare the AB type monomer.

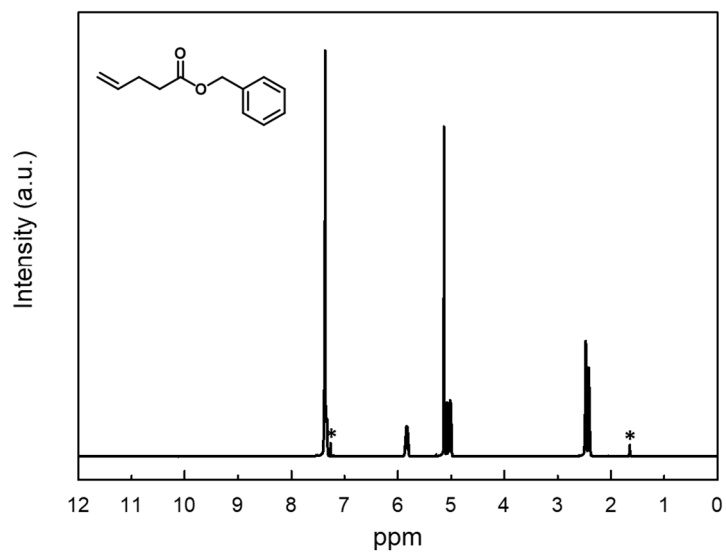


**Figure 5.1**  $^1\text{H}$  NMR spectrum of benzyl 4-pentenoate.

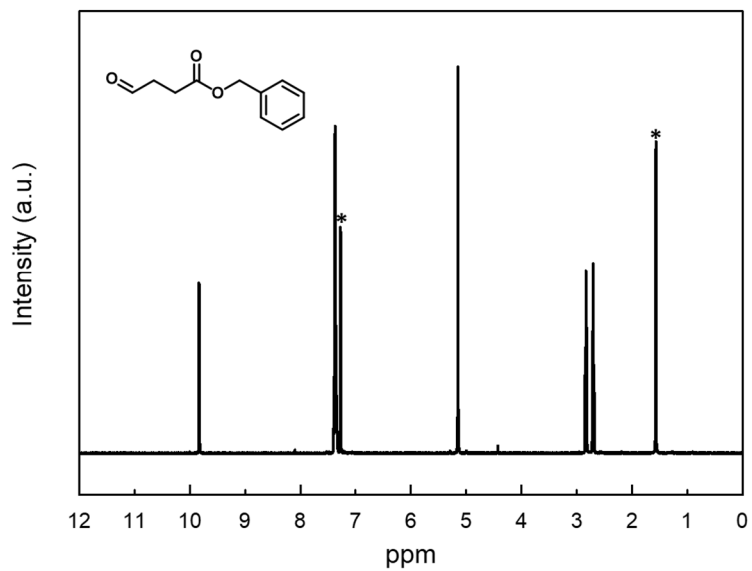


**Figure 5.2**  $^1\text{H}$  NMR spectrum of benzyl 4-oxobutanoate.

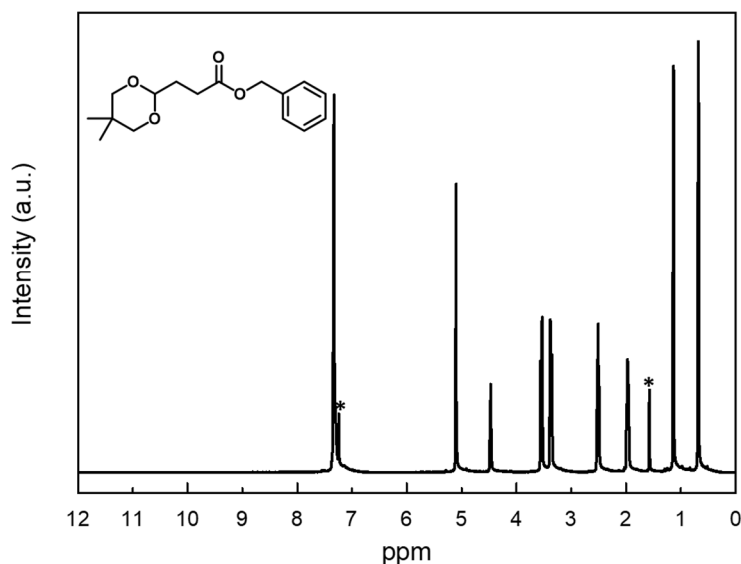
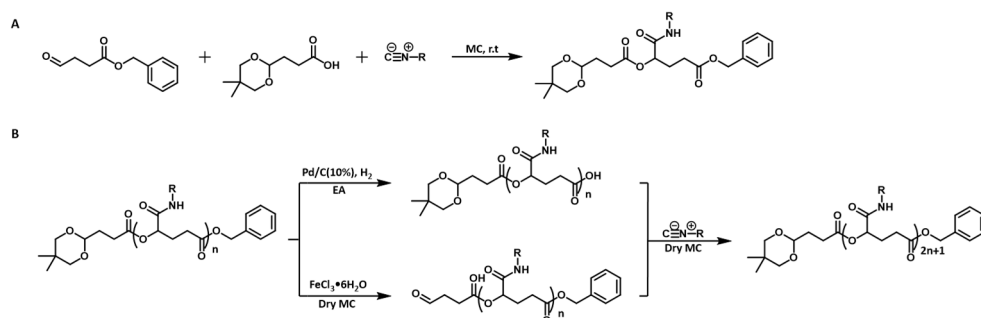


**Figure 5.3**  $^1\text{H}$  NMR spectrum of AB type monomer containing both aldehyde and carboxylic acid groups protected with each of orthogonal protection groups, respectively.

### 5.3.3 Synthesis of sequence-defined polymer

The AB type monomer was converted to two the only one side deprotected monomer via orthogonal deprotection and the dimer was synthesized through Passerini 3-component reaction using deprotected AB type monomers (Scheme 5.3a).<sup>[16,17]</sup> The Passerini 3-component reaction used only a small amount of solvent in very high concentration under room temperature.<sup>[18-20]</sup> This reaction was facile and very fast, yielding more than 95%. A dimer was synthesized using modified AB type monomers and cyclohexyl isocyanide, and was analyzed by  $^1\text{H}$  NMR (Figure 5.4). In addition, the cross-convergent strategy<sup>[9]</sup>, which includes a method of dividing into two paths, was introduced to synthesize sequence-defined polymers in earnest

(Scheme 5.3b). So, in the first manner ‘n-mer’ protected with both chain ends was converted into ‘n-mer’ having carboxylic acid group at the one chain end by deprotecting of benzyl group (Scheme 5.3b, upper reaction). And the second way is deacetalization of ‘n-mer’ in mild condition (Scheme 5.3b, under reaction). When ‘n-mer’ was deprotected under more acidic condition, dissociation of ester bonds, a side reaction in deacetalization, was observed. As a result, each deprotected dimer synthesized according to the above procedure was analyzed by  $^1\text{H}$  NMR (Figure 5.5 and 5.6). New isocyanide is introduced along with each ‘n-mer’ that has undergone the deprotection process, and ‘(2n+1)-mer’ is synthesized again through passerini 3-component reaction. The trimer synthesized through this process was analyzed by  $^1\text{H}$  NMR (Figure 5.7).



**Scheme 5.3** a) Passerini 3-component reaction using AB type monomers. b) Cross-convergent synthesis of sequence-defined polymers via Passerini 3-component reaction.

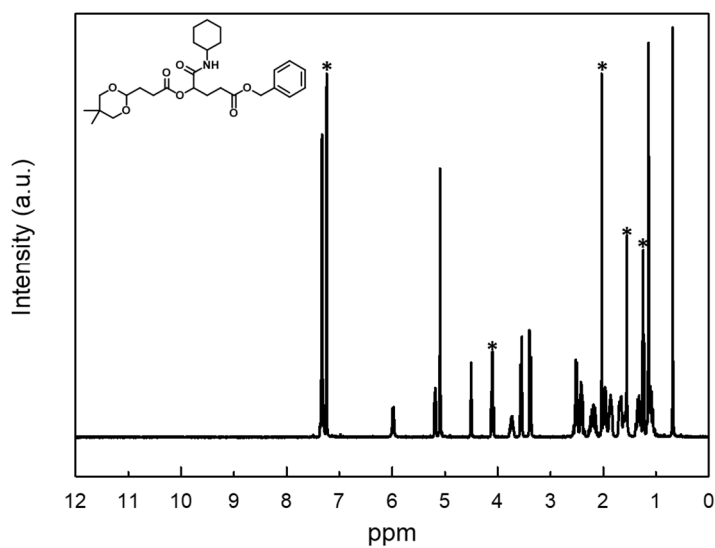


**Figure 5.4**  $^1\text{H}$  NMR spectrum of AB type monomer.

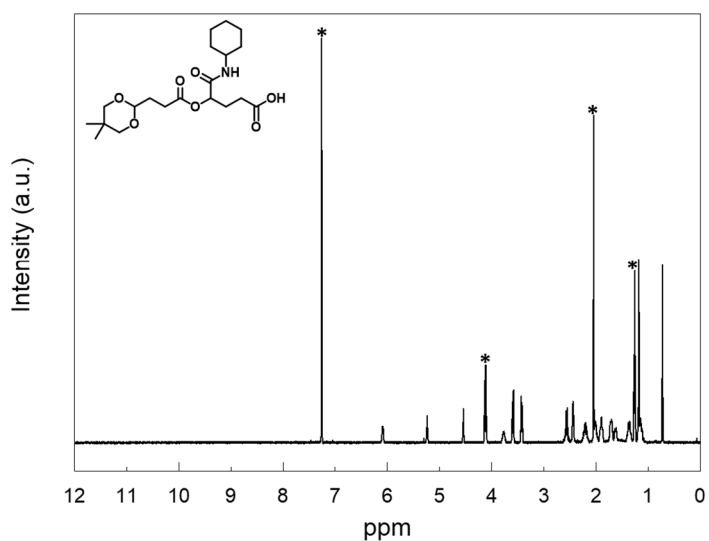


**Figure 5.5**  $^1\text{H}$  NMR spectrum of benzyl deprotected dimer.



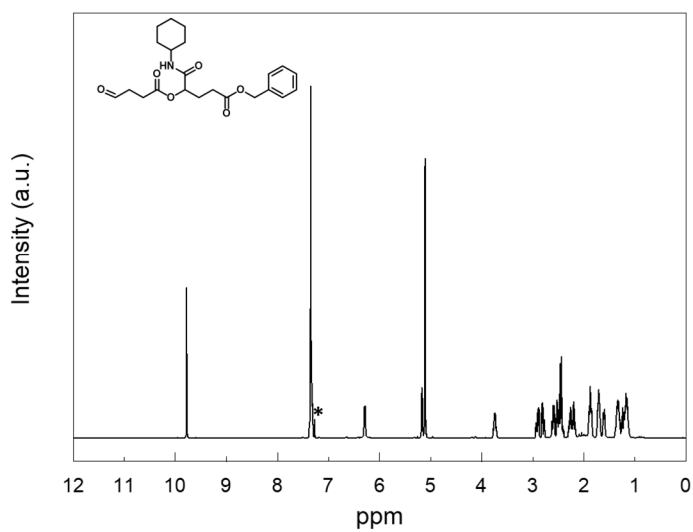


**Figure 5.6**  $^1\text{H}$  NMR spectrum of deacetalized dimer.

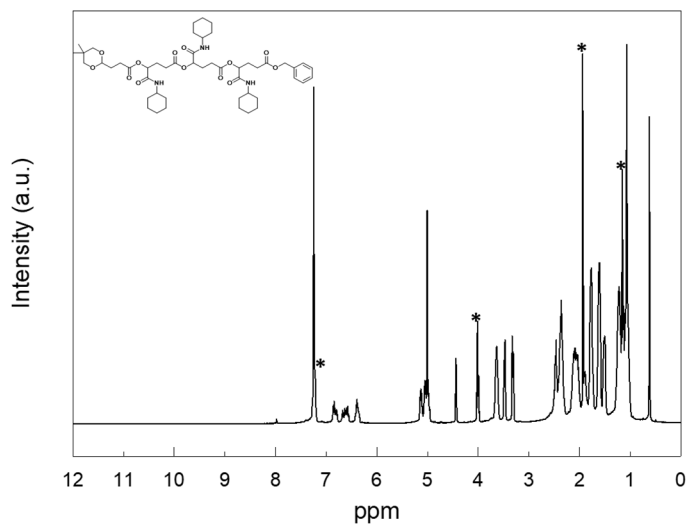


**Figure 5.7**  $^1\text{H}$  NMR spectrum of trimer synthesized through Passerini 3-component reaction.

In the meantime, we have gone through the process of screening and using various monomers in order to give different functional groups to one monomer. Specifically, various protection groups were applied to deprotect the functional groups without damaging the ester bond at the polymer stage.<sup>[21,22]</sup> For example, tert-butyltrimethylsilyl (TBDMS) and ethyl groups<sup>[8,9]</sup> were used to protect carboxylic acids, while ethylene glycol<sup>[18]</sup> and 2,2-Dimethylpropane-1,3-dithiol<sup>[23]</sup> were used to protect aldehydes. In addition, an attempt was made to increase the reaction economy by adding two functional groups to one reaction using the Ugi 4-component reaction. In addition, a highly economical Ugi 4-component reaction was attempted by adding two functional groups to one reaction. However, after several trials and errors, it was found that the currently reported methodology is the most optimal for our goal.

## **5.4 Conclusion**

In summary, we suggested new strategy of synthesizing sequence-defined polymers via multi-component reaction. This method introduces the cross-convergent synthesis reported in previous studies into a multi-component reaction, and is a methodology that can efficiently increase repeating units in a single reaction while assigning the functional group sequences to desired positions. We envisage that the system disclosed here could realize development of various research field such as synthesizing foldable polymers, alternating polymers, etc.

## **5.5 Experimental**

### **5.5.1 Materials**

All reagents and chemicals were used as received from Sigma Aldrich, Alfa Aesar and TCI. Dichloromethane (MC) was dried over CaH<sub>2</sub> under N<sub>2</sub> and Tetrahydrofuran

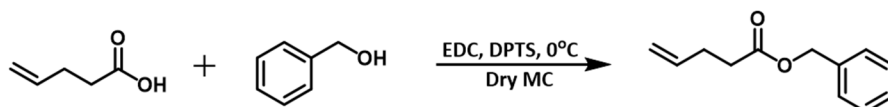
(THF) was refluxed over a mixture of Na and benzophenone under N<sub>2</sub> and distilled before use. All reactions were performed under N<sub>2</sub> unless otherwise note.

## 5.5.2 Techniques

<sup>1</sup>H NMR spectra was recorded at 400 MHz and 500 MHz, respectively on an Agilent 400-MR DD2 spectrometer and a Bruker DRX (500 MHz) NMR spectrometer. All NMR spectra were measured at 25 °C in the indicated deuterated solvents. CDCl<sub>3</sub> was used as standard solution in <sup>1</sup>H NMR spectra.

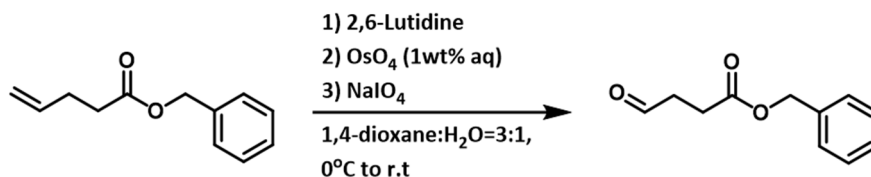
## 5.5.3 Synthesis

### 5.3.3.1 Synthesis of AB type monomer.



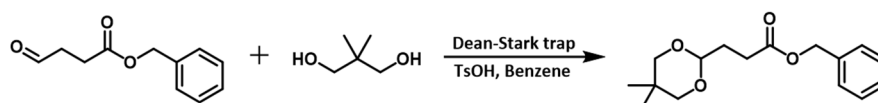
**Scheme 5.4** Preparation of benzyl 4-pentenoate.<sup>[9,13]</sup>

3g of 4-pentenoic acid and 1.62g of benzyl alcohol were added into 50mL of Dry MC. The mixture was cooled to 0 °C on an ice bath. 3.44g of 1-Ethyl-3-(3-dimethylaminopropyl)carbodiimide (EDC) and 0.66g of 1,4-Dimethylpyridinium *p*-toluene sulfonate (DPTS) were added to the mixture. The reaction mixture was stirred for 2-3h. Then the reaction mixture was washed with D.I water and brine. The combined organic layer was dried over MgSO<sub>4</sub>, and concentrated by vacuum rotary. The crude was purified by automated column chromatography with a mobile phase of EA/n-Hexane 10% to yield benzyl 4-pentenoate.



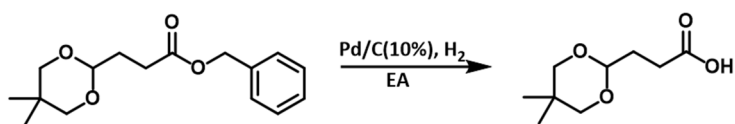
**Scheme 5.5** Preparation of benzyl 4-oxobutanoate.<sup>[14]</sup>

2.5g of benzyl 4-pentenoate was dissolved in mixture of 1,4-dioxane and D.I water (3:1 volume ratio, total 480mL). The reaction vessel was cooled to 0 °C on an ice bath. 2.8g of 2,6-Lutidine was first added, then 0.42mL of 1wt% OsO<sub>4</sub> aqueous solution was added and finally 8.43g of sodium periodate was added. The reaction mixture was stirred overnight. Then the reaction mixture was solved in 500mL of MC and washed with 1L of D.I water and Brine. The organic layer was dried over Na<sub>2</sub>SO<sub>4</sub> and concentrated under reduced pressure. The crude was purified by automated column chromatography with a mobile phase of EA/n-Hexane 20% to yield benzyl 4-oxobutanoate.



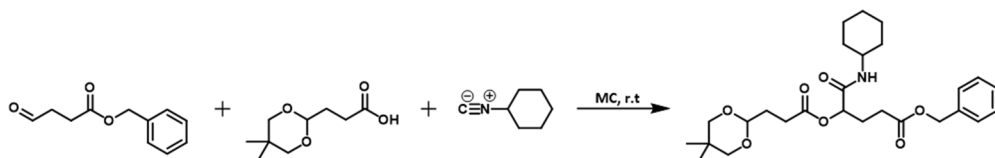
**Scheme 5.6** Preparation of AB type monomer.<sup>[15]</sup>

1g of benzyl 4-oxobutanoate, 0.54g of neopentyl glycol and 0.03g of p-toluene sulfonic acid were dissolved in 30mL of benzene. Then using Dean-stark apparatus, reaction mixture was distilled at 120°C for 2h. Cooled to r.t and concentrated organic layer under high vacuum condition. The crude was purified by automated column chromatography with a mobile phase of EA/n-Hexane 20% to yield AB type monomer.



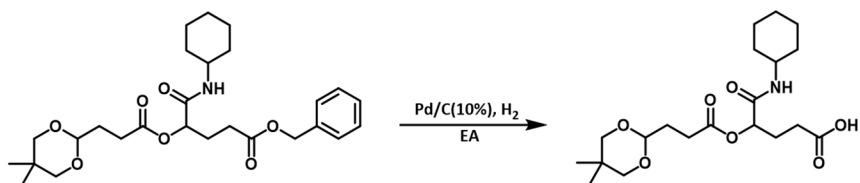
**Scheme 5.7** Preparation of 3-(5,5-dimethyl-1,3-dioxan-2-yl)propanoic acid.<sup>[9]</sup>

1g of AB type monomer was added in 100ml schlenk flask with EA(14mL) and 0.1g of Pd/C(10%). Vacuum the flask 2s for several times. A balloon of H<sub>2</sub> gas was injected into the vacuumed flask to purge. After that bubbling the H<sub>2</sub> gas for 2h with stirring. Then the reaction mixture was filtered with filter paper and washed with EA. The organic layers concentrated by rotary evaporator to yield 3-(5,5-dimethyl-1,3-dioxan-2-yl)propanoic acid.



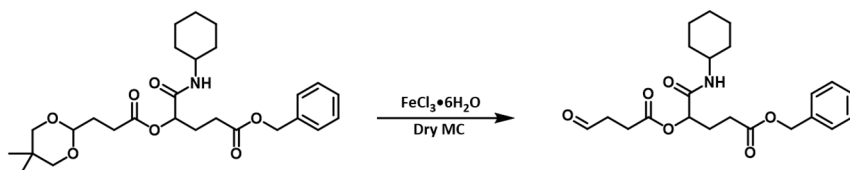
**Scheme 5.8** Preparation of dimer.<sup>[18-20]</sup>

0.82g of benzyl 4-oxobutanoate, 0.8g of 3-(5,5-dimethyl-1,3-dioxan-2-yl)propanoic acid and 0.56g of cyclohexyl isocyanide were dissolve in 2mL of dry MC. Then reaction mixture was stirred for 2h. The reaction mixture was concentrated by vacuum rotary. The crude was purified by automated column chromatography with a mobile phase of EA/n-Hexane 20% to yield dimer.



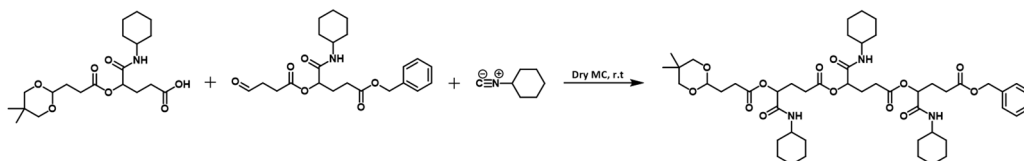
**Scheme 5.9** Hydrogenation of dimer.

0.6g of dimer was added in 100ml schlenk flask with EA(20mL) and 0.25g of Pd/C(10%). Vacuum the flask 2s for several times. A balloon of H<sub>2</sub> gas was injected into the vacuumed flask to purge. After that bubbling the H<sub>2</sub> gas for 2h with stirring. Then the reaction mixture was filtered with filter paper and washed with EA. The organic layers concentrated by rotary evaporator to yield 5-(cyclohexylamino)-4-((3-(5,5-dimethyl-1,3-dioxan-2-yl)propanoyl)oxy)-5-oxopentanoic acid .



**Scheme 5.10** Deacetalization of dimer.<sup>[21,22]</sup>

0.2g of dimer, 0.5g of iron chloride and dry MC (50mL) were added into 100ml Schlenk flask and stirred overnight under N<sub>2</sub> condition. Then reaction mixture was washed with D.I water and brine. The organic layer was dried over MgSO<sub>4</sub> and concentrated under reduced pressure. The crude was purified by automated column chromatography with a mobile phase of EA/n-Hexane 50% to yield benzyl 5-(cyclohexylamino)-5-oxo-4-((4-oxobutanoyl)oxy)pentanoate.



**Scheme 5.11** Preparation of trimer.

0.4g of each dimer and 0.13g of cyclohexyl isocyanide were dissolved in 2 mL of dry MC. Then reaction mixture was stirred for 2h. The reaction mixture was concentrated by vacuum rotary. The crude was purified by automated column chromatography with a mobile phase of EA/n-Hexane 55% to yield trimer.

### 5.5.4 Characterization

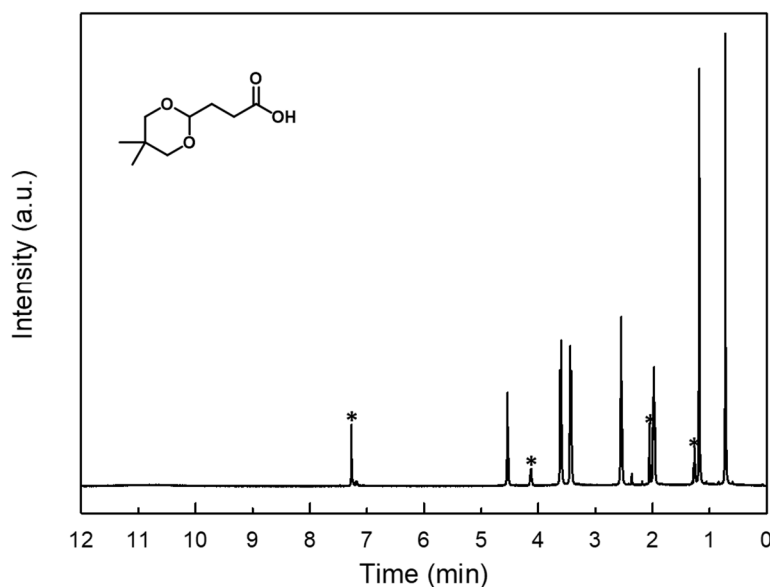


**Figure 5.8**  $^1\text{H}$  NMR spectrum of 3-(5,5-dimethyl-1,3-dioxan-2-yl)propanoic acid.

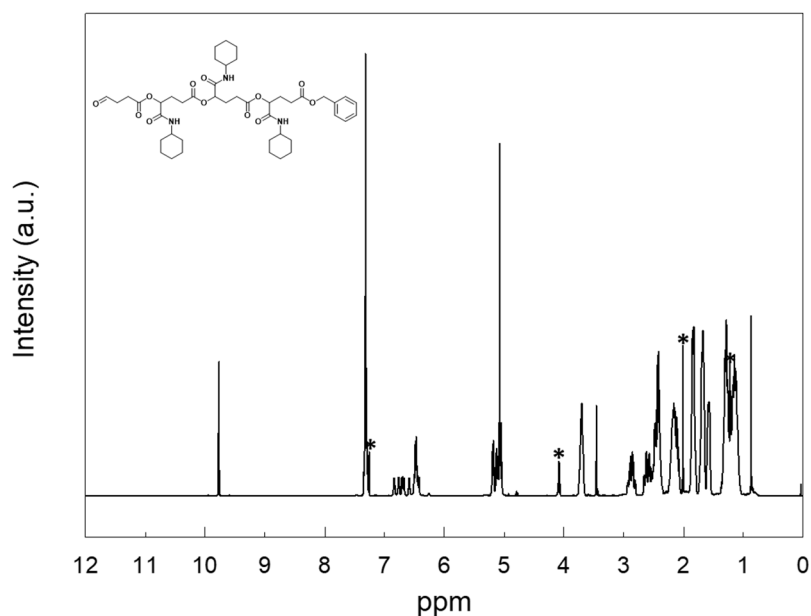


**Figure 5.9**  $^1\text{H}$  NMR spectrum of deacetalized trimer.

## 5.6 Reference

- [1] Brauch, S.; Berkela, S. S. V.; Westermann, B. *Chem. Soc. Rev.* **2013**, *42*, 4948.
- [2] Dömling, A.; Wang, W.; Wang, K. *Chem. Rev.* **2012**, *112*, 3083–3135.
- [3] Ugi, I.; Dömling, A.; Hörl, W. *Endeavour* **1994**, *18*, 115–122.
- [4] Badi, M.; Lutz, J. F. *Chem. Soc. Rev.* **2009**, *38*, 3383–3390.
- [5] Meier, M. A. R.; Kowollik, C. B. *Adv. Mater.* **2019**, *31*, 1806027.
- [6] Lutz, J. F.; Ouchi, M.; Liu, D. R.; Sawamoto, M. *Science* **2013**, *341*, 1238149.
- [7] Lutz, J. F. *Polym. Chem.* **2010**, *1*, 55–62.
- [8] Lee, J. M.; Koo, M. B.; Lee, S. W.; Lee, H.; Kwon, J.; Shim, Y. H.; Kim, S. Y.; Kim, K. T. *Nat. Commun.* **2020**, *11*.
- [9] Lee, J. M.; Kwon, J.; Lee, S. J.; Jang, H.; Kim, D. G.; Song, J.; Kim, K. T. *Sci.*



*Adv.* **2022**, *8*, eabl8614.

- [10] Mlitz, K. *Data Center Storage Capacity Worldwide From 2016 To 2021, By Segment* (Statista,2021).
- [11] Banfi, L.; Riva, R. *Org. React.* **2005**, *65*.
- [12] Dömling, A.; Ugi, I. *Angew. Chem. Int. Ed.* **2000**, *39*, 3168–3210.
- [13] Jordan, A.; Whymark, K. D.; Sydenham, J.; Sneddon, H. F. *Green Chem.* **2021**, *23*, 6405.
- [14] Yu, W.; Mei, Y.; Kang, Y.; Hua, Z.; Jin, Z. *Org. Lett.* **2004**, *6*.
- [15] Herdewijn, P.; Claes, P. J.; Vanderhaeghe, H. *J. Med. Chem.* **1986**, *29*, 661–664.
- [16] Sen, S. E.; Roach, S. L.; Boggs, J. K.; Ewing, G. J.; Magrath, J. *J. Org. Chem.* **1997**, *62*, 6684–6686.
- [17] Salomon, C. J.; Mata, E. G.; Mascaretti, C. A. *Tetrahedron* **1993**, *49*, 3691–3748.
- [18] Sehlinger, A.; Kreye, O.; Meier, M. A. R. *Macromolecules* **2013**, *46*, 6031–6037.
- [19] Zhang, L. J.; Deng, X. X.; Du, F. S.; Li, Z. C. *Macromolecules* **2013**, *46*, 9554–9562.
- [20] Zhang, J.; Zhang, M.; Du, F. S.; Li, Z. C. *Macromolecules* **2016**, *49*, 2592–2600.
- [21] Diness, F.; Meldal, M. *Eur. J. Org. Chem.* **2015**, *7*, 1433–1436.
- [22] Zhang, H. J.; Priebbenow, D. L.; Bolm, C. *Chem. Soc. Rev.* **2013**, *42*, 8540.
- [23] Firouzabadi, H.; Iranpoor, N.; Hazarkhani, H. *J. Org. Chem.* **2001**, *66*, 7527–7529.

# 국문초록

## 고밀도 작용기를 포함하는 블록공중합체의 수용액상의 자기조립체의 구조적 다양성 탐구와 응용

이수정

고분자화학전공

화학부

서울대학교

블록 공중합체의 용액상의 자기조립은 미세 구조체를 손쉽게 합성할 수 있는 방법들 중 하나이다. 이 방법을 이용하기 위해서는 잘 정의된 블록 공중합체를 합성하는 것이 필수적으로 선행되어야 한다. 이렇게 합성된 블록 공중합체는 한 분자 안에 친수성 블록과 소수성 블록을 한 번에 포함하여 양친성을 나타내기 때문에 용액상에서 일종의 계면활성제와 같이 거동한다. 각각의 블록과 용매들 사이 상호작용하는 요소들이 벌크상의 자기조립에 비해 보다 다양하기 때문에 상대적으로 더욱 섬세한 미세구조체들의 합성이 가능하다. 이 양친성 입자들의 거동에 의해 형성되는 자기조립 구조체에 영향을 미치는 요인들은 다수 있으나 가장 영향력 있는 요소로 블록 비율(block ratio)과 critical packing parameters를 정의할 수 있다. 선행 연구에서는 이 요소들이 고분자의 화학 구조와 밀접한 연관이 있음을 밝혔다. 이를 바탕으로 본 논문에서는 앞서 언급했던 요인들에 기반하여 양친성 블록 공중합체를 합성하고 여러 가지 자기조립 구조체들의 관찰 및 응용을 선보이고자 한다. 우리는 동일한 화학 구조를 가지며 소수성 블록의 극단적인 분자량 차이를 가지는 블록 공중합체들의 이원블렌드를 통해 선행 연구에서 보고된 적이 없는 자기조립 구조체를 보고하였다. 이는 폴리머의 큰 분자량에서 기인하는 비에르고딕적 거동으로 인해 발생하는

현상으로, 말단 작용기를 포함하는 저분자량의 블록 공중합체의 합성 및 금 나노 입자를 이용한 표지법을 이용하여 자기조립 구조체 내에서 표면에너지가 높은 곳에 저분자량의 블록 공중합체들의 밀집을 통해 구조체 전체가 안정화될 것이라는 가정을 실험적으로 증명하였다.

또한 우리는 선행 연구에서 보고되었던 고분자 큐보솜 표면에 고밀도 작용기를 부여하여하고자 하였다. 이 구조체는 내부에 잘 정의된 서로 독립된 두 개의 수로를 포함하며 표면에 미세 기공을 포함하고 있어 표면적이 넓다는 특징을 가진다. 이러한 장점을 응용하고자 표면에 알카인 작용기를 부여하고 구리 촉매를 이용한 알카인-아자이드 클릭 반응을 이용하여 작용기의 활성을 확인하였다. 그 결과 표면에 고밀도 작용기를 포함하는 고분자 큐보솜은 L-proline 도입을 통해 알돌 반응의 나노 반응기로 사용될 수 있을 것이라고 전망되었다.

뿐만 아니라 친수성 블록의 말단을 각각 벤질기, 하이드록시기, t-Boc 글라이신, 아민으로 개질하여 용액상의 자기조립을 하는 과정에서 다양한 형태학적 전이를 관찰할 수 있었다. 그 결과 선행 연구에서 보고된 적 없었던 표면에 고밀도 아민기를 포함하는 고분자 큐보솜을 합성할 수 있었다. 여기에 Ni-NTA 복합체를 도입하여 고분자 큐보솜을 히스티딘 표지 단백질을 선택적으로 정제할 수 있는 금속이온-친화성 크로마토그래피의 고정상으로 응용하고자 하였다.

그리고 작용기를 포함하는 폴리머 합성 연구의 계보를 이어 4-pentenoic acid 단량체를 이용한 Passerini 3-컴퍼넌트 반응으로 서열이 정의된 단일 분자량을 가지는 고분자 합성 연구를 진행하였다. 이 방법은 선행 연구에서 보고된 반복 지수 성장법을 멀티컴퍼넌트 반응에 융합하여 보다 효율적으로 원하는 위치에 원하는 작용기를 포함하는 고분자 사슬을 합성하여 고분자의 물성을 조절할 수 있는 새로운 수단이 될 수 있을 것이라 기대 받고 있다.

**주요어:** 블록공중합체, 자기조립, 고분자 큐보솜, 기능성 고분자, 고분자 나노구조체, 단일분자량고분자

**학번:** 2016-20357